# Muon Physics

# Muon Physics

By

Nicolai Popov

Cambridge
Scholars
Publishing

Muon Physics

By Nicolai Popov

This book first published 2019

Cambridge Scholars Publishing

Lady Stephenson Library, Newcastle upon Tyne, NE6 2PA, UK

British Library Cataloguing in Publication Data
A catalogue record for this book is available from the British Library



ISBN (10): 1-5275-2023-4
ISBN (13): 978-1-5275-2023-3

The author dedicates this book to his late wife, Antonina Popova.

# CONTENTS

# ABSTRACT

The muon plays an important role in elementary particle and nuclear physics. The muon was discovered in cosmic radiation by Carl D. Anderson and Seth Neddermeyer in 1936. The muon was a puzzle for physicists for a long time as the only difference between a muon and an electron seemed to be the difference in their masses: the mass of a muon is about 207 times greater than that of the electron. “Who ordered that?” asked Isidor Rabi.

At present the muon is very important in the framework of the Standard Model. With the discovery of the charm quantum number muon and the accompanying muon, the neutrino plays an important role in the quark-lepton model of elementary particles. Namely, the muon and the muon neutrino, together with their correspondent quarks, have been combined in the second generation of the Standard Model.

Muonic processes provide important information on the low energy limit of a weak interaction. The equality of the muon decay coupling constant and the vector one of beta-decay proved the Conserved Vector Current (CVC) hypothesis. The most accurate information on induced (via a strong interaction) pseudoscalar coupling ($g_p$) was obtained from the muon capture process. The most important problem is the exchange-current effects in the nuclear muon capture, as well as a possible T-violation beyond the kaon system.

A negative muon entering a gaseous mixture of light elements initiates a complicated chain of atomic and molecular processes, which forms an unavoidable background to the experimental investigation of a weak muon capture by hydrogen and helium nuclei. The experimental investigation of atomic and molecular processes, ending with nuclear fusion of light elements induced by muons (called Muon Catalyzed Fusion: μCF), is an interesting test for the verification of different approaches to theoretical calculations.

The investigation of muonic atoms gives essential information about the structure of light and heavy atomic nuclei, including nuclear formfactors. A very precise value of the root-mean-square charge radius of the proton was obtained from the measurement of the Lamb-shift in a $p\mu$ atom. The investigation of muonic atoms enables quantum electrodynamics to be tested using the high order of perturbation theory.

The behaviour of the muon and muonium in condensed matter is currently very topical, due to the fact that it is important for solid state physics.

Finally, muonic research is widely used in chemistry, biology, and medicine.

# ACKNOWLEDGMENTS

I am very grateful to Dr. Wilhelm Czaplinski for his long-term and fruitful collaboration, as well as his valuable discussions during the preparation of this book.

# 1. INTRODUCTION

The research into muon participation plays an important role in elementary particle and nuclear physics; as well as in applied physics. There are many excellent reviews concerning muon physics (see references, 1–4) that have been published some years ago. I will now provide a contemporary description of this topic.

The muon was discovered in cosmic rays in 1936 [5] and it was first named "muon" in 1947 [6]. However, this particle puzzled physicists for a long time as the only distinction between a muon and an electron appeared to be their mass: a muon is ~207 times heavier than an electron. Despite the numerous investigations into the muon, the nature of this particle remained unclear for a long time, leading Isidor Rabi to declare: "Who ordered this?" The numerous attempts to find any additional muon interactions in comparison with electrons, which could prove responsible for its mass, were unsuccessful. However, when the Standard Model was developed it proved that the muon plays an important role in the quark-lepton scheme of the elementary particles. The muon and the muon neutrino were combined with the correspondent quarks to the second generation of the Standard Model [7]; this evolved naturally after the discovery of charm particles.

Muonic processes provided important information on the low energy limits of this weak interaction [8]. The equality of the muon decay

coupling constant to vector one of beta-decay proved the Conserved Vector Current (CVC) hypothesis [9].

The investigation of muon capture by proton provided the best information on the induced pseudoscalar interaction [10]. The kinetics of muonic atoms in the hydrogen isotopes mixture is very important for weak muon capture. The investigation of muon catalyzed fusion (μCF) was predicted ~70 years ago [11] and it was effectively investigated over a thirty-year period [3, 12–14]. However, the hope that it would be possible to use μCF as an alternative source of energy has met with difficulties and is yet to be realized. At the same time, the numerous theoretical and experimental results that were obtained within the μCF investigations have made a very important contribution to mesic atomic physics.

In addition, the investigation of muon capture in light nuclei (e.g., by helium) is an important process in the research on weak interaction; this also includes the particle correlations for the determination of weak interaction constants. The possible exchange currents could prove to be very important when explaining the difference between the pseudoscalar formfactor in nuclei and that of the free proton. The information about nuclear formfactors and the verification of quantum electrodynamics in high order perturbation theory was obtained through the investigation of the muonic atoms; this also included mesic hydrogen [15].

Heavy muonic atoms are used to investigate problems in nuclear fission [16]. The prompt (by cascade transitions) and delayed (by weak muon capture) fissions will be discussed by comparing the experimental results with the theoretical explanation.

It is also very important to use the muon as a probe for the verification of the structure of condensed matter (e.g., the behaviour of muonium in the solid-state target) [3, 17]. However, these problems could form the subject of another book, so I have only provided a brief discussion on this topic.

Finally, muon research is used in biology and medicine [18–20]. With regard to medical goals, the characteristic gamma-ray emission of muonic atoms is used for diagnosis; this also included cosmic medicine.

The aim of this monograph is to demonstrate the wide role of muon physics when discussing problems in elementary particles and nuclear physics. This also includes applied research.

# 2. MUON IN THE VACUUM

## 2.1 Mass and spin

Different methods to determine particle masses exist [21]. The numerous amounts of data on muon mass have been obtained by measuring muon tracks using photo-emulsion and gamma-spectra from $\pi p$ reactions. Additionally, X-rays from *C*, *P*, and *Si* muonic atoms were published in 1954. The determination of the muon mass ($m_\mu/m_e$), as well as the muon magnetic moment $(\mu_\mu/\mu_p)$, has been obtained using the precision measurement of the ground state hyperfine structure interval of muonium $(\mu^+e^-)$, which is a hydrogen-like atom consisting of a positive muon and an electron [22, 23]. The muonium Zeeman hyperfine transitions, (1/2,1/2) $\leftrightarrow$ (1/2, -1/2) and (-1/2, -1/2) $\leftrightarrow$ (-1/2, 1/2) under a high magnetic field, have been made at LAMPF using the microwave magnetic resonance spectroscopy method [2]. The Hamiltonian of the interaction between the magnetic moments of two particles is: $H = -\frac{8}{3}\pi\vec{\mu}_\mu \cdot \vec{\mu}_e \delta(\vec{r}_\mu - \vec{r}_e)$ [24], where $\vec{\mu}_i = \frac{e\hbar}{m_i c}\vec{S}_i$. This is the magnetic moment operator of corresponding particle ($i$ = $\mu$, $e$) with the spin operator, $\vec{S}_i$, and known constants $e$, $\hbar$, $c$; $m_i$ is the mass of the particle. The magnetic moment depends on the muon mass, which can be obtained from this experiment: $(m_\mu/m_e)$ = 206.768277(24) with $(\mu_\mu/\mu_p)$ = 3.18334513(39). The recent experimental data of the muon mass, $m_\mu$ =

105.6583715(35)$MeV$ [4] and $(m_\mu/m_e)$ -206.768276(24) ≤ 1.2 × $10^{-7}$ [23], coincided with earlier experimental data [22].

There has been research into muon spin since 1941 [25]. The comparison of these calculations with the experimental data from cosmic rays indicated a muon spin 1/2 [26]. However, the direct proof of the muon spin 1/2 follows on from the gyromagnetic factor, $(g_\mu/2)$ = 1.0011659203(15) [3,27], where $g_\mu$ is determined from $\vec{\mu}_\mu = g_\mu \frac{e\hbar}{2m_\mu}\vec{S}_\mu$. The experimental data for $a_\mu = (g_\mu - 2)/2$ was presented in [23] using $a_\mu^{\exp} = 11659209.1(5.4)(3.3)\times 10^{-10}$, where the first errors are statistical and the second errors are systematic. The recent data for $g_\mu - 2$ has also been provided [see reference 28].

## 2.2 The lifetime and decay spectrum

The lifetime of the muon, $\tau_\mu$, can be obtained by using $\mu^+$ decay in the reaction, $\mu^+ \to e^+ + \overline{\nu}_\mu + \nu_e$. The analogous reaction of $\mu^-$ decay, $\mu^- \to e^- + \nu_\mu + \overline{\nu}_e$, can compete with the muon capture reaction in a proton or nuclei. Here, $\nu_e$ and $\nu_\mu$ are the electron and the muon neutrinos, respectively, while $\overline{\nu}_e$ and $\overline{\nu}_\mu$ are the antineutrinos.

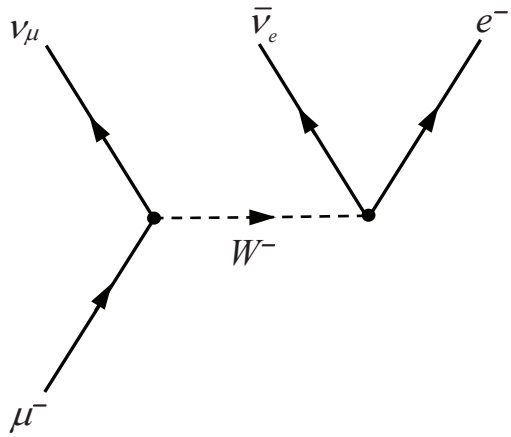


Fig.1. A muon transmutes into a muon neutrino by emitting a $W^-$ boson. The $W^-$ boson subsequently decays into an electron and an electron antineutrino.

The initial investigations of $\tau_\mu$ began in 1941 using cosmic rays [29, 30]. The data for $\tau_\mu$ were first obtained in the 1970s and 1980s [27, 31] and later, as evidenced in reference 32.

The recent determination of $\tau_\mu$ was performed in the Paul Scherrer Institute (PSI) [33]. The experiment was conducted using a time-structured and nearly 100% polarized surface muon beam, along with a segmented, fast-timing plastic scintillator array.

Approximately $1,6\times10^{12}$ positrons were accumulated and the following was obtained, $\tau_\mu = 2.1969803(22)\times10^{-6}s$; this is 30 times more precise than previous generations of lifetime experiments. The weighted average of all results gives a lifetime of $\tau_\mu = 2.1969811(22)\times10^{-6}s$. The detailed description of this experiment [33] has also been given in the reference 4.

The measurement of the lifetime of $\mu^-$ inflight resulted in 2.1948 $(10)\times10^{-6}s$ [34, 3]. As indicated above with regard to the stopped negative muon and muon decay, the muon capture process is possible. Therefore, the measurement of the negative muon's lifetime is determined by the total disappearance rate; this includes the decay and capture rates.

The contribution of the capture rate to the disappearance rate varies from ~0.1% in hydrogen to >90% in heavy elements [4]. Despite the complicated extraction of the lifetime of $\mu^-$, due to the atomic and molecular processes that occur in the hydrogen isotope mixtures, the lifetime of $\mu^-$ from the singlet state of $\mu p$ atom coincides with the lifetime of $\mu^+$ [10]. The muon decay spectrum was considered in, for example, reference 35. All the measurements of the $\mu^\pm$ decay have been successfully described by the V-A lepton number conserving four-fermion interaction. The members of each generation's weak isospin doublet are

$$\begin{pmatrix} e^- \\ \nu_e \end{pmatrix}, \begin{pmatrix} \mu^- \\ \nu_\mu \end{pmatrix}, \begin{pmatrix} \tau^- \\ \nu_\tau \end{pmatrix}.$$

These assigned lepton numbers are conserved under the Standard Model.

Electrons and electron neutrinos have an electronic number of $L_e = 1$, while the number for muons and muon neutrinos is $L_\mu = 1$. For $\tau$ the number is $L_\tau = 1$. Antileptons have a lepton number of -1. The conservation of $e^-, \mu^-$ and $\tau^-$ - type lepton numbers indicates that $\Delta L_e = \Delta L_\mu = \Delta L_\tau = 0$.

The initial consideration of the electron (positron) spectrum (beyond the Standard Model) was calculated using the Michel parameter $\rho$; however, the QED corrections $(\hbar = c = 1)$ have been ignored:

$$\Gamma dx = 12\,\Gamma_0 \left[ 1 - x - \frac{2}{9}\rho(3-4x) \right] x^2\, dx \quad ,$$

where $x = E/E_{\max}$ with $E_{\max} = m_\mu/2$ and $\Gamma_0 = \tau_\mu^{-1} = \dfrac{G_F{}^2 m_\mu^5}{192\pi^3}$ is the total decay rate with $G_F = 1.1663787(6)\times 10^{-5}\,(GeV)^{-2}$ [33] as the weak interaction constant. The spectrum dependence over the parameter, $\rho$, is given in Fig. 2, which has been taken from reference 1b. However, in the framework of the Standard Model using a lepton number conservation and a weak V-A interaction of $\rho = \dfrac{3}{4} = 0.75$, the electron spectrum is given by $\dfrac{d\Gamma}{dx} = 2\Gamma_0(3-2x)x^2$.

The following is the differential decay probability for $\mu^\pm \to e^\pm$ decay with respect to muon polarization:

$$\frac{d^2\Gamma}{dx\,d\cos\vartheta} = \Gamma_0[3 - 2x \pm P_\mu(2x-1)\cos\vartheta]x^2 \quad .$$

Where the upper sign corresponds to $\mu^+$ decay and the lower sign to $\mu^-$ decay, $P_\mu$ is residual muon polarization and $\vartheta$ is the angle of electron (positron) momentum with respect to the muon polarization vector $\vec{P}_\mu$.

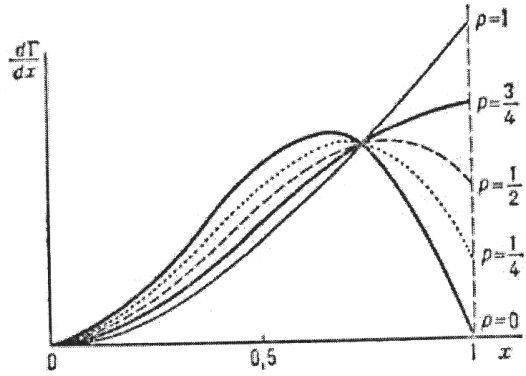


Fig. 2. The energy spectrum of electrons (positrons) from muon decay using the different Michel parameters taken from 1b.

The experiments agree with the standard Michel parameter, $\rho = 3/4 = 0.75$, for the emission of both the neutrino and antineutrino. In the case of $\rho = 0$, the electron (positron) emission could be accompanied by two neutrinos or two antineutrinos, which contradicts the conservation of the lepton numbers. The energy spectrum of positrons is described in Fig. 3.

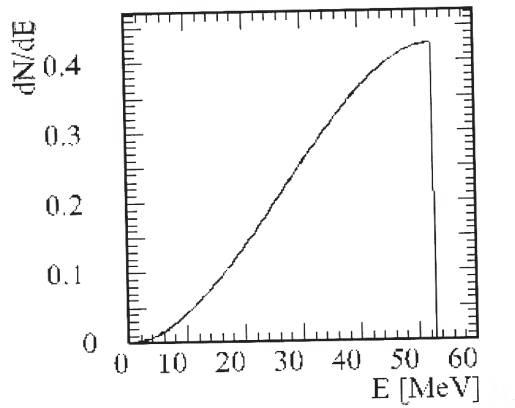


Fig.3. The Michel spectrum of positrons from muon decay at rest ($\rho = 3/4$).

The positron asymmetry, $N(\vartheta, E) \propto 1 + A(E)\cos\vartheta$, where $A(E) = (2x-1)(3-2x)^{-1}$, which for high energy positrons ($x \to 1$) approaches $A$ = +1, so positrons are preferentially emitted in the muon spin direction (i.e. opposite to the muon momentum). For low-energy positrons ($x \to 0$) the asymmetry approaches $A$ = -1/3 and positrons are preferentially emitted opposite the muon spin direction. When they are integrated over the energy distribution of emitted positrons, the asymmetry is $A$ = +1/3 (i.e., positrons are preferentially emitted alongside the muon spin). The muon decay is realized with *P*- and *C*-violation for parity. The backward asymmetry is for emitted electrons.

## 2.3 Rare decays and other processes

The fundamental law of flavour conservation has been confirmed through observations that set an upper limit on flavour conservation-violating processes, such as $\mu^{\pm} \to e^{\pm} + \gamma$, $\mu^{\pm} \to 3e^{\pm}$ or $\mu^{-}N \to e^{-}N$ and so on. The conservation of lepton numbers means that when the particles interact the number of the same type leptons remains the same. The process, $\mu^{\pm} \to e^{\pm} + \gamma$, represents the ultra-rare decay mode. The decay mode, $\mu^{+} \to e^{+} + \gamma$, was researched at PSI [36]. The decay mode features the back-to-back emission from both a positron and a gamma ray, each with energies that equal $m_{\mu}/2 \approx 53\,MeV$. A tracking drift chamber system and high-resolution liquid xenon scintillation detector were also [4]. Their results to data ratio set the limit, $BR_{e\gamma} < 5.7 \times 10^{-13}\,(90\%\,CL.)$ [36].

Searches for the $\mu \to 3e$ also resulted in the upper limit of flavour violation [37]. The total energy of three electrons should be close to the muon's mass. Therefore, possible background processes, such as internal-conversion decay, generally yield lower event energy sums and distort the momentum balance; this means they should not be considered. So, the results to data ratio of the $\mu \to 3e$ set the limit $BR_{3e} < 1.0 \times 10^{-12}$ [37, 4].

The reactions, $\mu^- N \to e^- N$, were researched using different nuclei, including *Ti* and *Pb* [8]. This recent experiment was performed on *Al* [38, 4]. The signature for the $(\mu^-, e^-)$ reaction is particularly simple and unique as the electron will become mono-energetic with an energy of ~106*MeV*, while, in the free muon decay, an electron only reaches ~53*MeV*. This process involves the formation of a muonic atom with a nucleus (i.e. $\mu Al$ – atom) followed by the coherent conversion of the muon to an electron, which is then ejected with an energy close to the muon rest mass. The coherent conversion measurements will correspond to

$BR_{\mu e} = \dfrac{\Gamma\left[\mu^- + (A,Z) \to e^- + (A,Z)\right]}{\Gamma\left[\mu^- + (A,Z) \to \nu_\mu + (A,Z-1)\right]}$, where the denominator corresponds to the muon capture rate. Searches for the $(\mu^-, e^-)$ reaction have set an impressive limit on lepton number conservation: $BR_{\mu e} < 7 \times 10^{-13}$ [38, 4]. Therefore, the searches for all of these reactions have indicated the placement of strong limits on lepton number conservation.

## 2.4 The muon and the Standard Model

The Standard Model of elementary particles is illustrated in Fig. 4. The second degeneration of the model is represented by muon $\mu$ and the muon neutrino $\nu_\mu$, as well as the strange *s* and charm *c* quarks. At the same time, the first degeneration corresponds to the electron *e* and its neutrino $\nu_e$; it also relates to both the down *d* and up *u* quarks. The third degeneration is determined by tau meson $\tau$, its neutrino $\nu_\tau$, and the bottom *b* and top *t* quarks. The interaction between fermions is realized by the photon $\gamma$, gluon *g*, and gauge bosons, *W* and *Z*. The Higgs boson (H) with a mass of about $126GeV$ using the Large Hadron Collider (LHC) at CERN was confirmed to exist on 14th March 2013. The Higgs boson was predicted by Standard Model's explanation of spontaneous breaking of gauge symmetry and appearance of masses of elementary particles.

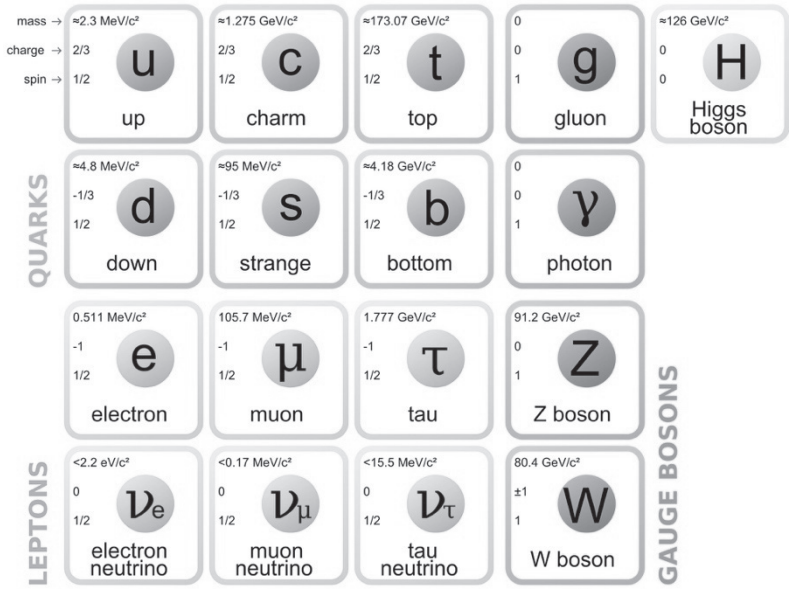


Fig. 4. The Standard Model of elementary particles

Four interactions exist in nature: electromagnetic, weak, strong, and gravitational.

**Table 1. Fundamental interactions**

| Force | Range (cm) | Particle | Strength | Boson |
|---|---|---|---|---|
| Electromagnetism | $\infty$ | charged particles | $10^{-2}$ | photon |
| Weak | $\approx 10^{-16}$ | leptons and quarks | $10^{-6}$ | $W^{\pm}, Z$ |
| Strong | $\approx 10^{-13}$ | quarks | 1 | gluons |
| Gravity | $\infty$ | all particles | $10^{-38}$ | graviton |

The initial unification of these interactions corresponds to the electromagnetic interaction within Maxwell's unification of electrostatic and magnetic interactions. The local gauge invariance corresponds to the electrodynamics used to conserve electric charge. The range of electromagnetic interactions is infinite and, therefore, is in the agreement with the quantum mechanics principle of uncertainty $R \sim \hbar/mc$ we should have $m = 0$ for the photon's mass realized the interaction between fermions in the agreement with the gauge invariance. At the same time the ranges of weak and strong interactions are limited by the distances indicated in Table 1. Therefore, the requirements of the gauge invariance are violated. However, the initial ideas formulated in reference 39–41 allowed us to keep the gauge invariance when formulating the Standard Model of elementary particles. The initial gauge invariance with massless bosons can be breached because of a spontaneous broken symmetry due to the interaction of fermions with the scalar field, as demonstrated by the Higgs boson [40–42]. The result is that the bosons get their masses. The discovery of Higgs boson in 2013 was a very important result that confirmed the legitimacy of the Standard Model. The Nobel Prize in Physics 2013 was awarded to P. Engler and P. W. Higgs for their prediction of the Higgs boson in 1964. The Higgs boson $H$ was obtained by research into the following decay: $H \rightarrow \gamma\gamma$ and $H \rightarrow 4l$, where $l = e^{\pm}$ or $\mu^{\pm}$. The experimental lifetime of $H$ is $\tau_H \geq 10^{-24}\, s$ and this agrees with the theoretical prediction $\tau_H = 1{,}6 \cdot 10^{-22}\, s$.

Further investigations into the LHC could be connected to the following areas of research: $H \rightarrow \tau^+\tau^-$ (~ 6%), $\rightarrow \mu^+\mu^-$ (~ 0,02%), $\rightarrow Z\gamma$ (~

0,15%), and so on. However, the Standard Model does not explain gravity whilst model of super-symmetry is far from complete. It is unable to explain dark matter and dark energy. Cosmological observations tell us that the Standard Model explains only ~5% of the energy present in the Universe. The Standard Model cannot explain matter-antimatter asymmetry in the initial stages of the Universe.

The proton radius puzzle is another problem for the Standard Model. The Standard Model makes precise theoretical predictions regarding the radius of proton of ordinary hydrogen and that of muonic hydrogen. However, the extremely precise extraction of the proton radius from the measured energy difference between the 2P and 2S states of muonic hydrogen (Lamb shift) disagrees significantly with that extracted from electronic hydrogen or elastic electron-proton scattering. The definition of the proton's charge radius from e-p scattering is: $r_p = 0,879(8)\,fm$ [43]. Collectively the charge radius from hydrogen spectroscopy is: $r_p = 0,8758(77)\,fm$ [23]. At the same time, the muonic Lamb shift of $\mu p$ atom induced by laser frequency, corresponding to $\Delta E_{2s-2p}$ results in $r_p = 0,84087(39)\,fm$ [44,45a]. The comparison of different results for the proton charge radii was presented in Fig.1 of reference 45b. The $\mu d$ value is also smaller than the $r_d$ value from the electronic deuterium spectroscopy. The so-called proton radius puzzle remains unsolved. Finally, according to the Standard Model, neutrinos are massless particles with left-handed helicity for a neutrino and right-handed helicity for an antineutrino. However, neutrino oscillation experiments have shown that neutrinos do have mass.

## The mass of the muon neutrino

W. Pauli proposed the third particle (i.e., a neutrino) in the final state of the reaction to explain the solid spectra of beta-electrons [46]. A neutrino is a massless Dirac particle within the framework of the Standard Model. F. Reines and C. Cowan first detected the antineutrinos that are emitted by a nuclear reactor [47]. In 1957, B. Pontecorvo suggested that multiple types, or flavours, of neutrinos exist and that they can change, or oscillate, from one to another [48]. The existence of both $\nu_e$ and $\nu_\mu$ was observed at Brookhaven National Laboratory in 1962 by L. Lederman and M. Schwartz. A third type of neutrino, $\nu_\tau$, was predicted in 1975 and discovered in 2000. R. Davis found that the experiment detected only 30% of solar-neutrinos according to $\nu_e$ [49] (i.e., the deficit with respect to the prediction of the Standard Solar Model as developed by Bahcall). This discrepancy can only be explained by the oscillation of neutrinos during their travel from the Sun to the Earth [50]. Finally, in 1998, Kajita used the data from the Super-Kamiokande Observatory experiment to show that the ratio of $\nu_e$ to $\nu_\mu$ was different on the opposite sides of the Earth. This means that these neutrinos oscillated as they passed through the Earth. At the same time, McDonald and colleagues in the Sudbury Neutrino Observatory (SNO) experiment reported in 2001–-2002 how many of the $\nu_e$ that are produced in the Sun change into $\nu_\mu$ or $\nu_\tau$ as they travel to the Earth. This was possible due to the fact that the SNO experiment could measure the number of neutrinos of all flavours that arrived from the Sun, as well as the number of $\nu_e$ that also travelled to Earth from the Sun. These measurements allowed McDonald and his colleagues to both

confirm theoretical prediction of the solar $\nu_e$ flux and also show that about two-thirds of the solar $\nu_e$ change flavour by the time they reach the Earth; this result agrees with R. Davis' experiment. This means that the neutrino oscillations were proved and it, therefore, implies that the neutrino has a nonzero mass, due to its state as a Majorana fermion [51] beyond the framework of the Standard Model. This neutrino violates the conservation of its lepton number also being its own antiparticle. There are many very good reviews connected with neutrino oscillations [52]. Information about neutrino mass can be obtained by measuring the $\beta$-decay spectrum near the end point of the tritium, as well as from astrophysical data. E. Fermi proposed the first theory of $\beta$-decay [53] which was based on the neutrino hypothesis of Pauli [46]. The form of solid $\beta$-spectrum is given by

$\frac{dN}{dE} \propto p\tilde{E}(Q-E)\sqrt{(Q-E)^2 - m_{ve}^2}$, where $p, \tilde{E}, E$ is the momentum, energy, and kinetic energy of the electron; $Q$ is the maximum kinetic energy of the electron in the case of zero neutrino mass. We can ignore the $F(\tilde{E})$ and the nucleus recoil, where $F(\tilde{E})$ is the Fermi function. This takes into account the Coulomb interaction between the electron and the daughter nucleus. The Kurie plot is, therefore, a straight line for $m_{ve} = 0$. In the case of $m_{ve} \neq 0$, the Kurie plot is: $K(E) = \{(Q-E)\sqrt{(Q-E)^2 - m_{ve}{}^2}\}^{1/2}$

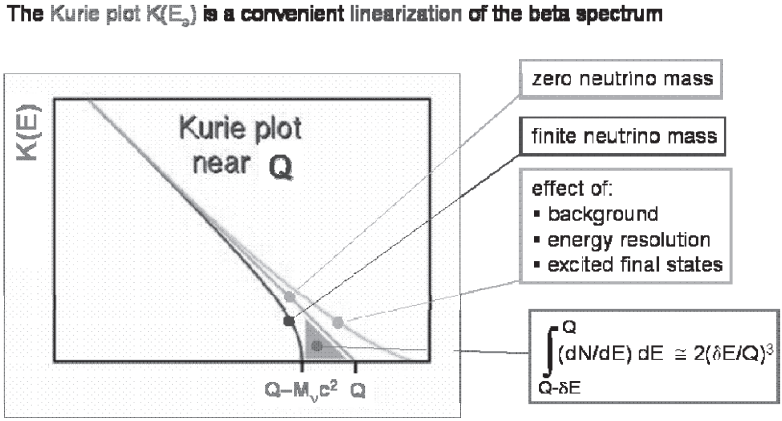


Fig. 5: Kurie plot

Information about the neutrino mass can be obtained by measuring the spectrum of electrons near the end point in the tritium decay: ${}^3H \to {}^3He + e^- + \overline{\nu}_e$. This is with maximum $\beta$-electron energy at 18,6 $keV$ and a lifetime of 13.3 years. The most stringent upper boundary in the $\overline{\nu}_e$ mass was obtained in reference 54's experiment: $m_{\overline{\nu}e} < 2.05eV$ at 90% *CL*. A similar result was obtained in the experiment from reference 55: $m_{\overline{\nu}e} < 2.3eV$ at 95% *CL*. In March 2013 the Planck Collaboration published their first constraints on $\sum_j m_j$ using cosmological and astrophysical data. Assuming the existence of three light massive neutrinos, they reported an upper limit for the sum of the neutrino masses: $\sum_j m_j < 0.57$ $eV$ at 95% *CL* [56] and later $\sum_j m_j < 0.23eV$ at 95% *CL*. It follows from this data that neutrino masses are much smaller than the masses of charged leptons and quarks: $m_j / m_{l,q} \le 10^{-6}$, $l$ = $e,\mu,\tau$, $q$ =

*d,s,b,u,c,t.* However, neutrino oscillations exist with $m \neq 0$, therefore, it is possible that new physics exists beyond that predicted by the Standard Model.

Mixing the neutrino with different lepton numbers (flavours) and their correspondent masses can be presented by $\nu_l = \sum_{i=1}^{N} U_{li}\nu_i$, where $U$ is orthogonal matrix of the mixture $(U^*U = 1)$, and $N$ is the number of neutrino with a definite mass. The mixture of states with the distance $L$ from the formation of neutrino corresponds to

$$\nu_l(L) = \sum_{i=1}^{N} \exp(i\sqrt{E_\nu{}^2 - m_i{}^2}\,L)\, U_{li}\nu_i ,$$

where $E_\nu$ is neutrino energy. It can be described for two generations as follows: $\begin{pmatrix} \nu_l \\ \nu_{l'} \end{pmatrix} = \begin{pmatrix} \cos\theta & \sin\theta \\ -\sin\theta & \cos\theta \end{pmatrix} \begin{pmatrix} \nu_1 \\ \nu_2 \end{pmatrix}$, where $\nu_{l,l'}$ and $\nu_{1,2}$ are the weak and mass eigenstates, respectively. If the neutrino masses are different (i.e., $m_1 \neq m_2$), any phase $\Theta$ between the states can develop and this can lead to neutrino oscillations between the different flavours. The oscillation probability (i.e., the appearance of the neutrino $\nu_{l'}$) for $l' \neq l$ with $l$, $l$' = $e$, $\mu$, $\tau$ on distance $L$ is:

$$P(\nu_l \rightarrow \nu_{l'}) = \sin^2 2\theta \cdot \sin^2\left(\frac{\Delta m^2}{4E_\nu} L\right)$$

where $\Delta m^2 = m_1{}^2 - m_2{}^2$.

In the case of $m_i$ expressed in *eV*, *L* in *m* (*km*) and $E_\nu$ in *MeV* (*GeV*),

$$P(\nu_l \to \nu_{l'}) = \sin^2 2\theta \cdot \sin^2 \left[ 1.27 \cdot \left( \frac{\Delta m^2}{eV^2} \right) \cdot \left( \frac{MeV}{E_\nu} \right) \cdot \left( \frac{L}{m} \right) \right]$$ is obtained,

taking into account $\hbar c = 197\, MeV \cdot fm = 1{,}97 \cdot 10^{-7}\, eV \cdot m = 1$ (as we took $\hbar = c = 1$), i.e., $1eV = 10^7 / 1.97m$, $1MeV = 10^{13} / 1.97m$, we obtain the factor $\frac{10^{14} \cdot 1.97m^2}{4 \cdot 3.88m^2 \cdot 10^{13}} = \frac{10}{4 \cdot 1{,}97} \approx 1.27$.

The absence of neutrino oscillations corresponds to $P(\nu_l \to \nu_l) = 1 - P(\nu_l \to \nu_{l'})$. The neutrino mixing for three generations can be described as:

$$\begin{pmatrix} \nu_e \\ \nu_\mu \\ \nu_\tau \end{pmatrix} = U \begin{pmatrix} \nu_1 \\ \nu_2 \\ \nu_3 \end{pmatrix}.$$

The data for neutrino oscillations was obtained by the T2K Collaboration in Japan [57]. About 500 collaborators from 59 institutes in different countries participated in this experiment. Fig. 6 illustrates the realization of this experiment by two Japanese institutes. This shows that the accelerator, J-PARC, for the production of $\nu_\mu$ and registration of $\nu_e$ at a distance of 295*km* by the Super-Kamiokande, due to $\nu_\mu \to \nu_e$ oscillations. Earlier, the Super-Kamiokande detector was used to register the atmospheric neutrino.

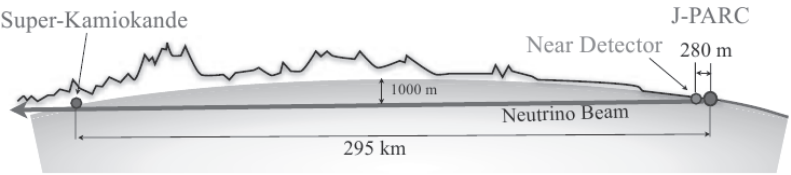


Fig. 6. The scheme of the T2K experiment: neutrinos in flight from the neutrino channel, J-PARC, to near the detector ND280 and then during *μsec* under the land leading to the Super-Kamiokande detector.

As evidenced in Fig. 7, the neutrino oscillations in the T2K experiment showed $\nu_\mu \to \nu_e$ oscillations with $\left|\Delta m^2_{ii'}\right| = 2.6\times10^{-3}(eV)^2$ at 99.3% *CL* exist. This agrees with the other experiments (e.g., MINOS) discussed.

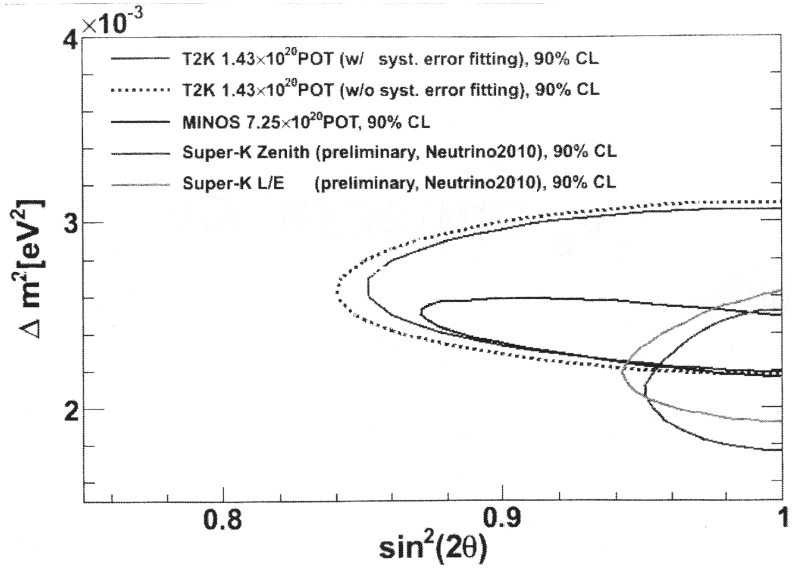


Fig. 7. Neutrino oscillations in the T2K experiment.

The current researches of neutrino oscillations in the MINOS Collaboration using beam and atmospheric data, including masses, mixing angles and the *CP* violation, were presented in reference 58.

At the same time, the possibilities of heavy muon neutrinos with masses in the range of 100–500*keV* appeared in the analysis of astrophysical data from white dwarf stars [59]. The majority of the available neutrino oscillation data can be best described by the three-flavour neutrino model (Fig. 4); however, this is beyond the Standard Model because of the non-zero neutrino mass. At the same time, a few experimental results, including those from the Liquid Scintillator Neutrino Detector (LSND, Los Alamos) [60] and the MiniBooNE [61] experiments, cannot be explained by three-neutrino mixing. Both experiments observed an excess of electron antineutrinos in the muon antineutrino beam and suggested mixing it with a new neutrino state. Precision electroweak measurements exclude the standard coupling of this additional neutrino state for masses of up to half the Z-boson mass, so that states, beyond the three known active states, are referred to as sterile. Sterile neutrinos are hypothetical particles that only interact via gravity and do not interact using any of the fundamental interactions of the Standard Model. The term, “sterile neutrino” ($\nu_4$), is used to distinguish it from the known active neutrinos ($\nu_e, \nu_\mu, \nu_\tau$) in the Standard Model, which are charged by the weak interactions. Mixing one (or more) light sterile neutrinos and the active neutrino flavours has discernible effects on the measurements of neutrino oscillations. Oscillations from muon to electron (anti)neutrinos are driven by a sterile neutrino, which requires electron and muon neutrino flavours to connect to the additional neutrino mass eigenstates. Consequently, oscillations between active and sterile states will also result in the

disappearance of muon (anti)neutrinos, as well as electron (anti) neutrinos [62]. The limits on active to sterile neutrino oscillations from disappearance searches in the MINOS, Daya Bay (Hong Kong) and Bugey-3 experiments were presented in reference 63. They obtained a deficiency of 6% of $\overline{\nu}_e$ in comparison with the Standard Model. The experiments constrain

$\sin^2 2\theta_{\mu e} < [3.0\times10^{-4}(90\%\ CL), 4.5\times10^{-4}(95\%\ CL)]$ and correspond to $\Delta m^2_{41} = 1.2\ eV^2$. The sterile-neutrino mixing phase space allowed by the LSND and MiniBooNE experiments is excluded by a mass region of $\Delta m^2_{41} < 0.8\,eV^2$ at 95% *CL*. Sterile neutrinos are also candidates for dark radiation. The Daya Bay collaboration measured the antineutrino energy spectrum and found that antineutrinos at an energy of around $5MeV$ were in excess of the theoretical expectation. The Planck Satellite's 2013 cosmological data are compatible with the existence of a sterile neutrino for a mass range of < $3eV$. Any evidence of a sterile neutrino was absent in the research results at the IceCube Neutrino Observatory in 2016. However, global analyses in reference 64 indicated the mass region $10\,eV \le m_{\nu 4} \le 1TeV$, so the question about possible mass of the sterile neutrino is still open. At the same time, the natural explanation for small masses of active neutrinos with simultaneous large masses of heavy sterile neutrinos, alongside the violation of their lepton number, could be within the framework of the seesaw mechanism. This could suggest that sterile neutrinos exist, or that our understanding of the neutrino is not yet complete.

A nonzero neutrino mass is possible in the case of both *CP* invariance and *CP* non-invariance of the weak interaction. The verification of the neutrino mass, with a simultaneous *CP* violation, is important due to the possible modification of the neutrino oscillations [65]. The investigation of the effects of the neutrino mass and *T*-violation (under the assumption of *CPT* invariance) in nuclear muon capture by consideration of particle correlations was considered in reference 66. The muon capture by nuclei will be considered in section 4.2; therefore, we will confine ourselves to the neutrino mass problem.

The partial nuclear muon capture

$\mu^- + (A,Z)_{J_i} \to (A,Z-1)_{J_f} + \nu_\mu$ will be considered. As the Majorana neutrino is not the only possibility for a massive neutrino the massive left-handed Dirac neutrino was used in reference 66. The Dirac bispinor is commonly used for neutrino wave function ($\hbar = c = 1$) [67]

$$\Psi_{\nu_\mu} = \frac{1}{\sqrt{2}} \exp(i\vec{q}\vec{r}) \begin{pmatrix} -c_1(\vec{\sigma}_\mu \cdot \hat{\vec{q}}) \\ c_0 \end{pmatrix} \otimes \chi_\nu ,$$

where $\vec{q}$ is the vector for neutrino momentum and $\hat{\vec{q}}$ denotes that the lepton spin is quantized along the direction of the neutrino momentum; in addition, $\vec{\sigma}_\mu$ is the muon polarization vector and coefficients are $c_0 = \sqrt{1 + m_\nu / q}$ and $c_1 = \sqrt{1 - m_\nu / q}$.

In the case of massive neutrino, it is important to consider the neutrino polarization vector

$$\left\langle \vec{s}_{\nu} \right\rangle = [a + (c - \mathrm{Re}\, b)(\vec{\sigma}_{\mu} \cdot \hat{\vec{q}})]\, \hat{\vec{q}} + \mathrm{Re}\, b \vec{\sigma}_{\mu} + \mathrm{Im}\, b\, \hat{\vec{q}} \times \vec{\sigma}_{\mu}$$

The correlation coefficient $b$ determines the neutrino transversal polarization along the direction of the cross product $\hat{\vec{q}} \times \vec{\sigma}_{\mu}$. The coefficient $b$ is proportional to $\sigma_{\mu}(m_{\mu}/q)\sqrt{1+(m_{\nu}/q)^2}$, (i.e., this polarization is determined by the neutrino mass $m_{\nu}$ that exhibits a *CP*-odd correlation). However, due to $\sigma \approx 10\%$ for spinless target nuclei and $\sigma_{\mu} \approx 1\%$ for nuclei with $J_i \neq 0$ and $q \approx 100\ MeV$, we should expect $b < 10^{-10}$ for active neutrinos $\nu_e, \nu_{\mu}, \nu_{\tau}$ with $m_{\nu_{\mu}} < 1.0\ eV$ (T2K, MINOS etc.). At the same time the observation of neutrino transversal polarization $b$~0.1 is possible for a heavy sterile neutrino with $m_{\nu_4} \approx 100\ MeV$. The registration of transversal polarization could provide evidence of a heavy sterile neutrino with a simultaneous *CP* violation. The muon capture, with three particle final states (e.g., $\mu d \to nn\nu_{\mu}$ or $\mu\, {}^3He \to dn\nu_{\mu}$) could potentially be more suitable at verifying the nonzero mass of a neutrino, including the Majorana.

# 3. MUON CAPTURE BY HYDROGEN

## 3.1 The formation of the muonic hydrogen atom

Both the slowing down and Coulomb capture of negative muons in hydrogen have been considered in references 68–72. After slowing down to the atomic velocity of $v \sim \alpha \cdot c$ (where $\alpha \approx 1/137$ is the fine structure constant), the $\mu^-$ is replaced with the electron from a hydrogen atom (molecule) forming the muonic atom in an excited state with the following principal quantum number $n \approx 14$. The corresponding Bohr orbit of the muonic atom $a_n^\mu \sim \frac{\hbar^2 \cdot n^2}{e^2 \cdot m_\mu}$ is equal to the K-orbit of the hydrogen atom, $a^e \sim \hbar^2/(e^2 m_e)$, as indicated in $n \approx \sqrt{m_\mu / m_e} \approx 14.$. The kinetic energy of the muonic atom, immediately after its formation, ranges between 1 and 10*eV*. The lifetime of the highly excited state of an isolated muonic atom is limited by the muon's lifetime ( $\tau_\mu$ ) due to the small probability of radiative transitions. The destiny of the muonic hydrogen isotope in a mixture of hydrogen isotopes is determined by many competing processes. If it collides with the surrounding hydrogen molecules it will lead to a rapid de-excitation to the states, $n$ = 4, 5, dependent on the time of the target conditions. For $n$ >10, de-excitation is dominated by the target molecule dissociation [70]. The reaction of the molecule dissociation in hydrogen isotope target corresponds to $(\mu h)_n + H_2 \rightarrow (\mu h)_{n'} + H + H$, where the nuclei, *h* = *p, d, t*, and *H* is hydrogen isotope. Additionally, the

$n \to n'$ transition energy coincides with the dissociation energy of the hydrogen molecule ~4.7*eV*. The reaction of the molecule dissociation in the mixtures of two or three hydrogen isotopes corresponds to $(\mu h)_n + HH' \to (\mu h)_{n'} + H + H'$, where *H* or *H'* marks the hydrogen isotope atoms with the corresponding nucleus, *h*. The cross section of the chemical process of molecule dissociation was estimated by $\sigma_{chem} \approx (1/2)\pi (a_n^{\mu})^2$ [70]. Below $n \approx 10$ the chemical process of the molecule dissociation becomes less important and the Auger de-excitation, due to the ionization of hydrogen molecules or atoms, is preferred for $n \le 10$, where transitions $n \to n-1$ dominate in

$$(\mu h)_n + H \to (\mu h)_{n-1} + H^+ + e^-.$$

Initially Wightman has semi-classically calculated the Auger de-excitation rates for $(n,l) \to (n',l')$ transitions (where *l* is orbital quantum number) in $p\pi^-$ and $pK^-$ atoms [69]. A hydrogen and a mesic atom were held at fixed distance apart and the motion of the meson was described by the Bohr-Sommerfeld orbit. Transition probabilities were calculated for the Auger processes induced by the mesic atom's oscillating electric dipole field. The corresponding cross sections were found to be much larger than the geometrical ones ($\sigma_A \approx (1/2)\pi a_n^2$, where $a_n$ is the Bohr radius), especially for the large *n*. It was also found that radiative transition predominated in $n < 4$.

Russel and Shaw numerically calculated the Auger cross sections, $\sigma_A$, and rates ($\lambda_A = N_0 v \sigma_A$, where *v* is the relative velocity of the colliding atoms,

and $N_0 = 4.25 \cdot 10^{22} cm^{-3}$ is the atomic concentration of the liquid hydrogen, LHD) in the Bohr approximation [73]. The relative motion of the colliding $K^-$ and hydrogen atoms was approximated by plane waves in the initial and, also, in the final channels of the process. It was found that for $v \le 10^6 cm/s$, $\sigma_A$ pronounces 1/*v* behaviour. It was underlined, however, that Born approximation does not take into account the strong deformation of the wave functions of the atomic relative motion in the initial and final channels.

Using the Bohr approximation, Leon and Bethe calculated $\sigma_A$ of $\pi^-$ and $K^-$ mesic atoms in gaseous hydrogen [70]. They also used dipole approximation in order to describe the interaction between the colliding atoms. The molecular structure of hydrogen target was introduced by replacing the ionization energy from a hydrogen atom with a hydrogen molecule. The 1/*v* behaviour of $\sigma_A$ was obtained and kept in the whole energy range. The estimated total cascade time of the $p\pi^-$ atom in LHD is $\approx 10^{-12} s$.

Bukhvostov and Popov calculated the Auger de-excitation rates for muonic hydrogen using the eikonal approximation [74]. The cross section for the process has the following form:

$$\sigma_A = \int d^2\rho \,(1 - e^{I(\rho)}), \qquad I(\rho) = (1/v) \int_{-\infty}^{\infty} dz \; w(\vec{\rho} - z\vec{v}/v),$$

where $\vec{v}$ is the relative velocity of the atoms and $\rho$ is the impact parameter.

In the quasi-static approximation, the atoms are assumed to be moving in classic straight-line trajectories and the rate, $w(\vec{R})$, as a function of the relative inter-atomic distance $\vec{R}$ has been determined using perturbation theory as if, in a given moment, the atoms were fixed.

In the Born approximation, which corresponds to the expansion of the exponential function up to the first term, the analogous role is played by the quantity $I(\rho)$; therefore, the condition for its application is $I(\rho) << 1$. This condition is not satisfied, even for relatively large collision velocities: $v \approx 10^6\ cm/s$. However, the results obtained in reference 74 and 70 are of the same order of magnitude.

Menshikov also estimated the Auger cross section using a quasi-classical approximation [75]. The two-step Auger process, with the formation of an intermediate bound complex, was considered in reference 75. The formed complex is decayed due to the secondary Auger process, so that the muonic hydrogen in the initial n-state occurs in the state n-2. It was stated that the two-step Auger transition for $n \leq 4$ may lead to the remarkable acceleration of muonic atoms.

The acceleration of mesic atoms can reach energies of up to ~$100eV$ due to an external Auger process that was also considered in reference 76–77.

So, one of the most important parts of the de-excitation process, which covers the wide range of the principal quantum number, $4 < n \leq 10$, is Auger de-excitation. This practically determines the characteristic time of the whole cascade and the initial energy distribution of the muonic atoms

in the ground state. For $n \leq 3$ radiative transitions to the 1*s*-state are dominant.

The mesic atom passes near, or through, a hydrogen atom and feels the *H* atom electric field. Therefore, Stark mixing occurs in states that have degenerated in angular momentum *l* for definite *n*. The linear Stark effect is the fastest collisional process, with a cross section that is determined by the size of the hydrogen atom. The rate of Stark mixing can be $\sim Nv\pi a_B^2$, where *N* is density of the target, *v* is the velocity of mesic atom and $a_B$ is Bohr radius of hydrogen atom. The Stark mixing rate for a liquid target (i.e., $N = N_0$) can be $10^{12} s^{-1}$.It is also worth noting that, the possible flight time of mesic atom through the hydrogen atom can be $a_B / v = 0.5 \cdot 10^{-14} s$ for $v \approx 10^6 \, cm/s$, which corresponds to the energy of the mesic atom after the previously mentioned reaction of dissociation ~1$eV$. Stark transitions were calculated using the straight-line trajectory approximation [70] and presented in Fig. 8 taken from reference 71.

The important reaction that determines the main characteristics of the mesic atom after the cascade is the Coulomb de-excitation,

$$(\mu h)_n + H_2 \rightarrow (\mu h)_{n'} + H_2,$$

in which the de-excitation energy is shared by the separating nuclei. Theoretical analysis was completed in a number of papers 78-84 using the framework of the semi-classical approach. The WKB approximation [85] was used in reference 79 and this is valid for excited states $n \geq 2$, according to the condition $d\lambda / dR = (3Mn)^{-1/2} << 1$, where $\lambda$ is the

wavelength of the muonic atom and *M* is the reduced mass of the system; *R* is the inter-nuclear distance.

The cross section is expressed as $\sigma = \pi \int_0^{\rho_{\max}^2} P\, d\rho^2$, where *P* is the reaction probability $P = 2e^{-2\delta}(1 - e^{-2\delta})$ and $\delta$ is the Massey parameter, given by $\delta = \left| \mathrm{Im} \int_{\mathrm{Re}\, R_c}^{R_c} (p_R^{(1)} - p_R^{(2)})\, dR \right|$. The radial momentum $p_R^{(i)} = Mv\sqrt{1 - U^{(i)}/\varepsilon - (\rho/R)^2}$, where *v* is the relative velocity of the colliding particles at $R \to \infty; \varepsilon = Mv^2/2$ is the collision energy and $U^{(i)} \to U^{(i)} - U^{(1)}(\infty)$, where $U^{(i)}$ is the molecular term of the two-centre problem (with Coulomb repulsion taken into account) for initial (*i* = 1) and final (*i* = 2) states. The maximum value of the impact parameter, $\rho_{\max}$, is determined by the requirement that $p_R^{(i)}$ is real along the trajectory $R \geq \mathrm{Re}\, R_c$. The crossing points of the molecular terms corresponding to the initial and final states of the reaction, $R_c$, and the Massey parameters, $\delta$, are calculated in the complex *R*-plane.

Any possible contradictions in the results from reference 80 and 82 could be explained by screening corrections [81]. The electron screening was accurately taken into account in reference 84, which came to the conclusion that the Coulomb de-excitation rates for $3 \leq n \leq 5$ at energies > 0.5*eV*, where the screening is not important, are in reasonable agreement with the final results from reference 82 for isotope pairs, *pμp*, *dμp*, and *pμd*. For other isotope combinations the agreement is much worse. The electron screening for $5 < n \leq 10$ should be considered in the low collision

energies that leads to the considerable decrease of reaction rates due to the drop in the maximum impact parameter. The Coulomb de-excitation could compete with an Auger for the large *n*.

All the processes of the cascade are presented on Fig.8 taken from reference 71. The processes mentioned above allow one to obtain the energy distribution of muonic hydrogen's excited and ground states. This is important for the other kinetics characteristics of the muonic atom (e.g., for the formation of muonic molecules). Muonic atom acceleration during the de-excitation process will be much stronger, if one considers Coulomb de-excitation, in which all energy excess is realized in the kinetic energy of mesic hydrogen and the recoil of the nucleus, atom, or molecule.

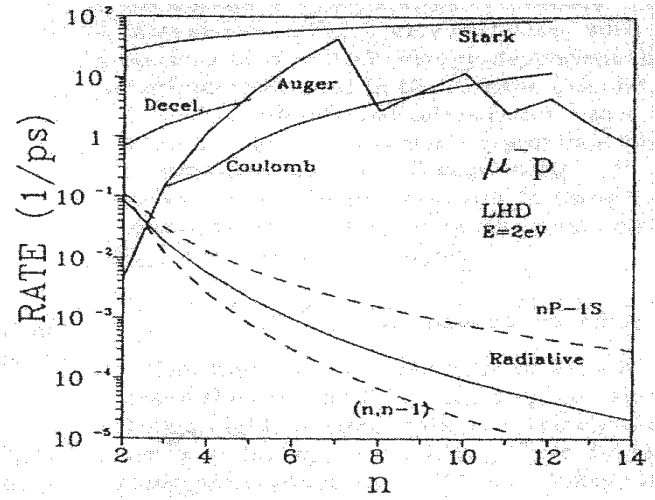


Fig. 8. The rates of the various cascade processes for LHD. The statistical population of the *nl* sublevels is assumed. The rates of the radiative transitions between the circular states ($n$, $n$-1) → ($n$-1, $n$-2) and for the K-lines ($nP \rightarrow 1S$).

## 3.2 The elastic scattering of muonic hydrogen atoms

During the cascade the muonic hydrogen can lose its kinetic energy in elastic collisions.

The elastic scatterings of muonic hydrogen on the hydrogen isotope nuclei and on light element nuclei were discussed in a number of reviews [2, 12, 13, 86–90]. It was shown in reference 91–93 that taking into account electron screening leads to a drastic change in the low-energy elastic cross sections. The previously mentioned WKB method was used in references 91, 92. The interaction potential for the scattering of the excited mesic hydrogen is determined asymptotically by the linear Stark effect. The interaction potential, especially in the effective region of the interaction, is very important for the determination of characteristic distances of interaction (i.e., $R_c$). This is why it is important to take into account the electron screening of the target nucleus, especially for a high principal quantum number *n*. The low energy elastic scattering of mesic atoms on nuclei can be described by the first two terms in the partial wave expansion $\sigma = \sum_J \sigma_J$, where $\sigma_J = (4\pi/k^2)(2J+1)\sin^2\delta_J$. Here *J* is the orbital momentum of three particles (muon and two nuclei). In $k = \sqrt{2M\varepsilon}$, *M* is the reduced mass of the mesic atom and the target atom, $\varepsilon$ is the collision energy and $\delta_J$ is the phase shift. The *p*-wave cross section is much smaller than the s-wave [92]. The phase shifts are obtained using a numerical calculation when solving the Schrödinger equation for the radial wavefunction of the relative motion of nuclei with boundary conditions that correspond to the states of the continuous spectrum:

$\chi(0)=0;\ \chi(R)\sim\sin(kR-\pi J/2+\delta_J)$ for $R\to\infty$. The contribution of large distances $R>>a^{\mu}$ was proved to be essential in calculating the phase shifts, especially when the phase shift value is close to the multiple $\pi$. For this reason, it is important to take into account the influence of the electron shell of the target atom during the scattering process. The successive treatment of the electron screening effect was carried out in reference 92 up to the second order of the perturbation theory. The electron shell contributes to the effective interaction potential in the first order of the perturbation theory is illustrated in Fig. 9.

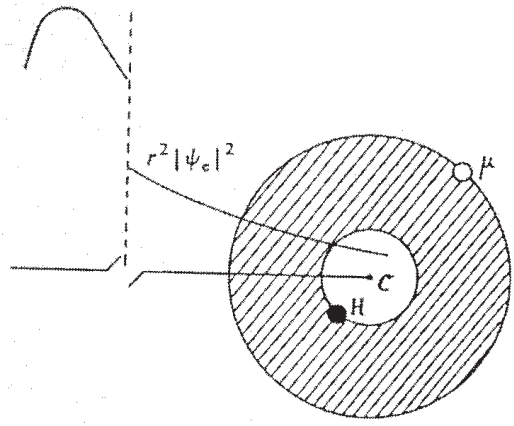


Fig. 9. The electrostatic interaction of the atomic electron with the mesic atom responsible for the electron screening in the first order of perturbation theory.

The electrostatic interaction of the mesic atom with the electron shell is determined by the dashed area of the uncompensated charge, so that the interaction potential is proportional to $-\int|\Psi_e|^2\left\langle r^{-1}\right\rangle dV\sim -m_{\mu}(m_e/m_{\mu})^3e^{-2R/a_B}$ ($a_B$ is Bohr radius).

The accurate calculation [92] yields a factor of $k_\mu = (M_H - m_\mu)(M_H + m_\mu)^{-1}$, so that the interaction with the electron shell vanishes (in the first order of the perturbation theory) for exotic atoms with equal masses $\left(e^+e^-, \mu^+\mu^-, p\bar{p}, etc.\right)$. The important role of the electron screening in the mesic hydrogen scattering on hydrogen is illustrated by the scattering lengths, calculated in reference 91 for even (g) and odd (u) channels (the scattering length is determined by $a = -(k\ ctg\ \delta_0)^{-1}$ for $kR << 1$).

**Table 2. Scattering lengths with $\tilde{a}_{g,u}$ and without $a_{g,u}$ electron screening (in mesic atomic units, $a_\mu \approx 2.56 \times 10^{-11} cm$).**

| | $a_g$ | $\tilde{a}_g$ | $a_u$ | $\tilde{a}_u$ |
|---|---|---|---|---|
| $\mu p + p$ | -29 | -37 | 3.5 | -2.4 |
| $\mu d + d$ | 4.9 | -6.2 | 3.0 | -8.3 |
| $\mu t + t$ | -8.8 | -27 | 2.2 | -14 |

The total elastic cross section for $\mu d$-scattering on deuterium, as well as the partial one in the lowest hyperfine structure state, was calculated with electron screening taken into account and was found to be ~$0.7 \cdot 10^{-19}$ $cm^2$ [91], in agreement with the experimental result, $(0.8 \pm 0.2) \cdot 10^{-19}$ $cm^2$ [94]. The calculation without the screening gives a value about two times greater than the experimental result. The analogous agreement of the calculations, with electron screening taken into consideration, gave the result indicated on Fig. 10 taken from reference 93. There is no doubt that

the electron screening should be considered.

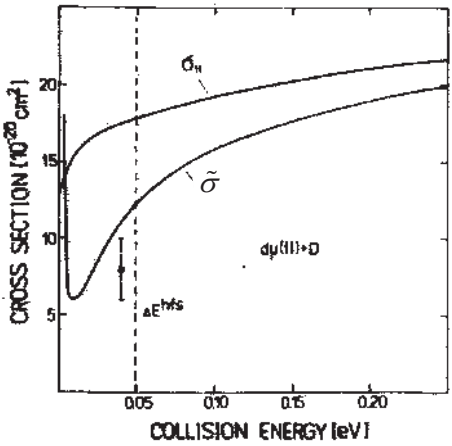


Fig. 10: Elastic cross sections for the muonic deuterium on the deuterium atom, averaged over states 1/2 and 3/2 of the total spin of the muon and two nuclei. The previously mentioned experimental value was taken from reference 93.

The total elastic and transport cross sections of the excited muonic hydrogen for all hydrogen isotopic mixtures were calculated using the energy range, $0.04 \leq \varepsilon \leq 10eV$. This considered the electron screening in reference 95. A method for the calculation of elastic cross sections of hydrogen mesic atoms on nuclei of hydrogen isotopes was developed in reference 96. The method consisted of expanding the system wave function over the adiabatic basis and reducing the multi-channel scattering problem with about 300 closed channels to the eigenvalue problem. The obtained elastic cross sections as well as scattering lengths were given in Table 2 from reference 96. The cross sections of the elastic scattering of deuterium mesic atoms in ortho and para states on deuterium nuclei with an energy of up to $50eV$ as well as spin-flip reaction were calculated in

reference 97. The method of calculation was analogous to that in reference 96. The calculated rate of the ortho-para transition for $\mu d$ atoms in deuterium target for 34K agreed with the experimental result [98]. The scattering lengths were presented in the Table from reference 97. The comparison of the calculated elastic cross sections with the experimental results [99] indicated the necessity to consider the account electron screening [90–93] and the effects of the molecular structure.

## 3.3 The muon transfer processes

a) Isotopic exchange reactions

The isotopic exchange reactions (i.e., a muon transfer to the heavier isotope nucleus) play an important role in the kinetics of the processes that occur in hydrogen isotope mixtures.

The isotopic exchange reactions for muonic atom in the ground 1s state are:

$\mu p + d \rightarrow \mu d + p$,
$\mu p + t \rightarrow \mu t + p$,
$\mu d + t \rightarrow \mu t + d$.

These have been studied both experimentally and theoretically. The theoretical and experimental data for the rates of muon transfer from the 1s state of muonic hydrogen together with transfer from excited states are given below in Table 3 taken from reference 100. The results of the calculations of the total cross sections of the elastic (see section 3.2), spin-flip (see section 3.5), and charge-exchange processes for the scattering of the muonic hydrogen isotope atoms in the ground state on the hydrogen isotope molecules were given in reference 101. The molecular effects,

including electron screening, and the rotational and vibrational excitations of target molecules, have been considered. The cross sections given for $\varepsilon$ ranged from 0.001 to 100 eV. The scheme of the muonic cascade together with the muon transfer from excited states is given in Fig. 11.

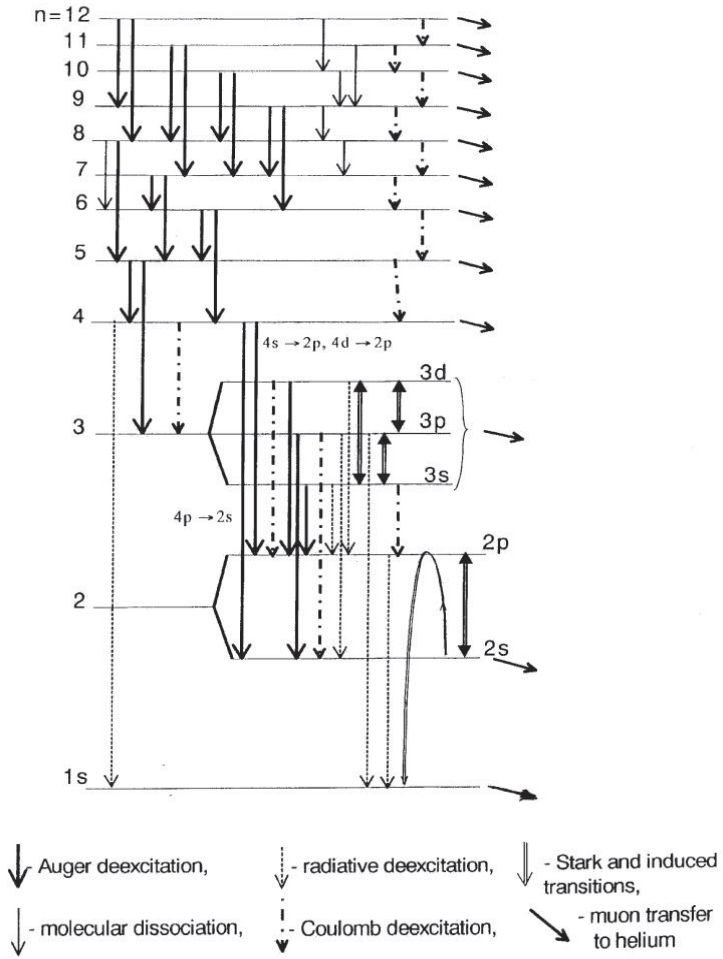


Fig.11. The muonic atom cascade scheme which was considered in s
The right arrows indicate the muon transfer into a heavier isotope nucleus.

However, muonic atoms should reach their ground states during the cascade at about $10^{-10}s$. It can depend, not only on the de-excitation process, but also on the muon transfer to a heavier nucleus in hydrogen isotopic mixtures. Therefore, the reactions

$$(\mu p)_n + d \to (\mu d)_n + p,$$
$$(\mu p)_n + t \to (\mu t)_n + p,$$
$$(\mu d)_n + t \to (\mu t)_n + d,$$

are very topical, when $n > 1$ corresponds to the excited states ($n = 1$ corresponds to the ground 1s state). The probability of the muon reaching the ground state is denoted in $q_{1s}$, which reflects the $\mu^-$ excited-state transfer to a heavier nucleus. Muon transfer in the excited muonic hydrogen has been considered in a number of papers [3,14,79a,102–116].

Muon transfer reactions represent quasi-resonant reactions in which the initial and final terms using the limit $R \to \infty$ differ by the small value of the resonance defect $\Delta U(\infty) = (\mu_2 - \mu_1)/2n^2$ which is equal to $135n^{-2}eV$ for *pd*, 183 $n^{-2}eV$ for *pt* and 48 $n^{-2}eV$ for *dt*. $\mu_1$ and $\mu_2$ are the reduced masses of the initial and final muonic atoms, respectively. For energies smaller than the resonance defect, these reactions are irreversible. It is clear, however, that for collision energy $\varepsilon > \Delta U$ inverse transfer reactions (with the replacement of → to ↔ in the above reactions) can proceed. The larger the *n*, the lower the threshold for inverse reactions.

The numerous calculations for the muon transfer in excited muonic hydrogen were obtained using the framework of WKB approximation. In addition to the formulae of this method, which was also used in section

3.2, the quasi-resonant charge exchange reactions could also use the Rozen-Zener-Demkov model [117] in which the molecular terms of the two-centre problem with Coulomb repulsion are considered to be branches of the complex potential $U(\vec{R})$ in a complex $\vec{R}$ plane [118]. The difference between the initial and final states $\Delta U(\vec{R})$ in the neighbourhood of the branch points of $U(\vec{R})$ can be represented by the exchange interaction and resonance defect [112]. Muon transfer occurs when $\Delta U(\vec{R}) = 0$. It is satisfactory for an infinite series of complex, equidistant branch points, which determine the transition probability, (for double passing the transition region) $P = (2\cosh^2 \delta)^{-1}$, which follows from the fact that there is an infinite family of branch points instead of a single one. $\delta$ is the Massey parameter $\delta = \left|\mathrm{Im}\int_C p_i d\vec{R}\right|$. Contour $C$ encloses the branch point, which is the closest one to the real axis $\mathrm{Re}\,\vec{R}$. In addition, $p_i = \sqrt{2M\left(\varepsilon - U_i - \varepsilon\rho^2 / R^2\right)}$ is the relative radial momentum of colliding atoms for the initial i =1 and final $i$ = 2 state. In the calculation, $U_i$, the electron screening of the field of the target nucleus was considered. Therefore, the numerical curves of $\lambda_n$ presented in reference 112 are some more accurate than given in Table 3, although in order of magnitude are the same. The data of population of ground state $q_{1s}$ are also given in reference 112 and their dependence on concentration of heavier hydrogen isotope indicated the evident decreasing with increasing of this concentration. The agreement with correspondent experimental data was also indicated in reference 3.

**Table 3. Isotopic exchange rates $\lambda_n(10^{11}s^{-1})$ [100] calculated for $\varepsilon = 0.04\,eV$ and the LHD and experimental data on the charge exchange rates from the ground state muonic hydrogen at room temperature.**

| $n$ | $\mu p \rightarrow \mu d$ | $\mu p \rightarrow \mu t$ | $\mu d \rightarrow \mu t$ |
|---|---|---|---|
| 1s | 0.17 [119] | 0.075 [119] | $2.7\cdot10^{-3}$ [120] |
| Experiment from 1s | $0.169 \pm 0.026$ [9] | | $(2.8 \pm 0.2)\cdot10^{-3}$ [121] |
| 2s | 17.6 | 13.7 | 15.5 |
| 3 | 13.4 | 10.3 | 12.0 |
| 4 | 18.3 | 14.1 | 16.4 |
| 5 | 22.3 | 17.1 | 20.0 |
| 6 | 25.4 | 19.2 | 23.0 |
| 7 | 27.5 | 20.4 | 25.5 |

The close results of the calculations were presented in Table 1 from reference 107. In fact, the same $\lambda_{1s} = 2.6\cdot10^{8}s^{-1}$ was calculated for $\mu d \rightarrow \mu t$ in reference 122. As for the experimental values of $\mu d \rightarrow \mu t$, the transfer rate from 1s state $(2.9 \pm 0.3)\cdot10^{8}s^{-1}$ was obtained in reference 123 and $(3.0 \pm 0.5)\cdot10^{8}s^{-1}$ in reference 124.

b) Muon transfer from muonic hydrogen to Z > 1 nuclei

The muon transfer from muonic hydrogen to the nucleus of elements with $Z > 1$ was reported in some reviews [12d, 86, 94, 100, 125–128] starting with the pioneer Gershtein's paper [128]. The high probability for the transfer of $\mu^-$ from hydrogen to nuclei from other elements is connected with the intersection of molecular terms corresponding to charge

exchange. Haff et al. developed the classical theory of the processes of charge exchange, where the cross section was determined by the maximum possible impact parameter $\rho_{\max}$; thereby, satisfying the condition of vanishing the Coulomb barrier between the nuclei [125]. This condition determines the internuclear distance that corresponds to the transition, which is larger than the turning point, (i.e. in a classical accessible region). As a result, the fall to the centre for all trajectories has the impact parameter of $\rho \le \rho_{\max}$.

A similar approach was used in reference 103 and the nonadiabatic transition probability was considered in a Rozen-Zener-Demkov model [117].

The potential energy of $\mu^-$ in the field of two nuclei (see Fig. 12) is $V = -r^{-1} - Z\left|\vec{R} - \vec{r}\right|^{-1}$, where *r* and *R* are distances of $\mu^-$ and nucleus *Z* from proton respectively. The maximum $V_{\max} = -\left(1+\sqrt{Z}\right)^2 R^{-1}$ is reached by $r_{\max} = R(1+\sqrt{Z})^{-1}$.

The smaller the *R*, the lower the potential barrier between $\mu^-$ and the nucleus *Z*, so the transition of $\mu^-$ from muonic hydrogen to nucleus *Z* could be possible for $R = R_0$. This transition can be considered as a so-called “second kind collision”, which were treated by Landau and Zener in 1932 [129]. In this case the quantum treatment of the muonic bound states is combined with the classical description of the motion of the colliding nuclei. It is well known that there is an adiabatic veto upon the probability

of the transition considered, which vanishes when the initial and final molecular terms intersect. This means that the transition takes place without change of the internuclear distance. Therefore, the adiabatically forbidden transition is removed by the intersection of the molecular terms for $R_0$.

The intersection of the molecular terms is possible for $E_0 + V_0(R_0) = E_n + V_n(R_0)$, where the energies of the muonic atoms of hydrogen and nucleus *Z* (in mesic atomic units) are

$E_0 = -\frac{1}{2} \cdot \frac{M_p}{1+M_p}$ and $E_n = -\frac{1}{2}\left(\frac{Z}{n}\right)^2 \frac{M_z}{1+M_z}$, where $M_p$ is mass of hydrogen nucleus and $M_Z$ is mass of *Z* nucleus. The muonic hydrogen in the ground state is polarized by the field of *Z* nucleus (quadratic Stark effect) and $V_0(R) = -\frac{9Z^2}{4R^4}$ for $R \to \infty$. The potential $V_n(R) = \frac{Z-1}{R}$ corresponds to the Coulomb interaction of the *Z* nucleus and $\mu^-$ with a proton.

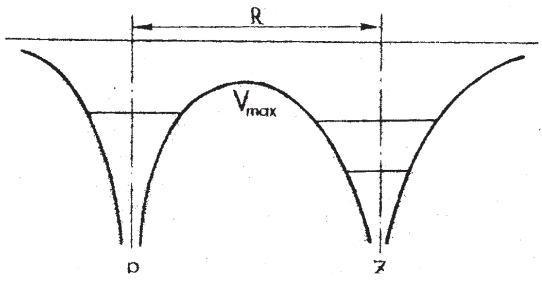


Fig. 12: The scheme of the potential acting in $\mu^-$ during the transfer process.

The classical distance of the muon transfer, $R_t$, can be obtained from the condition $V_n = V_{\max}$

$R_t = 2(1+2\sqrt{Z})$. As the wavelength of muonic hydrogen in the potential $V_0$ is $\lambda\!\!\!^{-} = \left[2M_p(\varepsilon + \frac{9Z^2}{4R^4})\right]^{-1/2}$ the satisfaction of semi-classic approach $d\lambda\!\!\!^{-}/dR << 1$ corresponds to $\frac{2R}{3Z}\sqrt{2/M_p}(1+\varepsilon\frac{4R^4}{9Z^2})^{-3/2} << 1$. We have $R << 3Z\sqrt{M_p/8} \approx 3Z$ (in mesic atomic units) in the limit $\varepsilon \to 0$ [128]. The obtained points of the intersections of molecular terms [128] satisfied this condition, therefore, the semi-classic consideration could be possible. The cross section of the muon transfer in this approximation $\sigma = 4\pi a_\mu^2 f v^*/v$, where $a_\mu$ is the Bohr radius of muonic hydrogen, *v* and *v** are relative velocities of the muonic atom and nucleus before and after the muon transfer, respectively; *f* is the squared of the matrix element of the transition calculated in mesic atomic units $\hbar = e = m_\mu = 1$. Therefore, $\lambda_{ex} = N_0 \sigma v = 4\pi a_\mu^2 f v^*$ for LHD. Taking into account the mesic atomic $v^* \approx \alpha Z c$, we can obtain

$\lambda_{ex} = 4\pi f N_0 a_\mu^3 \frac{\alpha Z c}{\lambda\!\!\!^{-}_\mu / \alpha} = 4\pi f N_0 a_\mu^3 Z\alpha^2 (1/t_\mu)\, s^{-1}$, where $t_\mu = \lambda\!\!\!^{-}_\mu / c$ and $\lambda\!\!\!^{-}_\mu$ is the muon Compton wavelength and c is the light velocity. Therefore, $\lambda_{ex} \approx 10^{10} Z f\, s^{-1}$, which for $f = 1$ reaches to $10^{11}$ $s^{-1}$, has been

confirmed by a lot of experiments [130,127]. However, if one considers the electron screening of the target nucleus, the simple linear $Z$ dependence of charge exchange rate will change. Fiorentini and Torelli, using the Thomas-Fermi model, obtained for $\lambda_{ex}$ a $Z^{2/3}$ - dependence [131]. In the case of $f \neq 1$ (i.e., in the absence of intersection of molecular terms), for example in the muon transfer from muonic hydrogen to helium nuclei, the rates should be reduced. In fact, the transition between muon states occurs at a specific mesoatomic time ~$10^{-19}$ $s$, which is too short to transfer energy to heavy nuclei. In the absence of the intersection of molecular terms, the muon transfer is realized with the change of $R$, or, in other words, with the violation of the Franck-Condon principle [132]. The direct muon transfer from muonic hydrogen to He was considered in reference 128. The intersection of molecular terms for $(\mu pHe)^{++}$ exists for $R \approx 20$, where the wave functions of $\mu p$ and $\mu He$ can overlap with each other in a small way and the transfer rate is $\lambda_{ex}^{He} \approx 10^6 s^{-1}$ [128, 133].

The alternative mechanism of the charge exchange with the formation of the intermediate quasi-stationary molecular state $\mu h + He \rightarrow \mu hHe \rightarrow \mu He + h$ was considered in references 134 and 12g.

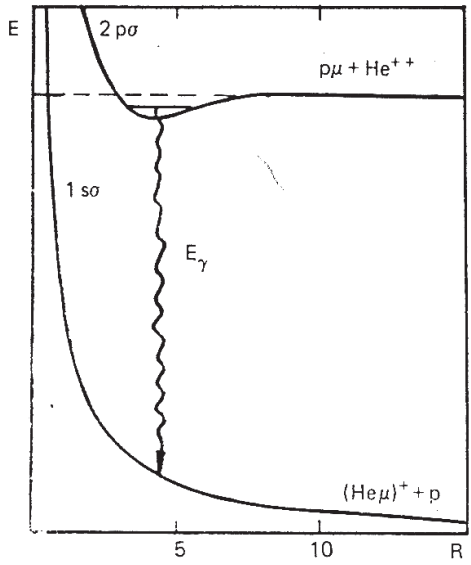


Fig.13: The mesomolecular charge exchange of muonic hydrogen on helium nuclei.

The analogous reaction of stimulated emission and population conversion in atomic physics was considered in reference 135. The mesomolecule $\mu hHe$ is formed in the Auger process $\mu h + He \rightarrow [(\mu hHe)^{2+} e]^{+} + e$

due to the polarization of the muonic hydrogen atom in the field of the helium nucleus (quadratic Stark effect). However, one should be sure the molecular bound state really exists. As described in Fig. 13 $2p\sigma$ -term with asymptote $\mu h$ + $He^{++}$ has a potential energy minimum of $U_{\min} \approx 200\,eV$ at $R_{\min} \approx 4$ due to the quadratic Stark effect. The levels of mesomolecules can be calculated using an approximation of the effective interaction potentials of Morse functions:

$U(R) = U_{\min}(e^{-2\beta(R-R_{\min})} - 2e^{-\beta(R-R_{\min})})$. The possibility of the existence [129a] of at least one level ($\beta^{-1}\sqrt{2M_{1,2}U_{\min}} \geq 1/2$) is satisfied for all masses ($M_{1,2}$) and variation parameters $\beta$.

The calculated muon transfer rates obtained in reference 134, together with experimental results are given in Table 4, which has been taken from reference 100.

**Table 4. The rates of molecular muon transfer from muonic hydrogen to helium nuclei $\tilde{\lambda}_e^{He}(10^8 s^{-1})$ calculated for $\varepsilon = 0.04 eV$, LHD, and experimental muon transfer rates.**

| | Theory | Experiment |
|---|---|---|
| $\mu p \to \mu He^3$ | 0.53 | |
| $\mu p \to \mu He^4$ | 0.35 | 0.36 ± 0.10 [136]<br>0.81 ± 0.08 [137] |
| $\mu d \to \mu He^3$ | 1.43 | 1.27 ± 0.11 [138] |
| $\mu d \to \mu He^4$ | 3.22 | 3.68 ± 0.18 [138] |
| $\mu t \to \mu He^3$ | 8.56 | 15.0 ± 2.5 [139] |
| $\mu t \to \mu He^4$ | 1.32 | |

The decay modes of hydrogen-helium muonic molecules were considered in references 134 and 140–143. The dissociation of the muonic molecule can be accompanied by the emission of the gamma quanta or electron with the energy of ~6.8$keV$. Such a spectrum was calculated in references 134, 140, 142, and 143 and experimentally observed in reference 144. As the relative momentum of the heavy particles in the final state is about 1 MeV,

the *d*-wave contribution is proved to be important due to the fact that it decreases the lifetime of the muonic molecule. At the same time the shape of the $\gamma$ -spectra is mainly determined by the wave function of the initial bound state. Experimental $\gamma$ -spectra from the decay of $\mu p^4He$ and $\mu d^{3,4}He$ [144a, b] agree with the calculations [142]. The molecule can also decay into two particles (e.g. $\mu dHe \to \mu He + d$ ); this is also known as the predissociation process [129a]. All modes of decay in the muonic hydrogen-helium molecule were calculated with the rates presented in Table 1 from reference 141. All the dissociation rates are proportional to $10^{11}$ $s^{-1}$ and the coefficient conversion for the Auger transition reaches ~25%, (i.e., $\beta = \lambda_e / \lambda_\gamma \approx 0.25$ ). At the same time, the predissociation decay mode dominates $\mu p^{3,4}He$ and $\mu d^3He$ .

The molecular charge exchange can be an important channel only if the direct one is suppressed. The molecular charge exchange was also considered for the $\mu hLi$ molecules in reference 145 in the reaction $\mu h + Li \to \mu hLi \to \mu Li + h.$ . The mesomolecule $\mu hLi$ is formed in the Auger process $\mu h + Li \to \left[(\mu hLi)^{3+}_J 2e\right]^+ + e.$ . As described in reference 145a $3d\sigma$ molecular term with asymptote $\mu h + Li^{+++}$ has potential energy minimum of $R_{\min} \approx 6$ due to the polarization of the muonic hydrogen atom in the field of lithium nucleus (quadratic Stark effect). The initial state corresponds to the low-energy *s*-scattering for $\varepsilon_0 \approx 0.04\,eV$ , so that the muonic molecules are produced in the dipole

transition to the final state $J$=1with binding energy $\varepsilon_{Jv} = \varepsilon_{10}$. The levels of muonic molecules were presented in the Table from reference 145a and Table 2 [145c]. The rates of the mesomolecular charge exchange of muonic hydrogen on lithium nuclei depend strongly on the details of the electron cloud. According to the calculations, the binding energy of the $\mu hLi$ molecule is not sufficiently large to emit a $1s^2$ electron from the lithium atom, so only the $2s$ valence electron can be emitted. The calculation was carried out with the use of Hartree-Fock wave functions for the atomic electrons [145a]. The results turned out to be sensitive to very subtle effects, which could hardly be observed in any other process (e.g. photoionization). The account of the intershell correlations [145b] (i.e. of virtual excitation of $1s^2$ electrons with the following emission of a $2s$ electrons), has a strong influence on the charge exchange rates. Table 3 from reference 100 contains the rates of $\mu hLi$ formation calculated for with and without the account of intershell correlations. It is evident that this investigation allows one to check some of the fine features of the atomic electron shell. The formation of such molecules was considered in reference 92, 145a, b, and d giving formation rates about 2 ÷ 3 order of magnitude smaller than those for $\mu hHe$. The decay channels of $\mu hLi$ are analogous to those for $\mu hHe$ and radiative $\lambda_\gamma$, Auger $\lambda_e$ and predissociation $\lambda_p$ decay, as presented in Table 2 from reference 145c, indicated that $\lambda_p$ is a dominating decay mode for $h = p, d$ while $\lambda_e$ dominates for $h = t$.

## 3.4. The formation of muonic molecules

The muonic molecule (in fact, the muonic molecular ion) is formed through the collision between muonic hydrogen $\mu h$ with the surrounding hydrogen isotope molecules, $H_2$. The bound energy may be realized in the form of radiation, carried off through the electron's emission (Auger conversion), or by transferring to a chemically bound neighbouring nucleus. The probability of radiative formation is much smaller than for the formation accompanied by an electron conversion

$$\mu h' + H_2 \rightarrow \left[(\mu h' h) he\right]^+ + e^- .$$

As the collisions between the muonic hydrogen and the nuclei with the formation of the muonic molecule correspond to very small collision velocities (largely thermal velocities), the muonic molecules are formed from the *s*-waves of the continuous spectrum. In the final bound state there are rotational levels of muonic molecules with $J = 0,1$. Due to the fact that this reaction mainly proceeds because of the dipole transition, the molecular state with the total angular momentum

$J = 1$ is mostly populated by slow *s*-wave collisions. In its lower lying rotational state, $J = 0$ is only populated in *p*-wave collisions. At the same time, the theoretically predicted rates of muonic molecules for $J = 1$ are fairly low: in the order of $10^6$ $s^{-1}$ (comparable to the $\mu^-$ free-decay rate). As for $J \neq 1$, the rates of formation of these molecules are essentially smaller. The rates of formation of muonic molecules for different hydrogen isotopes and *J* were presented in reference 13, 12c, d, and f or for $\mu dt$ molecules in reference 14. However, the resonant formation of muonic hydrogen molecules is also possible [146]. The dominant process

for $dd\mu$ and $dt\mu$ formation is resonant mechanism [12b, c, d, f, 146, 147] and I consider the formation of these molecules in Figs. 14 and 15 taken from reference 12c and f.

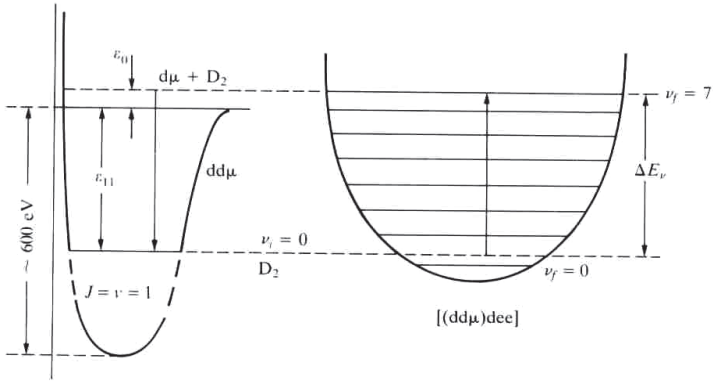


Fig. 14: The scheme of the resonant formation of the $dd\mu$ molecule. The molecular complex $[(dd\mu)dee]_{vK}$ is formed in the excited vibrational state $v_f = 7$.

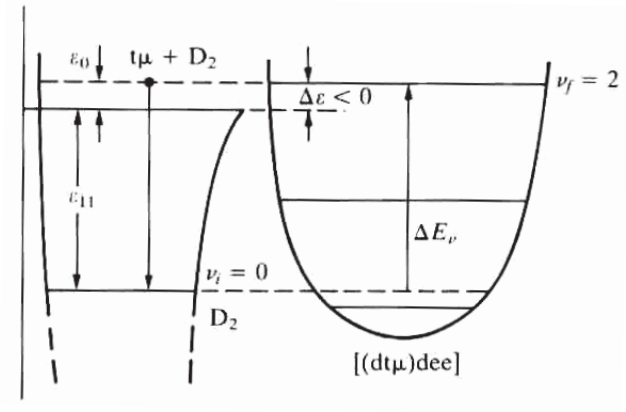


Fig. 15: The scheme of the resonant formation of the $dt\mu$ molecule. The molecular complex $[(dt\mu)dee]_{vK}$ is formed in the excited vibrational state $v_f = 2$.

The resonant mechanism of the muonic molecule formation is only possible if at least one of the levels of the *ddμ*- or *dtμ*-molecule has an energy lower than the electron ionization energy (~15*eV*) and the $D_2$-molecule dissociation energy (~4.5*eV*). The suspicion of existing of such level was expressed in references 13 and 148. The resonant formation of *ddμ* and *dtμ* molecules is caused by the existence of their weakly-bound rotational-vibrational ($J$ = 1, ν = 1) states with energies $|\varepsilon_{11}|$ close to the difference in those of vibrational levels of the $D_2$ (or *DT*) molecule. The resonant reaction for *ddμ*

$$d\mu + D_2 \rightarrow \left[(dd\mu)dee\right]_\nu$$

corresponds to the formation of the weakly-bound state of *ddμ* (indicated above), which is the "nucleus" of the muonic molecular complex. Its binding energy $|\varepsilon_{11}|$ is transferred to the excitation of rotational-vibrational state of muonic molecular complex by energy $\Delta E_\nu$ in agreement with the resonance condition $\varepsilon_0 + |\varepsilon_{11}| = \Delta E_\nu$.

As for the non-resonant reactions for *ppμ* and *pdμ* molecules, the calculated rates for LHD [12c, d, 148, 149] are $\sim 2\times10^6 s^{-1}$ and $\sim 6\times10^6 s^{-1}$, respectively, which agree with the experimental results [150]. However, the experimental results, including the temperature dependence of rates of molecular formation $\lambda_{dd\mu}$ [151], are an order of magnitude higher than that calculated for the non-resonant electron conversion reaction [12c]. The accurate calculations proved the existence of the *ddμ* and *dtμ* molecule levels ($J$ = $\nu$ = 1), which have extremely small bound

energy: $|\varepsilon_{11}| \approx 1.97eV$ and $|\varepsilon_{11}| \approx 0.66\,eV$, respectively. Such energies are not enough to separate the electron from the $D_2$ molecule or to cause its dissociation in collisions with $d\mu$ or $t\mu$. As for the previously discussed reaction for the formation of the $dd\mu$ (see Fig. 14), the resonant condition is fulfilled for $\nu_f = 7$ of the molecule $D_2$ at $\varepsilon_0 \approx 0.04\,eV$. The calculated resonant rate of the $dd\mu$ molecule formation for LHD and room temperature (300K) $\lambda_{dd\mu} \approx 3\times10^6 s^{-1}$ [12b] agrees with the experimental results. At the same time, the temperature dependence of $\lambda_{dd\mu}(T)$ has been obtained in numerous experiments. Fig. 16 taken from reference 12c and d demonstrates a very good agreement with the theoretical calculations from the experimental data.

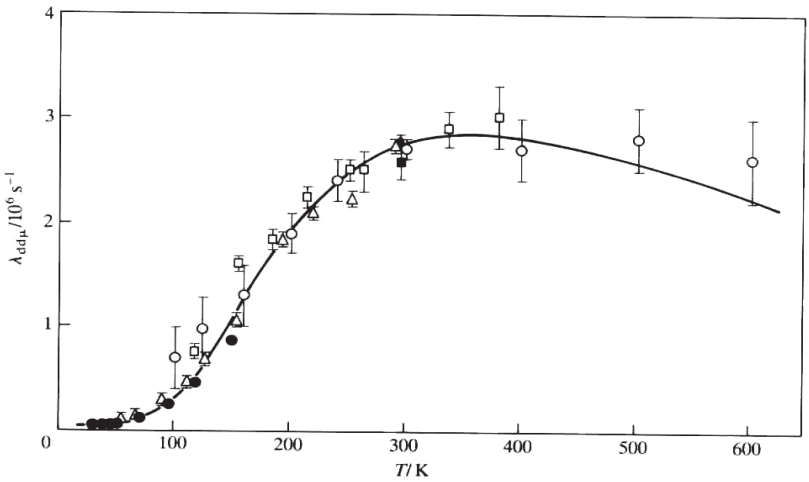


Fig.16. A comparison of the experimental data with the theoretical calculations of mesic molecule $dd\mu$ formation. Experimental points: ● - PSI [152], ○ - Los Alamos [153], Δ - Gatchina [154], □, ■ – Dubna [155]. The solid line presents the calculations of resonant formation of $dd\mu$ [156].

The same resonance reaction is also possible in the case of the $dt\mu$ mesic molecule formation. However, in this case, the transition

$$t\mu + D_2 \rightarrow \left[ (dt\mu) dee \right]_{\nu}$$

occurs in the vibrational state $\nu_f = 2$ of the final complex. Moreover, as the rate of the mesic molecule resonant formation depends exponentially on the number $\nu_f$, the rate of the formation of $dt\mu$ is about 100 times higher than that of $dd\mu$ (i.e. $\lambda_{dt\mu} \geq 10^8 s^{-1}$) [12c].

The formation of a large hydrogen-helium muonic molecule was proposed and calculated in reference 157.

## 3.5 Spin-flip reactions

The binding energy of the muonic hydrogen $\mu h$ in the ground state ($K$-shell) could have a hyperfine structure (h.f.s.) splitting due to the interaction of the magnetic moments of muon $\mu_{1/2}$ and the nucleus of hydrogen isotope $\mu_I$, where spin of protium $I$ = 1/2, deuterium $I$ = 1 and tritium $I$ = 1/2. Therefore, the binding energy of the $K$-shell should split on two sublevels, with a total spin of the muon and nucleus $F_{\pm} = I \pm \frac{1}{2}$, and a binding energy of $\varepsilon(F_+) > \varepsilon(F_-)$ (see Table 5 taken from Fig.1 from reference 12d).

**Table 5. The hyperfine structure of the *μp*, *μd*, and *μt* atoms.**

| Muonic hydrogen | Binding energy (eV) | $\Delta_{h.f.s.}$ (eV) |
|---|---|---|
| *μp* | 2528.4 | $F = 1$<br>$F = 0$ 0.183 |
| *μd* | 2663.1 | $F = 3/2$<br>$F = 1/2$ 0.048 |
| *μt* | 2711.2 | $F = 1$<br>$F = 0$ 0.241 |

The h.f.s. states form an incoherent mixture as the muon lifetime is large in comparison with $1/\Delta_{h.f.s.}$, where $\Delta_{h.f.s.}$ is the h.f.s. splitting. The small h.f.s. excludes any radiative transition. The fast spin-flip transition

$$\mu p(\uparrow\uparrow) + p \rightarrow \mu p(\uparrow\downarrow) + p$$
$$\mu d(\uparrow\uparrow) + d \rightarrow \mu d(\uparrow\downarrow) + d$$
$$\mu t(\uparrow\uparrow) + t \rightarrow \mu t(\uparrow\downarrow) + t$$

could be realized by collisions with nuclei from the same isotope [12c, d]. It is not related to relatively weak spin-spin interactions but is governed by the exchange process probability, which is in this resonant case fairly large. The rates of spin-flip reactions at low collision energies can be expressed in terms of the scattering lengths as proportional to $(a_g - a_u)^2$ [12d]. The scattering lengths, $a_g$ and $a_u$, correspond to scattering in the

symmetric $\Sigma_g$ and asymmetric $\Sigma_u$ muon state, which is relative to the two Coulomb centres of the nuclei. The accurate calculations take into account the electron screening of the target nuclei give rates: $\lambda_{dd} = 3.7 \times 10^7 s^{-1}$ and $\lambda_{tt} = 1.2 \times 10^9 s^{-1}$ [12c, d, e]. The relatively small $\lambda_{dd}$ is explained by the scattering lengths $a_g$ and $a_u$ having the same sign and close values. The $\lambda_{pp}$ is about one order of magnitude larger than that of $\lambda_{tt}$. This is explained by the scattering lengths having rather a large value and the $a_g$ a sign opposite to that of $a_u$.

The h.f.s. effects in collisions of the 2s metastable muonic hydrogen with hydrogen atoms were considered in reference 158.

So far, the investigation of hyperfine effects in the scattering of muonic hydrogen has been limited to the consideration of the ground-state $\mu p$, $\mu d$, and $\mu t$ [159-162, 98]. However, in the existing studies on the scattering of the muonic hydrogen in the 2*s* state [163–166, 103, 105], spin has not been taken into account. Unlike the electronic hydrogen atom, the $2s_{1/2}$ energy level of the muonic hydrogen is situated below the $2p_{1/2}$ one and the $2s_{1/2} - 2p_{1/2}$ energy splitting is mainly due to $e^+ - e^-$ vacuum polarisation. This situation is in contrast to electronic hydrogen, where the Lamb-shift dominates and the vacuum polarisation is relatively unimportant. Consequently, the $2s_{1/2}$ state is metastable. The dominant $2s \to 1s$ de-excitation is a two-photon electric dipole transition with the rate, $1.66 \cdot 10^3 s^{-1}$, whereas 2*p* state decays to the ground state due to the

single-photon electric dipole transition with the rate $1.29\times10^{11}\ s^{-1}$ [167]. However, the collision of the 2*s* state muonic atom with a surrounding electronic molecule (or atom) leads to the 2*s*-2*p* Stark-mixing, thereby enabling the radiative $2p \to 1s$ transition. The effective de-excitation rate is, however, target density dependent. The 2*s* state is populated either due to the cascade processes (radiative or Auger) or due to the muon transfer from a lighter to a heavier hydrogen isotope. E. Borie and M. Leon have shown [168] that the percentage of muonic hydrogen atoms arriving during the cascade in the 2*s* state increases from 6% to 17% when the target pressure increases from 0 to $10^3$ atm. Therefore, the spin-flip processes in the 2*s* state may influence the population of the 1s spin states and, in addition, the kinetics of atomic and molecular processes in gaseous hydrogen isotope mixtures.

In references 163–164, the collision quenching of 2*s* muonic hydrogen was investigated. In reference, 103, the isotope exchange reactions for the excited muonic hydrogen were considered using a quasi-classical approach. In reference 165, calculations for the charge exchange process $(\mu p)_{2s} + d \to (\mu d)_{n=2} + p$ are presented using fully quantum treatment applying two coupled radial equations for the attractive $3d\sigma$ and $4f\sigma$ molecular terms. The same approximation, with the inclusion of electron screening and Lamb shift, was used in reference 166 for the *n* = *2* exchange processes $\mu p + d \to \mu d + p$, $\mu d + t \to \mu t + d$, and $\mu p + t \to \mu t + p$. However, since the hyperfine splitting in the 2s muonic hydrogen is of the order of $10^{-2}eV$ ($\Delta\varepsilon_{\text{hfs}} = 0.023eV$, $0.006eV$, and $0.03eV$ for $\mu p$, $\mu d$, and $\mu t$, respectively), the spin effects, neglected in the previous

studies, can be expected to play a significant role in $n = 2$ scattering thermal energies. Cross sections for elastic and spin-flip scattering for the symmetric systems $\mu p + p$, $\mu d + d$, and $\mu t + t$ were calculated in reference 158 using the adiabatic method for the attractive $3d\sigma_g$ and $4f\sigma_u$ molecular terms, with the inclusion of the Lamb shift and electron screening. The results averaged over the total spin of the colliding systems are presented in Fig. 17.

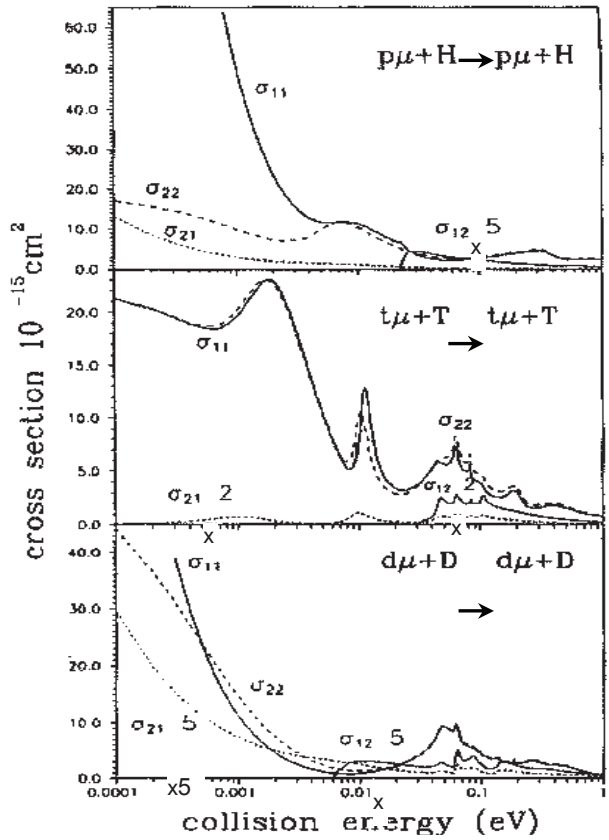


Fig. 17. Total spin-flip and elastic cross sections for the scattering of the 2*s* muonic hydrogen isotope atoms in symmetric systems.

These cross sections are significantly larger than their ground-state counterparts and reach values characteristic for electronic atom collisions. The corresponding reaction rates (normalized to the LHD) reach $10^{12}\ s^{-1}$. As can be seen from the figures, they exhibit a rather complicated structure, which is due to the contributions from several partial waves (at energies of about 0.15 eV, significant contributions come from $J$ to $J$=8).

## 3.6 Muon catalyzed fusion

The nuclear fusion reactions for different hydrogen isotopes with released energy are as follows:

$$
\begin{aligned}
&p + d \to He^3 + \gamma && (5.5\ MeV)\\
&d + d \to \begin{cases} He^3 + n & (3.3\,MeV)\\ t + p & (4.0\,MeV)\end{cases}\\
&d + t \to He^4 + n && (17.6\,MeV)\\
&p + t \to He^4 + \gamma && (20\ \ MeV)\\
&t + t \to He^4 + 2n && (11.3\,MeV).
\end{aligned}
$$

We do not consider the reaction of *pp*-fusion as weak beta-interaction is responsible for it with extremely small probability. Nevertheless, it plays a very important role in astrophysics, as it is one of the main source of stellar energy. The possible fusion reaction $d + d \to He^4 + \gamma$ is also improbable because of isotopic invariance and symmetry. In order for nuclear fusion to occur, the nuclei must approach to a distance in the radius of action of the nuclear forces, $\sim 1fm = 10^{-13}\ cm$. They should overcome the electrostatic repulsion between the nuclei by quantum mechanical tunnelling through the Coulomb barrier. Although the height of the Coulomb barrier for these reactions is some hundreds of *keV*, the

reaction of *dt* fusion is observed in accelerator energy ~10*keV*. The thermonuclear reactions occur at a temperature of ≈ $10^8 K$, which corresponds to $\varepsilon_0 \approx 10\,keV$. In fact, the Tokamak parameter for *dt* reactor corresponds to 30 *keV* [169]. The physics of magnetic fusion reactors for thermonuclear fusion was considered in a number of reviews [169, 170]. In agreement with the existent prognosis, the thermonuclear energetics (i.e., "hot" fusion), can be realized after ~2020 [170].

The alternative possibility for realization nuclear fusion could be cold fusion (e.g. Muon Catalyzed Fusion ($\mu$CF)). After fusion occurs, the muon, as a rule, is liberated and becomes available for the creation of a new muonic molecule. Therefore, a chain of nuclear fusions occurs.

This means that the muon works as a catalyst and the catalysis cycle can be repeated many times during the muon's lifetime. The history of $\mu$CF was described in detail by John David Jackson in reference 12h. The idea of $\mu$CF was first hypothesized in 1947 by Frederick Charles Frank [11a] and Andrey D. Sahkarov [11b] in 1948 (i.e., 70 years ago). A few years later, Ya.B. Zel'dovich indicated the possibility of an enhanced reaction rate if the weakly bound state of $dd\mu$ exists [11c]. These theoretical speculations occurred before the first experimental observation. The intensive research of these processes came after experimental discovery of $\mu$CF in both $pd\mu$ and $dd\mu$ molecules by Luis W. Alvarez with his group at the end of 1956 [11d]. Alvarez also hoped to find energy production inside the $\mu$CF. However, the comparison of energy spent on the creation of a muon with that realized in the $\mu$CF cycle could answer this question. The initial accurate calculations were performed by J.D. Jackson [12a] with an evaluation of the parameters relevant to power production. The important

stimulus for the investigation of $\mu$CF was related to the resonant formation of $dd\mu$ molecule, which was discovered in 1967 by E. Vesman [146] who connected it with the interpretation of Dubna's experimental data. The interest particularly increased after S.S. Gerstein and L.I. Ponomarev's 1977 prediction [12b] of the resonant formation of the $dt\mu$ molecule with ~100 fusions per muon. A 1983 experiment by Jones et al. [171] confirmed the temperature dependence of the molecular formation rate $\lambda_{dt\mu}$, this supported hopes over the potential for energy production in $\mu$CF. The different channels of the nuclear fusion in the muonic molecules are as follows:

$$pd\mu \rightarrow \begin{cases} {}^3\mathrm{He} + \mu \\ {}^3\mathrm{He}\mu + \gamma \quad (\omega_s) \end{cases}$$

$$dd\mu \rightarrow \begin{cases} {}^3\mathrm{He} + n + \mu \\ {}^3\mathrm{He}\mu + n \quad (\omega_s) \\ t + p + \mu \\ t\mu + p \qquad (\omega_s) \end{cases}$$

$$dt\mu \rightarrow \begin{cases} {}^4\mathrm{He} + n + \mu \\ {}^4\mathrm{He}\mu + n \quad (\omega_s) \end{cases}$$

$$pt\mu \rightarrow \begin{cases} {}^4\mathrm{He} + \mu \\ {}^4\mathrm{He}\mu + \gamma \qquad (\omega_s) \\ {}^4\mathrm{He}\mu + e^+ + e^- \quad (\omega_s) \end{cases}$$

$$tt\mu \rightarrow \begin{cases} {}^4\mathrm{He} + 2n + \mu \\ {}^4\mathrm{He}\mu + 2n \qquad (\omega_s). \end{cases}$$

However, only two reactions connected with the $\mu$CF are of interest, namely the $dt\mu$ reaction and the $dd\mu$ with a formation of ${}^3He$ in their final

states. Other reactions are not topical because of small molecule formation or fusion rates. The molecule formation rates have been discussed in section 3.4. The fusion rates are $\lambda_f(dt\mu) \approx 10^{12} s^{-1}$ and $\lambda_f(dd\mu) \approx 4\times10^{8} s^{-1}$ [12c, d, e, f, g, 14]. A very important parameter is the sticking probability $\omega_s$, which was initially discussed by Jackson [12a, h]. If the muon, when it is in the final states of previously discussed reactions, sticks to the helium (or tritium) nucleus it will be lost for further catalysis cycles. Therefore, the accurate calculations of sticking probability, $\omega_s$, as well as numerous experimental verifications were performed. The references for these results were given by Froelich in Table 10 [14] with a discussion of the calculated methods. Comparisons were also made with the numerous experiments on $dt\mu$ molecules in Fig. 24 from reference 14. The discussion of the loss of muons from cycles (i.e., parameter $\omega_s$) was discussed by Cohen in reference 12e and Bracci and Fiorentini in reference 12.

Since the fusion rate is rapid in comparison with the atomic and molecular rates, the nuclear reaction may be considered to be sudden; this means that the muon sticking is simply determined by the overlapping of initial and final wave functions in the matrix elements. The probability of sticking in state $\nu$ is [12a,e] $P_\nu = \left|\left\langle \psi_\nu^f \middle| \psi^i \right\rangle\right|^2$ with an initial wave function $\psi^i$; the normalized molecular wave function in the limit of zero internuclear distance $R \to 0$; and final wave function $\psi_\nu^f = \varphi_{nlm}(\vec{r})\, e^{i\vec{q}\cdot\vec{r}}$, where $\varphi_{nlm}$ is an atomic wave function of $(^4He\mu)^+$ for $dt\mu$ (or $(^3He\mu)^+$ for $dd\mu$) and

plane wave with $(He\mu)^+$ momentum $\vec{q}$ represents the motion of the atom with respect to the initial molecule and *r* is the muon coordinate with respect to the centre of the mass of the two nuclei. The total sticking is $\omega_s = \sum_\nu P_\nu$. The initial calculations in the Born-Oppenheimer approximation result in $(\omega_s)_{BO} = 1.2\%$ [172]. However, more accurate nonadiabatic calculations reduced $\omega_s$. The recent $\omega_s \approx 0.6\%$ for $dt\mu$ [12e, 173, 174]. The sticking for $dd\mu$, $\omega_s$, could be in the range of 8% to 12% [12d, e, f].

In the final states of the fusion reactions, $(^3He\mu)^+$ and $(^4He\mu)^+$ have a kinetic energy of $0.8MeV$ and $3.5MeV$, respectively. During their deceleration they collide with the target's nuclei and can lose the muon, with a stripping probability of *R* [12a, h]. Therefore, $\omega_s = \omega_s^0(1-R)$, where $\omega_s^0 = \sum_{nl} \omega_s^0(nl)$, or, in other words, the probability of sticking is the sum of initial sticking contributions which correspond to each orbital of the $(He\mu)^+$ ion [3]. The probability of the stripping process depends on the density of the target $\phi$ and can achieve up to the value of *R* = 0.35 for $dt\mu$ [12c]. This process was considered in reference 175, as well as in previous papers in reference 176. I have demonstrated the cross section of the stripping of $\mu^-$ in a hydrogen target in Fig. 18, which has been taken from reference 175. The experimental data were used from reference 177.

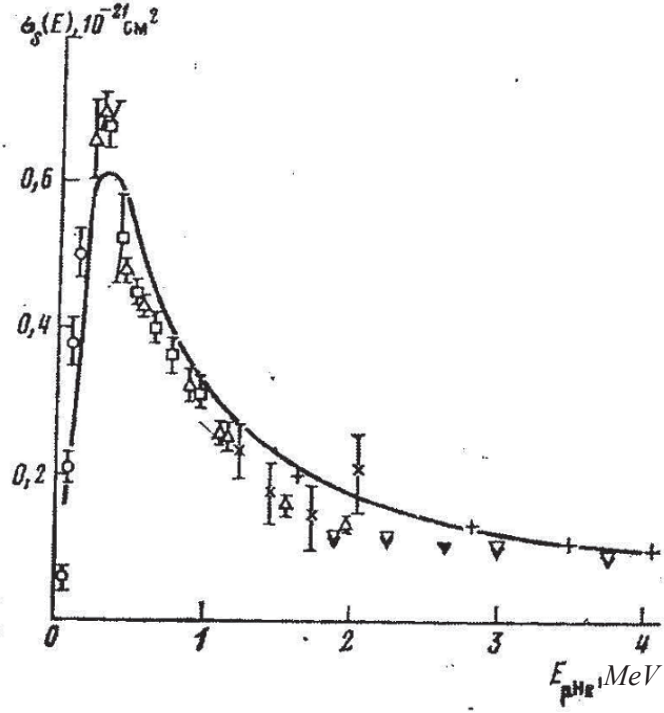


Fig. 18: The cross section of the stripping of $\mu^-$ on the slowing down of $(He\mu)^+$ in hydrogen.

The effective sticking probability $\omega_s = \sum_{nl}\left[1 - R(nl)\right]\omega_s^0(nl)$ is given in Fig. 19, which was taken from Nagamine [3, 12g].

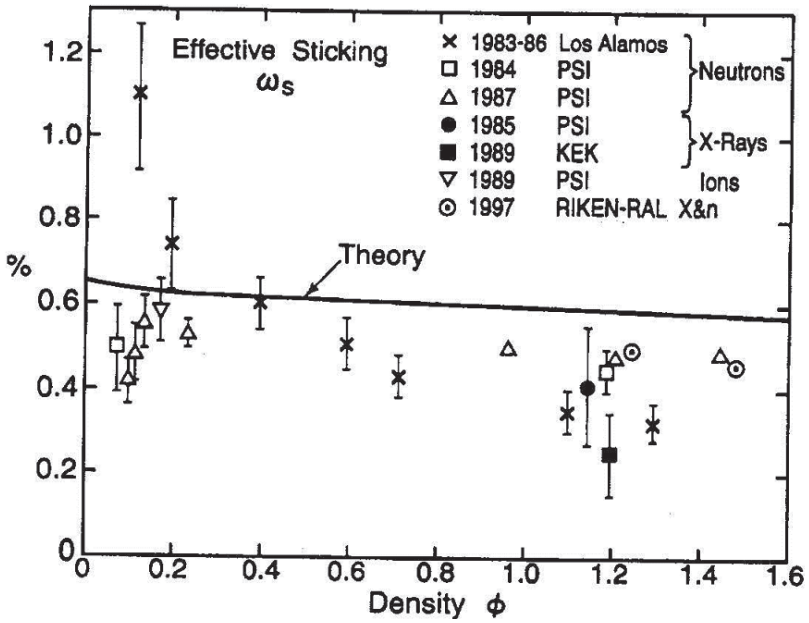


Fig. 19 The sticking probability $\omega_s$ vs density $\phi$ in $\mu$CF in a D-T mixture.

The important parameter for the $\mu$CF is the probability of muonic hydrogen reaching its ground 1*s* state $q_{1s}$. By solving the system of kinetic equations with the rates of the processes indicated in Fig. 11, one can obtain the ground state population $q_{1s}$ of muonic hydrogen. The data on $q_{1s}$ depending on the concentration of a heavier hydrogen isotope $C_i$ (in a D-T mixture $C_i \equiv C_t$) and the target density $\phi$ have been obtained in numerous papers [79a, 109, 111, 112, 178, 179]. Of course, the larger is either $C_i$ or $\phi$, and the smaller is $q_{1s}$. The parameter, $q_{1s}$, is important in the formation of the muonic molecule. For example, in the D-T mixture

the inverse of the cycling rate $\lambda_c^{-1}$ corresponds to the $d\mu$ waiting time for the muon transfer to *t*, together with the time taken to form $dt\mu$ molecule (i.e. $\frac{1}{\lambda_c} \cong \frac{q_{1s}C_d}{\lambda_{dt}C_t} + \frac{1}{\lambda_{dt\mu}C_d}$). Here, the factor, $q_{1s}C_d$, is the probability of the muon reaching the ground state of $d\mu$, reflecting the fact that the transfer rates from the excited states of $d\mu$ are very rapid [3]. $\lambda_{dt}$ is the rate of the muon transfer from $d\mu$ to tritium nucleus (see section 3.3). Fig. 20 represents the theoretical $q_{1s}$ for the D-T mixture as a function of $C_t$ at various $d\mu$ energies and target densities calculated in references 79a and 112 in comparison with the experimental results in reference 180, taken from 3, 12g.

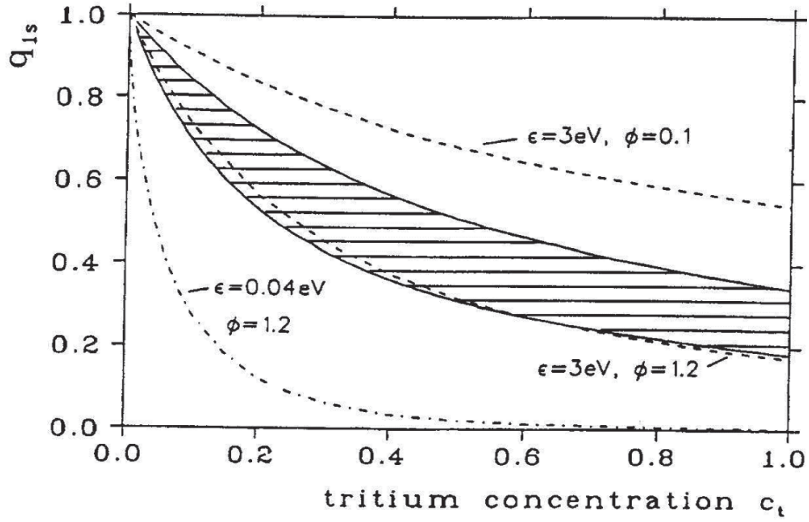


Fig. 20 The theoretical predictions of the $q_{1s}$ values (dashed lines) in the D-T mixture [112] together with the experimental values (shaded area) as a function of $C_t$ at various dμ energies and densities $\phi$ [180] taken from references 3 and 12g.

The previously mentioned parameters, especially $\omega_s$, indicate that on average a muon will not initiate more than 100 $\mu$CF cycles in a D-T mixture and not more than a dozen in pure liquid deuterium. Using this fact, with an estimated energy cost per muon at $10GeV$ and only $1.7GeV$ produced with 100 *dt* fusions [12h], the amount of energy gained is a net negative. At the same time, further investigations, especially at RIKEN, have been prolonged. The $\mu$CF in a dense low temperature plasma with about 1500 *dt* fusions per muon was considered by Menshikov and Somov [109]. Further perspectives of the $\mu$CF are discussed in references 3, 12c, e, g, i, 14, and 109. It is now impossible to consider $\mu$CF as an alternative source of energy. However, the previous experimental and theoretical investigations of this problem have considered $\mu$CF as one of the important alternative possibilities in the future. The research into $\mu$CF have been ongoing at the RIKEN-RAL Muon Facility by T. Matsuzaki et al. [181]. The muon transfer to $^3He$ is discussed in reference 181, as in the D-T mixture $^3He$ is originated from tritium $\beta$-decay. The muon transfer from $\mu d$, or $\mu t$, to $^3He$ is determined by the molecular mechanism discussed in section 3.3. The temperature dependence of the transfer rate was investigated in reference 181. The poisoning of the D-T target by helium due to tritium $\beta$-decay, or a nuclear fusion reaction, is a problem for $\mu$CF. The experiments are realized in a solid-state D-T target, where the process rates should be increased. A mixed gas of deuterium and tritium is cooled to temperatures below around $-250^{\circ}C$, causing the gas to form a liquid or solid state. In the RIKEN-RAL Muon Facility, $5GeV$ of energy is required to produce one muon that is capable of inducing *d-t* nuclear fusion 120 times before it decays, producing $2GeV$ of energy, which corresponds to an energy balance of 40%. A possible 100% energy

balance could be achieved when a single muon can induce *d-t* nuclear fusion at least 300 times before decaying. In fact, the efficiency level required is estimated to be $3 \div 10$ times higher than the indicated estimation. This means that a single muon needs to induce fusions $1000 \div 3000$ times before decaying. Previously, there were many scientific centres in the world that researched $\mu$CF, now only RIKEN-RAL performs fundamental experiments on this problem. The aim is to achieve the necessary conditions in an effort to put $\mu$CF into practical use. The key to successful research lies in two points: how to strip the muons from $He\mu$ efficiently, and how to create $dt\mu$ more efficiently. If the target is made much denser, $He\mu$ could be stripped of their muons more easily because of the increased probability of collision with deuterium or tritium atoms. Furthermore, a denser target will contribute to an increased probability that $dt\mu$ molecules can be created, as well as increasing of the frequency of nuclear fusion induced by a single muon and the efficiency of the $\mu$CF cycle. If $He\mu$ can be completely stripped of their muons at the present level of $\lambda_{dt\mu}$, then a single muon could induce nuclear fusion 340 times before decaying. Furthermore, if the target is 5 times denser than LHD, a single muon could induce nuclear fusion as many as 1200 times. The new target, which is 5–10 times denser than LHD, could be realized by combining it with laser-based inertial confinement fusion. The efficiency of the nuclear fusion cycle improves as the temperature of the solid target is increased from 5 to 17*K*. However, if the temperature is increased too far, the solid target will melt and become a liquid. The target, however, stays solid up to temperature of 30*K* provided that the pressure is maintained above 1000 atm. Other possibilities are connected with using a laser beam to enhance the production of $dt\mu$ molecules, as well as applying

the electric field to the target in order to increase the efficiency when stripping the muon from $He\mu$. Also, it can be important to use the Japan Accelerator Research Complex (J-PARC) to produce an intense muon beam. The $\mu$CF can be used for a hybrid (fusion/fission) reactor, as discussed by Yu. Petrov in reference 12, and as an intense 14 *MeV* neutron source [182]. Of course, $\mu$CF is far from being complete. At the same time, the movement from a plutonium bomb to atomic power stations is shorter than that from a hydrogen bomb to industrial plants that use hot or cold fusion.

## 3.7 Weak muon capture by proton

Muon capture by proton or deuterium is difficult as it only occurs at a rate of 0.1% in comparison with muon decay. However, any complications connected with the nuclear structure are absent in comparison with weak nuclear muon capture. Therefore, numerous experimental investigations into the weak muon capture by proton have been performed. The consideration of weak muon capture by proton have been discussed in a number of reviews [1, 4, 8, 9, 10, 13, 35, 183a, b, 184, 185]. The muon capture,

$$\mu^- + p \to n + \nu_\mu$$

is considered as a current-current V-A weak interaction [186–188]:

$$H_{\text{int}} = \frac{G_F}{\sqrt{2}} j_\lambda \bar{j}_\lambda + h.c.$$

where $G_F = \frac{g^2}{8M_W^2}\sqrt{2}$ is the Fermi constant (see section 2.2) with the weak coupling *g*, W-boson mass $M_W$ and $j_\lambda = j_\lambda^\mu + j_\lambda^h$. The matrix elements of the left-handed lepton current are given in terms of lepton fields: $\overline{\nu}_\mu and\ \mu$. $j_\lambda^\mu = \overline{\Psi}_{\nu_\mu}\gamma_\lambda(1+\gamma_5)\Psi_\mu$, $\gamma_\lambda$, and $\gamma_5$ are Dirac matrices (i.e.,

$$\overline{\gamma} = \begin{pmatrix} 0 & -i\overline{\sigma} \\ i\overline{\sigma} & 0 \end{pmatrix}, \quad \gamma_4 = \begin{pmatrix} 1 & 0 \\ 0 & -1 \end{pmatrix}, \quad \gamma_5 = -\begin{pmatrix} 0 & 1 \\ 1 & 0 \end{pmatrix}.)$$

The neutrino wave function, $\Psi_{\nu_\mu}$, was determined at the end of section 2.5. The muon wave function is given as the Dirac bispinor for the particle in the atomic 1s state (*K*-orbit)

$$\Psi_\mu = \begin{pmatrix} -iF(r)\chi_{1m}(\hat{r}) \\ G(r)\chi_{-1m}(\hat{r}) \end{pmatrix}$$

and the spherical spinors are defined as

$$\chi_{km}(\hat{r}) = [Y_l(\hat{r}) \otimes \chi_{1/2}]_{Jm} \qquad (J = l - \frac{1}{2}sign\,k),$$

where $G(r)$ and $F(r)$ are large and small radial components of wave functions in central-symmetrical field, respectively, and $k = \pm 1$. However, as the binding energy of the $\mu^-$ meson at *K* orbit is much smaller than its rest energy (i.e. mass), the non-relativistic approximation for the wave function of the muon at *K*-orbit is possible:

$$\Psi_{\mu}(r) = \begin{pmatrix} 0 \\ g(r)\chi_{\sigma} \end{pmatrix},$$

where $g(r) = 2(\alpha Zm_{\mu})^{3/2} \exp\left(-\alpha Zm_{\mu} r\right)$ and $\chi_{\sigma}$ is a normalised spinor. Although the lepton current and nucleonic one have similar parity violating V-A structures, the nucleonic current, because of its consistent and strong quark interaction, is more complicated. $j_{\lambda}^{h} = \cos\theta_c (V_{\lambda} - A_{\lambda})$, where the Cabibbo angle is determined experimentally, $\cos\theta_c = 0.9730 \pm 0.0024$ [189a] and $\sin\theta_c = 0.229 \pm 0.003$ [189b]: i.e. $\theta_c \approx 13^0$ and see also reference 189c. So, the matrix element of muon capture is

$$H_{\mu} = \frac{G_F}{\sqrt{2}} \cos\theta_c \left\langle \overline{n} \left| V_{\lambda} - A_{\lambda} \right| p \right\rangle L_{\lambda},$$

where $L_{\lambda}$ and $\left\langle \overline{n} \left| V_{\lambda} - A_{\lambda} \right| p \right\rangle$ are lepton and hadron matrix elements respectively. $L_{\lambda} = \overline{u}_{\nu} \gamma_{\lambda} (1 + \gamma_5) u_{\mu}$, where $u_i$, is a free spinor of the correspondent particle. Taking into account the Lorentz invariance vector and axial matrix elements of the weak nucleon $n \rightarrow p$ current, [190–193]. are:

$$\left\langle \overline{n} \left| V_{\lambda} \right| p \right\rangle = \overline{u}_n \left[ g_V(q^2) \gamma_{\lambda} + g_M(q^2) \sigma_{\lambda\nu} q_{\nu} / 2M \right] u_p$$

$$\left\langle \overline{n} \left| A_{\lambda} \right| p \right\rangle = \overline{u}_n \left[ g_A(q^2) \gamma_{\lambda} \gamma_5 + g_P(q^2) q_{\lambda} \gamma_5 / m_{\mu} \right] u_p,$$

where $q_\lambda = (p_n - p_p)_\lambda$ is the four-momentum transfer, with $q^2 \approx m_\mu{}^2$; $M = M_p = M_n$, $m_\mu$ are respectively proton or neutron and muon masses; $g_{V,A,M,P}(q^2)$ are vector, axial vector, weak magnetism and pseudoscalar form factors, respectively. In the $q^2 = 0$ limit, only $g_{V,A}$ contribute, and they are known experimentally as $g_V(0) = 1.000 \pm 0.0015$ [189] and $g_A(0) = 1.2723 \pm 0.0023$ [194a], or $g_A = 1.2701 \pm 0.0025$ [194b]. I have ignored right handed weak coupling parameters, taking into account the low experimental limits from the inelastic neutrino interactions < 0.009 [195]. The terms involving $g_V, g_A, g_M$ and $g_P$ are called first-class currents, while the terms involving $g_S$ and $g_T$ are called second-class currents [196]. First-class and second-class currents have opposite transformations under *G*-parity. The *G*-operation produces a rotation of 180° around the 2-axis in the isospin place, plus a charge configuration (i.e. $G = Ce^{i\pi T_2}$). This strong interaction is isotopic invariable with a conservation of charge parity *C,* so *G*-parity should be conserved. The hadronic components of the vector current, which transform $GVG^{-1} = V$ and the hadronic components of the axial current which transform $GAG^{-1} = -A$, are called currents of the first class. Second class currents (i.e., scalar in vector current or tensor in axial current) have the opposite behaviour under *G*-parity transformation. The conservation of *G*-parity is equal to isotopic invariance. Therefore, they should be forbidden to conserve *G*-parity. The *G*-operation transforms the matrix elements of

n → p into those from the inverse p → n process. Second-class contributions can only arise through breaking *G*-parity and any experimental evidence for second-class currents is absent for scalar $g_S$ [197] or tensor $g_T$ [198] contributions. The conserved vector current hypothesis (CVC) [9, 185, 186, 200, 201] indicates that the strangeness-conserving weak vector current and isovector electromagnetic current are the components of a single conserved vector-isovector current. The CVC leads to a relationship between the weak vector and isovector electromagnetic currents and relates the $g_V(0)$ and $g_M(0)$ to the charge and magnetic terms, respectively, of the isovector electromagnetic current, which has a simultaneous absence of any scalar term (i.e., $g_S(0)=0$). Therefore, in the experiments considered, $g_V(0)=1$ and $g_M(0)=\mu_p-\mu_n-1=3.706$, as well as $\mu_p$ and $\mu_n$ are all anomalous magnetic moments of proton and neutron, respectively.

Since the vector coupling constant is not renormalized by the presence of hadrons in framework of CVC, the constant $G_F$ determined in muon decay is close to < 2% of the weak-interaction coupling constant in beta-decay (e.g. the $0^+ \to 0^+$ transitions between levels belonging to a single isobaric multiplet). From the analysis of experimental results, one gets $G_F = 1.1663787(6)\times 10^{-5}\, GeV^{-2}$ [4, 194a]. In contrast with $g_V(0)$, the value of $g_A(0)\neq 1$ (i.e., it is modified by strong interactions), however, the partial conserved axial current hypothesis (PCAC) exists [9, 185, 191, 192, 199]. In the PCAC hypothesis, the divergence of the axial current is

proportional to the pion field operator $\phi_\pi$ (i.e. $\partial A_\lambda / \partial x_\lambda = g_\pi m_\pi^3 \phi_\pi$, where $g_\pi$ is determined by the process of pion decay in a muon and a neutrino, from which one gets $g_\pi = 0.9450 \pm 0.0008$ [202]). In order to estimate the $g_A(q^2)$ and $g_P(q^2)$, let us consider the matrix element of this operator between two free-nucleon states:

$$\left\langle n \left| \partial A_\lambda / \partial x_\lambda \right| p \right\rangle = g_\pi \, m_\pi^3 \left\langle n \left| \phi_\pi \right| p \right\rangle$$

We calculate that the left side uses the matrix element of axial current, while the right side can be obtained by the following equation:

$$(-\Box^2 + m_\pi^2)\, \phi_\pi = J_\pi$$

with the function $J_\pi$ of the pion field search from nucleons

Following the pole Feynman graph of one pion exchange we could obtain $g_A(0) = \sqrt{1/2}\, g_\pi m_\pi f_{\pi NN}(-m_\pi{}^2) / M$, where $f_{\pi NN}(-m_\pi{}^2) = (13.31 \pm 0.15)$ $(\mathrm{GeV})^{-1}$ represents the pion-nucleon coupling constant. The result, $g_A(0) = 1.3$, is in agreement with the discussed experimental value. As the pseudoscalar contribution depends on transfer momentum, its value, via PCAC, corresponds to

$$g_P(q^2) = \frac{2 m_\mu M}{q^2 + m_\pi^2}\, g_A(0)$$

.

Due to $q = 0.88\, m_\mu$, we have $g_P(0.88\, m_\mu^2) \approx 7 g_A(0) \approx 8.7$ (the precise value derived within the effective chiral theories of QCD corresponds to

$g_P = 8.26 \pm 0.23$ [203]) in agreement with the experimental result $g_P(0.88\, m_\mu^2) = 8.06 \pm 0.55$ [204]. In fact, the axial vector current is not conserved, whereas this would be the case if the pion had a vanishing mass. However, one may quantitatively understand the idea of PCAC by observing the pion mass, which is responsible for the non-conservation of axial vector current, is actually small with respect to the nucleon mass.

The $\mu p$ can be in two h.f.s. states, with $F = 0$ and 1 (see section 3.5) with a capture rate from a singlet $F = 0$ state [205]

$$\Lambda_s = N_p (G_V - 3G_A + G_P)^2$$

and from triplet $F$=1 state

$$\Lambda_t = N_p [(G_V + G_A)^2 - \frac{2}{3} G_P (G_V + G_A) + G_P^2],$$

where

$$G_V = g_V(q^2)(1 + \frac{q}{2M}),$$

$$G_A = g_A(q^2) - \frac{q}{2M}[g_V(q^2) + g_M(q^2)],$$

$$G_P = [g_P(q^2) - g_A(q^2) - g_V(q^2) - g_M(q^2)]\frac{q}{2M};$$

$$N_p = (G_F \cos\theta_c)^2 q^2 \frac{(\alpha m_\mu)^3}{2\pi^2} = 14.88 (G_F \cos\theta_c)^2.$$

On reaching the 1s ground state, the $\mu p$-atoms have a kinetic energy of typically $1eV$ and a statistical population of h.f.s. states

$$\Lambda = \frac{1}{4}\Lambda_s + \frac{3}{4}\Lambda_t \quad .$$

Due to the small probability of muon capture by proton in comparison with muon decay the initial experiments were performed at LHD, where muonic molecules formation is realized with ~82% of muon capture by proton. After the formation of muonic hydrogen in an excited state and de-excitation to the ground state during ~$10^{-3}\mu s$, the destiny of the muon is determined by the processes illustrated in Fig. 21. The small h.f.s. splitting of the *K*-shell ~$0.18eV$ excludes the radiative transition. However, de-excitation is realized due to the collisions between mesic and hydrogen atoms at the LHD target; this means that the triplet lifetime is ~$0.1ns$ at LHD and ~$10ns$ in 10 bar hydrogen gas. The muonic molecule is, as a rule, formatted in an ortho-state with $S_p = 1$ spin from both protons [13] and a rotational momentum of $K = 1$ (para-state corresponds to $S_p = 0$ and $K = 0$). The $p\mu p$ molecules are formed by collisions between the $\mu p$ atoms and the surrounding $H_2$ molecules via the Auger emission ($\mu p + H \rightarrow p\mu p + e$) with a rate of $\lambda_{p\mu p} = (1.94 \pm 0.06) \times 10^6 s^{-1}$ [206].

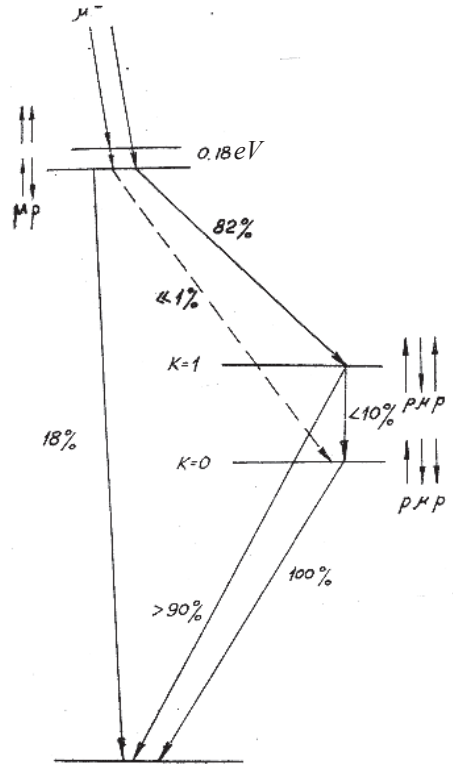


Fig. 21 The scheme of processes undergone by $\mu p$ atoms in pure hydrogen before the muon capture by nucleus.

As $\mu p$ atoms are essentially in a *s*-state, the calculated rate of the E1 Auger transition forming ortho-states $\lambda_{p\mu p}^{\text{ortho}} \approx \varphi \cdot 1.8 \times 10^6 s^{-1}$ is much faster than the E0 Auger transition forming para-states $\lambda_{p\mu p}^{para} \approx \varphi \cdot 0.75 \times 10^4 s^{-1}$, where $\varphi$ is the $H_2$ density normalized to LHD. The total rate of molecular formation $\lambda_{p\mu p} = \varphi \cdot (2.01 \pm 0.07) \times 10^6 s^{-1}$ [4] agrees with the theoretical predictions [13]. The ortho–para transition corresponds to

$\lambda_{op} = (6.6 \pm 3.4) \times 10^4 s^{-1}$ [207] (without any $\varphi$ dependence) with a change of the total spin $S_p$ and a correspondently magnetic moment of two protons, therefore it is sufficiently small, and the ortho-state of *pμp* molecule could be considered as metastable. The determined channel of the mesic atomic processes before the muon capture by proton was indicated in Fig. 21. The recent MuCap experiment at PSI [204] using an ultrapure 10-bar hydrogen gas was described in detail in reference 4. They obtained the rate, $\Lambda_s$, with a precision of 1%, $\Lambda_s = (714.9 \pm 5.4_{stat} \pm 5.1_{syst})\, s^{-1}$, and derived the pseudoscalar coupling, $g_P(0.88\, m_\mu^2)$, as indicated above.

The muon capture by deuteron, $\mu^- + d \rightarrow n + n + \nu_\mu$ was considered in references 9 and 183b and c. As the deuteron spin is equal to 1, the capture rate from the two h.f.s. states (namely the $F$ =1/2, doublet, and the $F$ = 3/2, quartet) of the muon-deuteron system is:

$$\Lambda_F(d) = N_d \int \Gamma_F(d)\, dE_n,$$

where $E_n$ is the energy of one of the neutrons released in the above reaction:

$$N_d = (G_F \cos\theta_c)^2 \frac{(\alpha m_\mu)^3}{\pi (2\pi)^3} \int \Gamma_F(d)\, dE_n =$$

$$= 44.16 (G_F \cos\theta_c)^2 \int \Gamma_F(d)\, dE_n.$$

The h.f.s. factors $\Gamma_F$ can be expressed using

$$\Gamma_{1/2}(d) = \{[(G_V - 2G_A)^2 + \frac{2}{3}G_P(2G_V - 4G_A + G_P)]I_t + \\ + \frac{1}{3}(3G_A - G_P)^2 I_s\} + \Gamma_{1/2,vel},$$

$$\Gamma_{3/2}(d) = \{[(G_V + G_A)^2 - \frac{2}{3}G_P(G_V + G_A - G_P)]I_t + \\ + \frac{1}{3}G_P^2 I_s\} + \Gamma_{3/2,vel}.$$

$\Gamma_{1/2,vel}$ and $\Gamma_{3/2,vel}$, which takes into account the velocity terms of the muon-nucleon coupling. $I_s$ and $I_t$ are integrals over the neutrino momentum $\vec{p}_\nu$ defined by

$$I_{s,t} = \int \left|M_{s,t}\right|^2 p_\nu dp_\nu,$$

where the nuclear matrix element is

$$M_{s,t} = \left\langle f_{s,t}(\vec{r},\vec{k}) \middle| \exp(-i\vec{p}_\nu \cdot \vec{r}/2) \middle| \Psi_d(\vec{r}) \right\rangle.$$

$\Psi_d(\vec{r})$ is the deuteron wave function and $f_{s,t}(\vec{r},\vec{k})$ is the wave function of the relative motion of the two neutrons in singlet *s* and triplet *t* spin state with relative momentum $\vec{k} = \vec{p}_n + \vec{p}_\nu/2$, where $\vec{p}_n$ is the neutron momentum. The relation $\vec{p}_n \cdot \vec{p}_\nu = p_n\, p_\nu \cos\vartheta = M(m_\mu - p_\nu) - \ p_n^2 - p_\nu^2/2$ follows from the conservation of the momentum-energy law. The limits of integration are determined from the condition of $\cos\vartheta = \pm 1$. The index *s* or *t* for $I_{s,t}$ denotes the spin of the two neutrons in a singlet or triplet state,

respectively. As follows from the calculations, $I_s$ dominates with respect to $I_t$ over the whole energy range [9]. Therefore, $\Gamma_{1/2} \sim (3G_A - G_P)^2$ leads to $\sim g_A^2$ dependence, whereas $\Gamma_{3/2} \sim G_P^2$ to $g_P^2$ one. In fact, $\Lambda_{3/2}(d)$ is smaller by about one order of magnitude in comparison with $\Lambda_{1/2}(d)$. This is explained by the sufficiently small energy of the two neutrons (i.e., they are in an s-state and in agreement with the Pauli principle that the total spin of two neutrons should be zero). The theoretical estimations of $\mu d$ capture that are founded on phenomenological potential models of nucleon-nucleon interactions resulted in $\Lambda_{1/2}(d) \sim 400 s^{-1}$ [208]. In the case of the statistical population of h.f.s. states we have $\Lambda(d) = \frac{1}{3}\Lambda_{1/2}(d) + \frac{2}{3}\Lambda_{3/2}(d)$.

The energy spectrum of two neutrons from muon capture by deuterium could provide a good possibility for determining the neutron-neutron scattering length ($a_{nn}$). The maximum sensitivity to the *s*-wave final-state interaction between the neutrons is verified when the neutrons are emitted at small angles and relative momentum. Moreover, only two hadrons are present in the final state of the process. Fig. 11 from reference 9 shows the sensitivity of the different capture rate to the $a_{nn}$ for a vanishing emission angle between the two neutrons (having a maximal differential distribution at a momentum of $p_n \approx 56\, MeV/c$) and how this sensitivity decreases with the increase of the angle. The average scattering length from different experimental data is $a_{nn} = -18.9 \pm 4\, fm$, which is in comparison to

$a_{pp} = -17.3 \pm 0.4\, fm$ [8]. Therefore, the experimental charge symmetry break is at $1.6 \pm 0.6\, fm$, whereas the theoretical estimate was $1.5 \pm 0.5\, fm$ [8].

Similar to pure hydrogen, the formation of muonic molecules formation is possible especially in LHD. The processes in p-d mixtures are illustrated by Fig. 22.

The processes in pure deuterium are accompanied by the formation of $d\mu d$ molecules with nuclear fusion reactions. Therefore, the hydrogen targets, which contain a small amount of deuterium impurities, were initially used with the possible formation of $p\mu d$ molecules, as indicated in Fig. 22. The bound energy of $\mu d$ is larger on $135eV$, in comparison with $\mu p$. Therefore, muons are transferred from $\mu p$ to the deuterium nuclei. The problem is the formation of $p\mu d$ molecules, which was initially realized in rotational momentum $K = 1$. However, the different nuclei, $p$ and $d$, results in 4 sublevels of h.f.s. states with $J = 0$, 1 (two levels), 2 and de-excitation to $K = 0$ is realized for $10^{-11}s$ due to the E1 Auger conversion on an atomic electron. The experiment in hydrogen gas at 7.6 atm. and deuterium impurity 5.2% was performed at CERN [209a], which obtained $\Lambda_{\exp}(d) = 451 \pm 70\, s^{-1}$ in agreement with the theoretical results. Similar experimental data was published later: $\Lambda_{\exp}(d) = 445 \pm 60\, s^{-1}$ [209b], $470 \pm 29s^{-1}$ [209c], $409 \pm 40s^{-1}$ [209d].

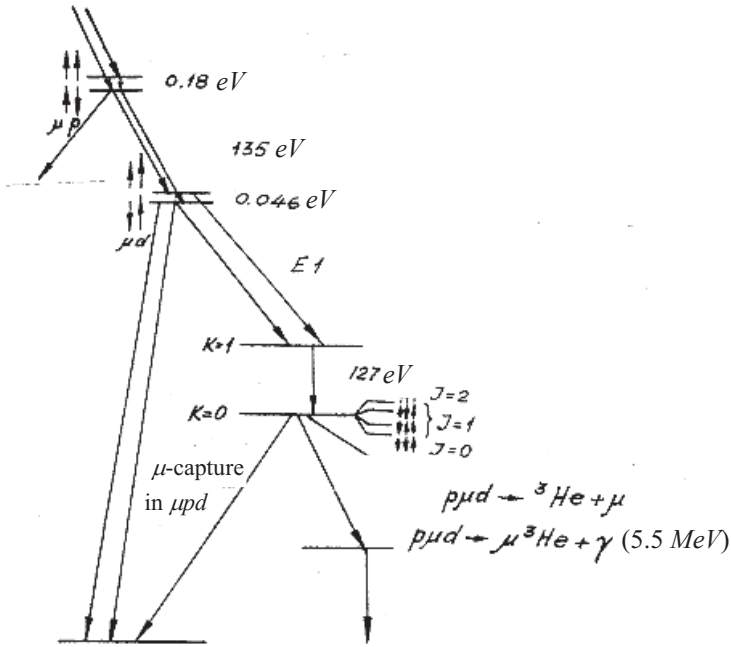


Fig. 22: A scheme of the processes undergone by $\mu d$ atoms in p-d mixture before the muon capture by nucleus.

However, recent experiments have been performed using pure deuterium gas targets. The experiments were undertaken by the MuSun collaboration [4, 210–214]. The scheme of processes undergone by $\mu d$ atoms in pure deuterium, before the nuclear muon capture, is presented in Fig. 23, which has been taken from reference 210. The MuSun experiment at PSI measured the rate of muon capture in a deuteron with a precision of 1.5%. A temperature of ~30$K$ and a pressure of ~5 bar were chosen to prepare the optimal population of doublet atoms. At this temperature and pressure, the quartet atoms with $F$ = 3/2 decay rather quickly to doublet atoms with $F$ = 1/2 and the regeneration of quartet atoms by muon recycling after

formation of *dμd* molecules and following *dd*-fusion (see Fig. 23) is quite small. At the same time, the upper limit in the ratio of rate of formation from a quartet atom to a doublet was obtained ($\Lambda_{3/2}(d)/\Lambda_{1/2}(d) < 0.275(90\%\,CL)$), as well as the hyperfine transition rate from quartet to doublet atom: $\lambda_{qd} = 34.71 \pm 0.21(stat) \pm 0.01(syst)\ (\mu s)^{-1}$ [214].

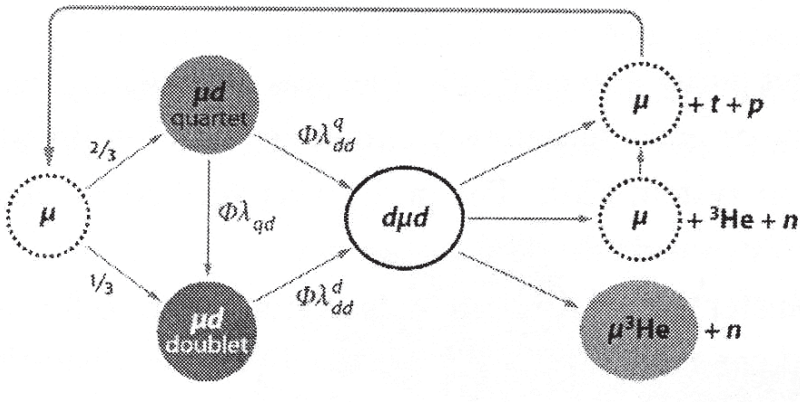


Fig. 23: A scheme of processes undergone by *μd* atoms in pure deuterium before the muon capture by nucleus.

The muon capture by tritium in the reaction $\mu + t \to n + n + n + \nu_\mu$ is a very slow process with an impulse approximation rate of $\approx 9.5 s^{-1}$ [215a] or with more accurate potential for neutrons in the final state $\Lambda_s = 137.5 s^{-1}$ and $\Lambda_t = 3.7 s^{-1}$ [215b]. When the radioactivity of the tritium target with such a low capture rate is taken into account, measuring muon capture by tritium is, in fact, impossible [8].

# 4. MUON CAPTURE IN LIGHT NUCLEI

## 4.1 The formation of muonic atoms

Fermi & Teller first discussed the formation of muonic atom using the *Z*-scaling law of $\mu^-$ muon capture [68]. This law predicts that the muon capture cross-section in an atom is proportional to the number of shell electrons present (i.e. *Z*). A more precise dependence corresponds to the $Z^{2/3}$- law [216]. The different models and approaches of $\mu^-$ capture have been considered by Cohen [72a] and also in references 12e and 217. After the formation of the muonic atom with $n \approx 14$, its destiny is determined by both radiative and Auger de-excitation. Contrary to the hydrogen targets, the channels of molecule dissociation and Coulomb de-excitation are absent for $Z > 1$. The de-excitation of the muonic hydrogen atom was considered in section 3.1. I will now discuss some aspects of the de-excitation of muonic atoms for $Z > 1$. The radiative transitions are not important for muonic hydrogen; however, they can be essential for heavy atoms, as the probability of radiative transition is proportional to $Z^4$ [218, 219]. The radiative rate is also proportional to $(E_{n'} - E_n)^3$ (i.e. such transitions are more essential for large $\Delta n$). The main transitions from $n >> 1$ correspond to $ns \to 2p$, as well as the decrease of the orbital quantum number (i.e. $l \to l-1$) for any *n*. However, the Auger transitions are more important for light muonic atoms. At the same time, the formation of muonic hydrogen is realized by the replacement electron from the hydrogen atom on muon and further process of the outer Auger

de-excitation of the muonic atom, which corresponds to the ionization of hydrogen atoms or molecules of the target with a density dependence. As for $Z > 1$, the process of the Auger de-excitation of the muonic atom is realized on the inner electrons of target atom without any density dependence. The relative importance of the Auger internal conversion and radiative transitions is illustrated in Fig. 24, which has been taken from references 1b, 218, 219, and 220. As indicated in Fig. 24, the rates of radiative transitions decrease with $n$ increasing contrary to the Auger transitions, which increase with an increase in $n$. At the same time, the rates of Auger transitions have very small $Z$.-dependence. We can see that Auger rates dominate for light atoms, while radiative ones are more important for heavy atoms.

The most prominent transitions are electric-dipole ones between circular orbits ($(n, l = n-1) \rightarrow (n-1, l = n-2)$) as indicated in Fig. 24 (i.e., $K_\alpha, L_\alpha$ and so on are radiative transitions that promote the population of the circular orbits). The time for the de-excitation of the light muonic atoms is $\sim 10^{-13}\, s$ and this is shorter for heavy muonic atoms.

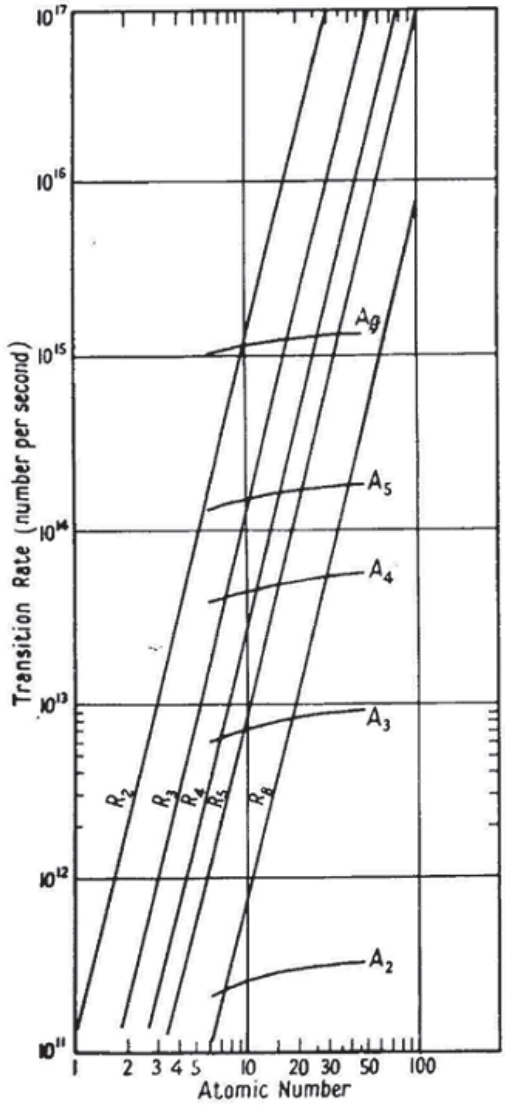


Fig. 24 The calculated radiative $R_n$ and Auger $A_n$ rates for $(n, l = n-1) \to (n-1, l-1)$ transitions in muonic atoms.

## 4.2 Weak muon capture

The reaction of $\mu^-$ capture by (*A, Z*) nucleus may be written as

$$\mu^- + (A,Z)_{j_0} \rightarrow (A,Z-1)_{j_1} + \nu_\mu$$

(where $j_0$ and $j_1$ is the spin of the initial and the final nucleus, respectively). This was considered in a number of reviews [8, 183a, b, 184, 193, 221–224]. The matrix element in the case of nuclear muon capture is

$$H_\mu = \int \Psi^*_{j_1\mu_1} \bar{H}\, \Psi_{j_0\mu_0} d\vec{r},$$

where $\Psi_{j_0\mu_0}$ and $\Psi_{j_1\mu_1}$ are the wave functions of initial and final nuclei. The correspondent consideration for muon capture by proton was given in sec.3.7.

The Hamiltonian $\bar{H}$ corresponds to the impulse approximation (IA), which supposes that the weak interaction of nucleons with leptons is realized independently from each other [222], as they are an additive contribution of the nucleons. The nuclear collective effects were included in the wave functions of both the initial and final nuclei. The nuclear wave functions are used within non-relativistic nuclear models, so that the non-relativistic limit of $\bar{H}$ is also used [223, 224a]. The non-relativistic muon function was determined in section 3.7. The effective Hamiltonian must be considered as applying to 2-component spinors for the particles in the Dirac field: $u = \sqrt{\frac{E+m}{2m}}\begin{pmatrix}\chi\\ \phi\end{pmatrix}$, where $\chi$ and $\phi$ are both 2-component

spinors with $\chi = -\frac{\vec{\sigma}\,\vec{p}}{E+m}\phi$ and $\vec{\sigma}$ Pauli matrix, $\vec{p}$ particle momentum. We can obtain the following expression for a system of nucleons [224a]:

$$H = \frac{1}{2}\left(1-\vec{\sigma}\,\hat{\vec{\nu}}\right)\sum_{i=1}^{A}\tau_i^{(-)}[G_V + G_A\vec{\sigma}\cdot\vec{\sigma}_i - G_P\left(\vec{\sigma}\cdot\hat{\vec{\nu}}\right)\left(\vec{\sigma}_i\cdot\hat{\vec{\nu}}\right) -$$
$$- g_V\left(\vec{\sigma}\cdot\hat{\vec{\nu}}\right)\left(\vec{\sigma}\cdot\vec{p}_i\right)/M - g_A(\vec{\sigma}\cdot\hat{\vec{\nu}})(\vec{\sigma}_i\cdot\vec{p}_i)/M]\delta(\vec{r}-\vec{r}_i)$$

$\vec{\sigma}_i, \vec{p}_i$ are the operators for the *i*-th nucleon and $\vec{\sigma}$ is lepton operator; $\hat{\vec{\nu}}$ is the unit vector in the direction of neutrino momentum $\vec{\nu}$; $\tau_i^{(-)}$ is isobaric-spin operator of transfer of proton to neutron (i.e. the operator that decreases the charge of the nucleon by one unit); $G_V, G_A, G_P$ were determined in section 3.7.

$\bar{H} = \bar{\Psi}_{\nu_\mu}(\vec{r})\,H\,\Psi_\mu(\vec{r})$ with both the neutrino and muon wave functions was determined in sections 2.5 and 3.7. We have supposed that the nucleon is on a mass surface as the bound energy $\varepsilon$ of the nucleon in the nucleus is sufficiently small: $p_i^2 + M^2 \approx 2\varepsilon M$. We have also neglected the possible contributions from the exchange currents between the nucleons.

The probability of a muon capture in light nuclei is proportional to ~$Z^4$ in agreement with Primakoff's law [1b, 8, 223]. For light nuclei the point nucleus concept is sufficient, so there are $Z$ protons and the probability of finding the muon in the nucleus increases to $Z^3$ (as a consequence of the muonic wave function in section 3.7); therefore, the capture rate increases to $Z^4$.

In fact, the probability is

$$\Lambda_C(A,Z) = (Z_{eff})^4 X_1 \left[1 - X_2\left(\frac{A-Z}{2A}\right)\right],$$

where $X_1 = 170\,s^{-1}$ and $X_2 = 3.125$ are proportional to $Z_{eff}^4$. However, $Z_{eff} \approx Z$ for light nuclei up to $^{12}C$ is in agreement with Table 4.2 in reference 8.

The simplest nucleus, after an investigation into a muon capture in hydrogen isotopes, is $^3He$ in the reaction:

$$\begin{aligned} \mu^- + {}^3He &\to {}^3H + \nu_\mu \quad (70\%) \quad \Lambda_t \\ &\to d + n + \nu_\mu \quad (20\%) \quad \Lambda_{nd} \\ &\to p + n + n + \nu_\mu \quad (10\%) \quad \Lambda_{nnp}. \end{aligned}$$

The experimental precise determination yields: $\Lambda_t = 1496 \pm 4\,s^{-1}$ [225], as well as $\Lambda_{nd} = 497 \pm 57\,s^{-1}$, $\Lambda_{nnp} = 190 \pm 7\,s^{-1}$ and $\Lambda_{br} \equiv \Lambda_{nd} + \Lambda_{nnp} \equiv$ $\equiv 687 \pm 60\,s^{-1}$ [226].

Numerous theroretical calculations have been obtained within different nuclear models. The elementary particle model (EPM) [227, 183b], which determined $\Lambda_t$ was used in reference 228. The nuclei, $^3He$ and $^3H$, are treated as elementary particles, while their structure reveals $\vec{q}$-dependent nuclear form factors, $F_V(q^2),\ F_M(q^2), F_A(q^2)$ and $F_P(q^2)$. The information from the electron scattering and beta decay of tritium allows

us to estimate these form factors [228]. The values for $F_V$ and $F_M$ follow from the isotriplet vector current hypothesis [186] and from the results of elastic scattering by $^3He$ and $^3H$. A world average for $q^2 = 0.954\, m_\mu^2$ muon capture by a helium reaction yields

$$F_V(0.954\, m_\mu{}^2) = 0.834 \pm 0.011,$$
$$F_M(0.954\, m_\mu{}^2) = -13.969 \pm 0.052.$$

The value of the axial form factor measured by $^3H$ beta decay corresponds to $F_A(0.954\, m_\mu^2) = 1.052 \pm 0.005$.

The pseudoscalar form factor can be estimated using PCAC prediction (see section 3.7), which is expressed via the axial form factor with a $\vec{q}$ - dependence. The calculated data, $\Lambda_t = 1497\, s^{-1}$, agrees with the experiment. In addition, impulse approximation calculations were performed in reference 228. The effective Hamiltonian was found by summing up the on-shell one-body currents from each of the nucleons. However, the calculation, $\Lambda_t = 1304\, s^{-1}$, was not close to the experimental result. The more accurate microscopic calculations were performed later. The calculation was studied using a hybrid chiral effective field theory approach ($\chi$ EFT) in reference 229, which yielded $\Lambda_t = 1499 \pm 16\, s^{-1}$; this agreed with the experiment. There were two main sources for the error: the experimental uncertainty on the tritium half-life of the beta decay, and the calculation of radiative corrections. The comparison of this rate with experimental date yields $g_P(0.954\, m_\mu{}^2) = 8.13 \pm 0.6$ [210, 229].

Later calculations were performed in reference 230, using a realistic model for the nuclear Hamiltonian and weak transition operator, which was derived either in meson-exchange or in the χEFT framework; this obtained the result, $\Lambda_t = 1484 \pm 13\, s^{-1}$, in agreement with the experiment. Fig.2 in reference 210 summarises the different theoretical results for $\Lambda_t$ in comparison with the experiment. The muon capture in $^3He$ through the two (*nd*) and three-body (*nnp*) channels was considered in reference 231. This indicated that the main contributions to the rates of both reactions are from regions with the highest neutrino energies. The calculation, $\Lambda_{nd} = 544\, s^{-1}$, is in agreement with the experiment. The $\Lambda_{nnp} = 154\, s^{-1}$ roughly agrees with the experiment.

The reactions of the muon capture by $^4He$

$$\begin{aligned} \mu^- + {}^4He &\rightarrow t + n + \nu_\mu \qquad (97.75\%) \\ &\rightarrow d + n + n + \nu_\mu \qquad (2\%) \\ &\rightarrow p + n + n + n + \nu_\mu \qquad (0.25\%), \end{aligned}$$

were considered in reference 8. The capture reaction has a very low rate, (e.g. $\Lambda^{\exp}_{^4He} = 364 \pm 46\, s^{-1}$ [232a]) and is therefore difficult to study.

The muon capture in different nuclei was considered in references 8 and 232b. The total muon capture rates from $^6Li$ to $^{18}O$ were indicated in Table 1 from reference 232b. Their values range between $\sim 10^3\, s^{-1}$ and $\sim 10^5\, s^{-1}$, which are in good agreement with the experimental data.

## 4.3. The particle correlations in muon capture

The theory of angular correlations in nuclear transitions was given in reference 233. More accurate information on weak interaction coupling constants in beta-decay and muon capture can be obtained from the study of the angular correlations of the participating particles, due to the weaker effect of the nuclear structure on the correlation coefficients in comparison with the process probability. In fact, angular correlation experiments have been important in the determination of weak interaction constants in beta-decay. Electron-neutrino angular correlation provides primary experimental evidence that the V-A interactions are mainly responsible for beta-decay. As for muon capture, the neutron-muon spin correlation can measure the $g_P$ [234].

The numerous correlations can arise via the excited state of the daughter nucleus with the subsequent emission of the gamma-ray:

$$\begin{array}{l} \mu^- + (A,Z)_{j_0} \rightarrow (A,Z-1)^*_{j_1} + \nu_\mu \\ \qquad\qquad\qquad\quad \downarrow \\ \qquad\qquad\qquad\quad (A,Z-1)_{j_2} + \gamma. \end{array}$$

The numerous correlations between the neutrino and gamma-ray have been considered in references 235–247. When the muon capture results in the excitation of the nucleus and the subsequent emission of the gamma-ray, the probability of the transition $j_0 \xrightarrow{\mu} j_1 \xrightarrow{\gamma} j_2$ takes the form of

$$W = \left\langle H_\gamma H_\mu \rho H^*_\mu H^*_\gamma \right\rangle,$$

where $H_\mu$ and $H_\gamma$ are both matrix elements of the muon capture (which was given in section 4.2) and gamma-transition, respectively. The brackets $\langle\ \rangle$ stand for the summation of those initial, intermediate, and final states which are not measured in the experiment. The matrix element of radiative transition, which omitted common factors that do not affect the correlation, takes the form of [233a, 248]

$$H_\gamma = \int \Psi^*_{j_2\mu_2} \hat{\vec{j}}\, \vec{A}_{\vec{k}}(\vec{r}) \Psi_{j_1\mu_1} d\vec{r}$$

where $\Psi_{j_1\mu_1}$ and $\Psi_{j_2\mu_2}$ are the wave functions of the nucleus in the initial and final state of radiative transition, respectively; $\hat{\vec{j}}$ is current operator of nucleons in the nucleus; and $\vec{A}_{\vec{k}}(\vec{r}) = \vec{\varepsilon}\, e^{-i\vec{k}\vec{r}}$ is vector-potential of electro-magnetic field. The following cumbersome calculations were also completed [241]:

$$H_\gamma = \sum_\beta C^{j_1\mu_1}_{L\beta j_2\mu_2} b_{L\eta} A_{L\pi} D^{L\ *}_{\beta\eta}(\varphi\theta 0)$$

,

where $D^L_{\beta\eta}(\varphi\theta 0)$ is the matrix rotation of the photon momentum, $\vec{k}$, and the polarisation vector, $\vec{\varepsilon}$, is in the direction of the coordinate axis *z* along, $\vec{k}$. $A_{L\pi}$ is the reduced matrix element of the radiative transition of multipole *L*. $\eta$ is +1 (-1) for the right-handed (left-handed) circular polarization of the photon. For the electric and magnetic multipole radiation of character $2^L$, we have used $b^{mag}_{L\eta} = \sqrt{2L+1},\ b^{el}_{L\eta} = \eta\, b^{mag}_{L\eta}$.

However, we have only considered the pure multipole radiation of the character $2^L$.

It is necessary to average over the muonic and nuclear polarization states using the density matrix $\rho$. If there is an Auger conversion between the two sublevels of the *K*-shell, the density matrix $\rho$ will determine the time dependence of the correlation coefficients [24, 241]

$$\rho(t) = \frac{p}{2j_0+2}\left(1+\frac{6\lambda_+}{2j_0+3}\hat{\vec{\sigma}}_\mu \vec{F}\right)P_+ + \frac{1-p}{2j_0}\left(1-\frac{6\lambda_-}{2j_0-1}\hat{\vec{\sigma}}_\mu \vec{F}\right)P_-,$$

, where $\vec{F} = \vec{j}_0 + \vec{S}$ is the total angular momentum of the mesoatom on the *K*-shell; $P_\pm$ is the projection operator on h.f.s. with $F = F_\pm$; $p$ is the population probability of the state $F_+$; $\hat{\vec{\sigma}}_\mu$ is the unit vector in the direction of muon polarization; $\lambda_\pm$ are the muon polarization values in the states, $F_\pm$. In the case of conversion between the two K-shell sublevels both $p$ and $\lambda_\pm$ are varying with time, which determines the time dependence of $\rho$. For the positive magnetic moment of the nucleus, when the $F_+$ level is higher than the $F_-$, we have $p = p^0 e^{-Rt}$, where $R$ is the conversion rate. When in the matrix element $H_\gamma$ we expand the potential of the electromagnetic wave in a series of multipoles we obtain the general expression for the angular correlation: $\vec{\nu}$, $\vec{k}$, and $\vec{\sigma}_\mu$ i.e., between the neutrino and photon momentum, and the muon polarization respectively for the allowed transition [235, 238, 239, 241].

$$W = 1 + \alpha\vec{\sigma}_\mu \cdot \hat{\vec{\nu}} + (\beta + \gamma\vec{\sigma}_\mu \cdot \hat{\vec{\nu}}) P_2(\hat{\vec{k}} \cdot \hat{\vec{\nu}}) + \eta(\hat{\vec{k}} \cdot \vec{\sigma}_\mu)(\hat{\vec{k}} \cdot \hat{\vec{\nu}}) +$$

$$+ \xi(\hat{\vec{k}} \cdot \hat{\vec{\nu}})\left[(\vec{\sigma}_\mu \times \hat{\vec{\nu}}) \cdot \hat{\vec{k}}\right] + \left[\varepsilon\vec{\sigma}_\mu \cdot \hat{\vec{k}} + \varsigma(\vec{\sigma}_\mu \times \hat{\vec{\nu}}) \cdot \hat{\vec{k}}\right] P_3(\hat{\vec{k}} \cdot \hat{\vec{\nu}})$$

where $\hat{\vec{\nu}}$ and $\hat{\vec{k}}$ are unit vectors, $P_i(\hat{\vec{k}} \cdot \hat{\vec{\nu}})$ is the Legendre polynomial. The gamma-neutrino correlation in the first forbidden nuclear muon capture has an additional term, $-(\kappa - \lambda\hat{\vec{\sigma}}_\mu \cdot \hat{\vec{\nu}}) P_4(\hat{\vec{k}} \cdot \hat{\vec{\nu}})$ with the correlation coefficients obtained in reference 237.

Let consider the allowed Gamow-Teller transition, $0^{\pm} \xrightarrow{\mu} 1^{\pm} \xrightarrow{\gamma} 0$, for an unpolarized muon capture. The initial orbital angular momentum is zero as the muon capture is realized from the 1s state (*K*-shell). Therefore, the whole angular momentum is determined by the muon spin i.e. 1/2. The neutrino helicity (i.e., the spin projection in the direction of emission) is negative: $\mu_{\nu_\mu} = -1/2$. Table 6 illustrates the conservation of the projections of the angular momenta on the direction of the neutrino emission: $\vec{\nu}$.

**Table 6. The projections of the angular momenta of a muon, a neutrino, and an intermediate nucleus.**

| $\mu_\mu$ | $\mu_{\nu_\mu}$ | $\mu_{j_1}$ |
|---|---|---|
| +1/2 | -1/2 | +1 |
| -1/2 | -1/2 | 0 |

As follows from the conservation of the projection of the angular momentum, the $m_{j_1} = -1$ sublevel cannot be populated. Therefore, the nucleus is orientated on the direction of the neutrino emission. Due to the conservation of space parity in the radiative transition the anisotropy of gamma-ray emission could be

$$W = 1 + \beta P_2(\hat{\vec{k}} \cdot \hat{\vec{\nu}}) .$$

The coefficient $\beta$, which determines the angular correlation of the photon and the recoil nucleus (neutrino) in the capture of an unpolarized muon, depends only on the interference of the correction terms (with the main pseudoscalar interaction $g_P$) with the Gamow-Teller main term for the transition. This is a consequence of the fact that the correlation, $P_2(\hat{\vec{k}} \cdot \hat{\vec{\nu}})$, must contain the "*d* waves of the neutrino" (the main contribution to the correlation is the interference of the *s*-waves and *d*-waves of the neutrino), which in an allowed muon capture can only arise from the Hamiltonian terms that contain the operator *p* or from terms in the matrix element that contain the Bessel function, $j_2(\nu r)$ [235]. Therefore, $\beta$ is proportional to $g_P$ and the gamma-neutrino correlation experiment could be decisive for the determination of the pseudoscalar contribution.

Grenacs et al. [249] have proposed a method to observe the correlations in terms of the Doppler broadening of the transition gamma ray due to the recoil of the nucleus upon the neutrino emission. The forms of the Doppler broadened gamma ray lines are given in Fig. 25 from reference 249.

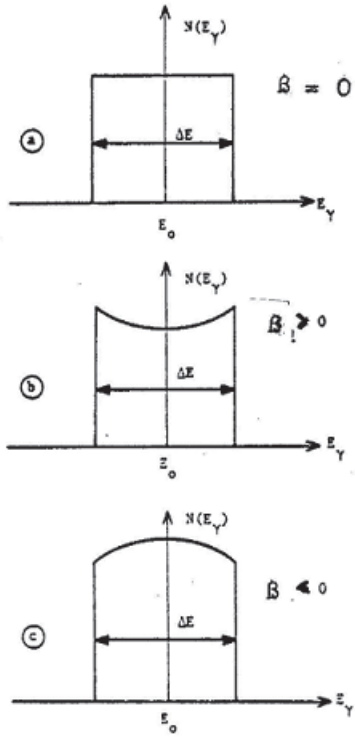


Fig. 25**:** The forms of the Doppler broadened gamma ray lines in a muon capture by an unpolarised muon taken from reference 249.

If the lifetime of the excited nucleus is smaller than the time of its slowing down, the gamma ray line has to be Doppler shifted due to the recoil of the nucleus upon the neutrino emission. Since the neutrino and nucleus have equal and opposite momenta, the energy of the $\gamma$ ray is given by $E = E_0(1 - v_0 \hat{k} \cdot \hat{v})$, where $E$ and $E_0$ are the energies of the Doppler-shifted $\gamma$ ray and of the $\gamma$ ray in the rest frame of the emitting nucleus, respectively. The Doppler broadened gamma ray is $\Delta E = 2E_0 v_0$, where

$v_0 = [m_\mu - (E_f - E_i)]/(A M_N)$ is the internuclear recoil velocity. The number of gamma ray $dn = N(E)\,dE$ for an unpolarized muon capture is given by the equation,

$$N(E) = 1 + \frac{1}{2}\beta\left[3\left(\frac{E - E_0}{E_0 v_0}\right)^2 - 1\right].$$

Experimental and theoretical efforts have concentrated on the $0^+ \xrightarrow{\mu} 1^+ \xrightarrow{\gamma} 0^+$ muon capture sequence:

$$\mu^- + {}^{28}Si \rightarrow {}^{28}Al^*(2201keV) + \nu_\mu$$
$$\downarrow$$
$${}^{28}Al^{**}(972.4keV) + \gamma.$$

Fig. 26 shows a nuclear level diagram of the lower levels in ${}^{28}Al$. The transitions indicated by heavy lines have been observed to be Doppler broadened in the initial experiment by Welsh et al. [250, 251].

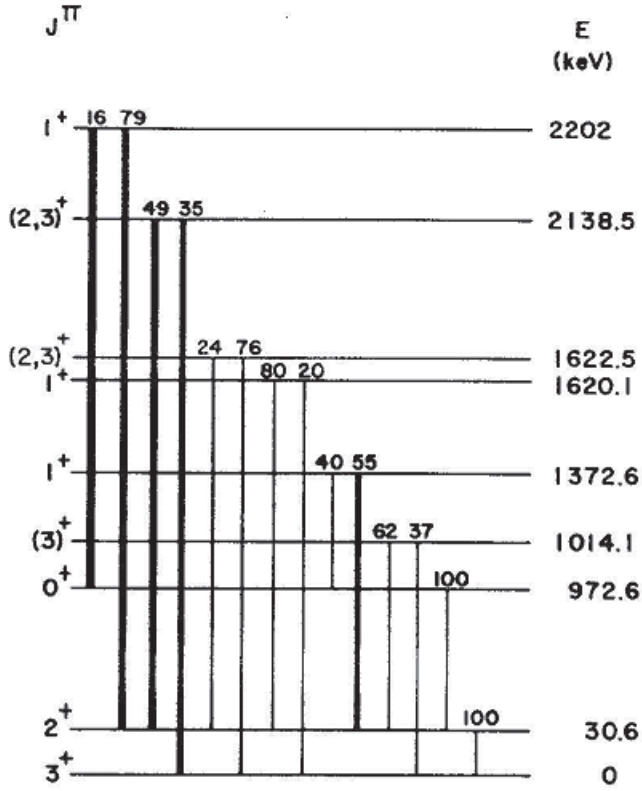


Fig. 26 Nuclear level diagram of $^{28}Al$ . The transitions denoted by heavy lines are observed to be Doppler broadened in the experiment from references 250 and 251.

The resulting 1229*keV* $\gamma$ ray had a Doppler broadened width of 9*keV*, which is wide enough to allow a line-shape measurement of the angular correlation using the detector with a ~2*keV* resolution (see Fig. 27). The value, $\beta = 0.29 \pm 0.30$, obtained from $^{28}SiO_2$ data, had high errors. They indicated that the result of the measurement of $\beta$ was in agreement with the theoretical predictions, but obtained, $g_P/g_A = 5 \pm 8$, which was

imprecise primarily as a result of the background level and detector resolution; this was in comparison with the value 7, which was predicted by PCAC for the free nucleon.

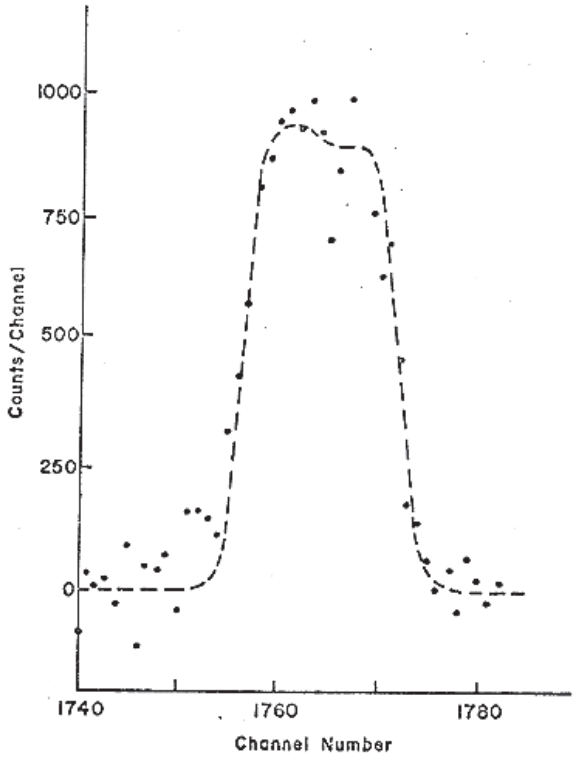


Fig. 27: The energy spectrum of the 1229 *keV* line in $^{28}Al$ from a muon capture in $^{28}Si$ (natural); this was taken from references 250 and 251.

Low statistics and poor signal-noise precluded a sensitive measurement of $g_P$ in that experiment. Brudanin et al. [252] performed a more precise measurement of the $\gamma - \nu$ correlation in this reaction. They obtained the

value, $\beta$ = 0.307 ± 0.041, and extracted, $g_P/g_A = 3.4 \pm 1.0$, which indicated a substantial quenching from the prediction of PCAC and the pion-pole dominance. That experiment, however, suffered from serious backgrounds that distorted the observed line-shape of the $1229eV$ $\gamma$ ray of interest.

Moftah et al. [253] obtained the energy spectra of the $1229keV$ gamma ray in $^{28}Al$ (see Fig. 28) and extracted $\beta = 0.360 \pm 0.059$.

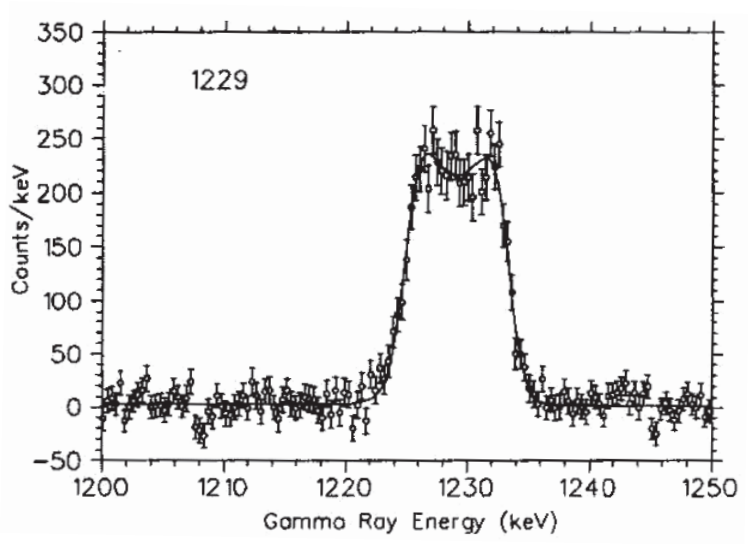


Fig. 28 The energy spectra in the region of the $1229keV$ gamma rays in $^{28}Al$, along with the result of the simultaneous fit taken from reference 253.

They obtained, $g_P/g_A = 5.3 \pm 2.0$, using Ciechanowicz's calculation [254] and $g_P/g_A = 4.2 \pm 2.5$ with the calculations by Parthasarathy and Sridhar [255]. In both cases the results are somewhat below the PCAC prediction.

This difference was explained by the other nuclear wave functions of the 70th. Using the calculations of Junker et al. [256a], they received $g_P/g_A = 0.0 \pm 3.2$, which was substantially smaller than the prediction of PCAC and the pion-pole dominance. The calculations of Junker et al. were very successful at explaining the Gamow-Teller transitions in muon capture, $\beta^+/\beta^-$ -decay, $(n,p)/(p,n)$ data for 1s-0d neutron-rich ($N >> Z$) nuclei (e.g. $N \approx 20$ and 28) [257]. At the same time in agreement with the Measday discussion [8], the alternative nuclear model of the $^{28}Si$ consideration [256b, c] could result in a different conclusion about $g_P$, namely $g_P = 5.1 \pm 0.8$, which would clearly be more satisfying.

The consideration of the correlation between muon spin (i.e. a polarized muon beam) with a gamma ray emission of $1229keV$ is discussed in reference 258. This obtained $-1 \le g_P/g_A \le 1.3$, which again confirmed the strong quenching of $g_P/g_A$, as reported earlier. However, in agreement with the Measday discussion, [8] both these experiments are subject to systematic uncertainties in their experimental and theoretical interpretations. It is necessary to consider the cascade influence from high levels, as well as the 5% (approx.) admixture of $^{29}Si$ in the natural silicon target. At last the alternative consideration of nuclear model [256c] results in $g_P/g_A = 4.4 \pm 0.3$. Previously, it has been known that $^{28}Si$ is not a simple shell-model nucleus and extensive tests are needed [8]. In fact, the coefficient $\beta$ coincided in different experiments at approximately 30% in agreement with the theory; however, the extracted pseudoscalar coupling,

$g_P/g_A$, was found to be nuclear-model dependent, but the results suggest some quenching from the PCAC prediction.

In the absence of a gamma ray, or without its registration, the only correlation is the asymmetry of the recoil nuclei relative to the polarization vector of muons:

$$W = 1 + \alpha\ \vec{\sigma}_\mu \cdot \hat{\vec{\nu}}\ .$$

The angular distribution of the recoil nuclei was considered in references 223, 239, 240, and 259–264. However, the coefficient $\alpha$ is relatively small due to the strong depolarization of the muon, especially in a non-zero spin, $j_0$, of the initial nucleus: e.g., $\alpha \leq 0.06$ for a muon capture by $^{11}B(3/2)$ [264]. An attempt to measure the residual muon polarization and angular correlation in the muon capture by gaseous $^3He$ at 0.75 atm. was realized by Dugan et al. [265]. The obtained muon polarization was 3.4 ± 1.1%, which limits the value of $\alpha$ and any possible information on weak coupling constants.

## 4.4 Radiative muon capture

Radiative muon capture (RMC) by free proton,

$$\mu^- + p \rightarrow n + \nu_\mu + \gamma\ ,$$

is a rather rare reaction, which has a rate that is roughly $10^{-4}$ times the ordinary muon capture (OMC) rate. In spite of the very difficult experimental investigation of radiative muon capture, this process enables us to obtain important information on the weak interaction form factors

and on $g_P(q^2)$. Due to three particle final kinematics, the investigation of the *q*-dependence of weak interaction form factors is possible within the limits of $-m_\mu^2 \le q^2 \le m_\mu^2$. This is contrary to the usual muon capture for $q^2 \approx m_\mu^2$. The reaction of the radiative muon capture by a proton can be chiefly described by the diagrams presented in Fig. 29, taken from reference 224.

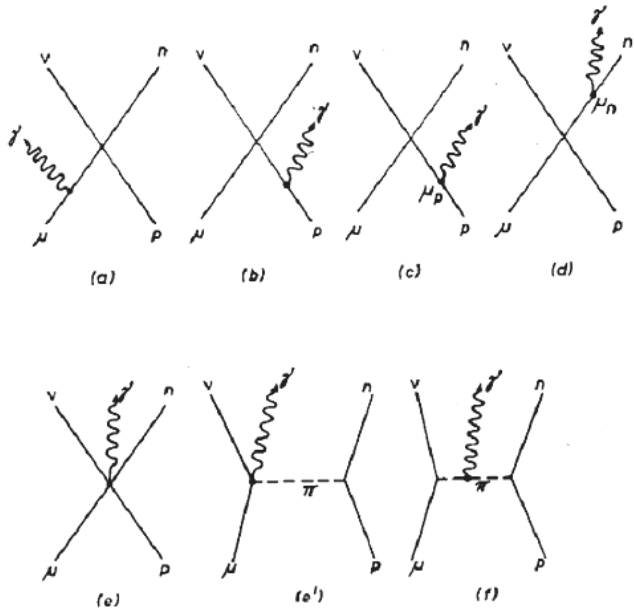


Fig. 29: Diagrams of radiative muon capture. The diagrams with $\mu_p$ and $\mu_n$ indicate the couplings via the anomalous magnetic moments of the proton and neutron, respectively.

The radiative muon capture by a proton was studied theoretically in reference 266. The ratio of $\tilde{\Lambda}_t$ and $\tilde{\Lambda}_s$ in a radiative muon capture by a proton is opposite to an ordinary muon capture by a proton due to the gamma ray emission of the particle with a spin 1 in agreement with calculations in reference 267: $\tilde{\Lambda}_t = 0.05\, s^{-1}$ and $\tilde{\Lambda}_s = 10^{-2}\, \tilde{\Lambda}_s$. The radiative muon capture by a proton is a doubly rare reaction, primarily because an ordinary muon capture corresponds to only about $\sim 10^{-3}$ of the muon decay (see sec. 3.7). Another factor arises from the ratio, $\sim 10^{-4}$, from the radiative muon capture to an ordinary muon capture by a proton. Therefore, experiments on radiative muon capture are very difficult to perform, especially with regard to hydrogen where an ordinary capture is rare in comparison with the decay of a muon in a *K* orbit. The bremsstrahlung of electrons from $\mu$ decay drowns the observable effect below ~60*MeV*. In order to exclude this background, the energies of the registered $\gamma$ rays are above 57*MeV* and can rise up to a maximum photon energy of 100*MeV*. Due to the low branching ratio, an intense muon beam and a high efficiency detector are required. The photon energy spectrum of radiative muon capture on the proton was realized for the first time in the experiment for LHD at TRIUMF [268a], as demonstrated in Fig. 30. The problem of background, including cosmic rays and so on, was discussed in this paper. In this experiment, they obtained the branching ratio to the muon decay, $(1.6 \pm 0.3) \times 10^{-8}$, for 250 ± 21 events.

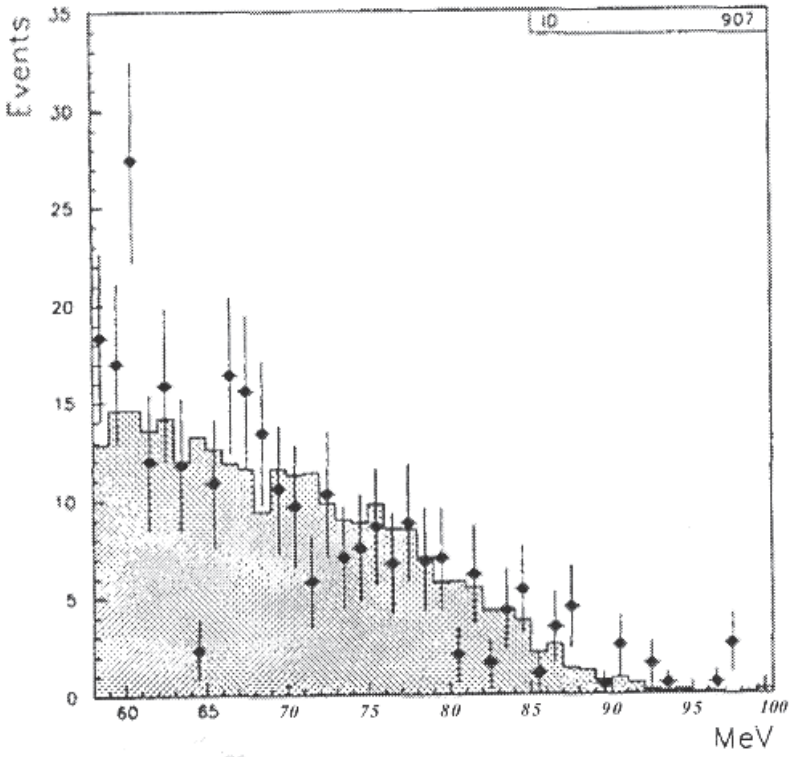


Fig. 30: The photon energy spectrum of the radia[illegible]n taken from reference 268a.

Later, experimental attempts for LHD were undertaken in references 268b and c. The final result was the accumulation of 279 ± 0.26 events for radiative muon capture with energies of $\gamma$ ray above $60MeV$ and the branching ratio of $(2.10\pm0.21)\times10^{-8}$. The result is very sensitive to $g_P(q^2)$, which corresponds to the discussion in reference 8. Surprisingly, the value of $g_P$ deduced in references 268b and c is ~1.5 times larger than the PCAC prediction. Many suggestions have been made to explain this

difference, including a supposition about $p\mu p$ molecular levels [268d]; there is, however, no confidence in any of these guesses.

Essentially, the rate of radiative muon capture is increased for the nucleus $Z > 1$ in the reaction

$$\mu^- + (A,Z) \rightarrow (A,Z-1) + \nu_\mu + \gamma \ ,$$

which has been studied in several nuclei over many years; all of these results have achieved a consensus. The first theoretical studies on radiative capture by nuclei were made by Cantwell [269] and Primakoff [223a]. Bernstein [270] calculated the spectrum and circular polarization of photons for partial transitions, including muon capture by $^{12}C$. Very complicated and cumbersome calculations of the radiative muon capture by nuclei were presented in references 224 and 271. The matrix element for radiative muon capture can be written as a sum of diagrams in Fig. 29:

$$M = M(a) + M(b) + M(c) + M(d) + M(e) + M(f) \ ,$$

where $M(a) = -(\tilde{V}_\lambda + \tilde{A}_\lambda)[\overline{u}_\nu \gamma_\lambda (1+\gamma_5) S(\mu')(\vec{\gamma}\cdot\vec{\varepsilon})u_\mu]$,

$\tilde{V}_\lambda = \langle \overline{n} | V_\lambda | p \rangle$ , and $\tilde{A}_\lambda = \langle \overline{n} | A_\lambda | p \rangle$ were presented in section 3.7.

$$M(b) + M(c) + M(d) = \left[\overline{u}_n (V_\lambda + A_\lambda) S(p')(\vec{\gamma}\cdot\vec{\varepsilon} + \right.$$

$$\left. \frac{\mu_p}{2M} \sigma_{\alpha\beta} k_\beta \varepsilon_\alpha) u_p + \overline{u}_n \frac{\mu_n}{2M} \sigma_{\alpha\beta} k_\beta \varepsilon_\alpha S(n')(V_\lambda + A_\lambda) u_p \ \right] \times L_\lambda$$

where $L_\lambda$ is the lepton matrix element given in section 3.7, as well as $V_\lambda$ and. $A_\lambda$.

$$M(e)+M(e')=\bar{u}_n\left[\ g_M\sigma_{\lambda\beta}\varepsilon_\beta\frac{1}{2M}+g_P^L\gamma_5\varepsilon_\lambda\frac{1}{m_\mu}\ \right]u_pL_\lambda$$

and

$$M(f)=-\left[\bar{u}_n g_P^H\gamma_5\frac{2\vec{\varepsilon}\cdot\vec{\nu}}{q_L^2+m_\pi^2}u_p\ \right]\left[\bar{u}_\nu(1-\gamma_5)u_\mu\ \right],$$

and $S(p)=\dfrac{1}{i\vec{\gamma}\cdot\vec{p}+m}$ is the propagator for fermion, where $m$ is the mass of the fermion (muon, proton, or neutron): $\mu'_\lambda=\mu_\lambda-k_\lambda$, $p'_\lambda=p_\lambda-k_\lambda$ and $n'_\lambda=n_\lambda-k_\lambda$. $\mu_\lambda, p_\lambda, n_\lambda$, and $\nu_\lambda$ are the muon, proton, neutron, and neutrino momentum four-vectors in the initial and final state, respectively. $k_\lambda$ and $\varepsilon_\lambda$ are the photon momentum and polarization four-vectors; the indexes *L* and *H* correspond to lepton and hadron, respectively, for the $\gamma$ emission.

The *q*-dependence of $g_P(q^2)$ obtained in the framework of PCAC (see section 3.7) occurs a different in diagrams in Fig. 29. The *q*-dependence corresponds to the square of energy and momentum transfer at the vertex of the weak interaction for diagrams (*a*) and (*e'*),

$$q_L^2=(p-n)^2=(\mu-\nu-k)^2,$$

while for other diagrams it is,

$$q_H^2 = (p'-n)^2 = (\mu-\nu)^2 .$$

Therefore, we have for both (*a*) and (*e'*) diagrams,

$$g_P^L = \frac{2M\,m_\mu}{m_\pi^2 + (\mu-\nu-k)^2}\, g_A ,$$

and for other diagrams,

$$g_P^H = \frac{2M\,m_\mu}{m_\pi^2 + (\mu-\nu)^2}\, g_A .$$

In this result we can have $g_P^H / g_P^L = 3$ for the maximum energy of a photon (i.e. $g_P$ in a radiative muon capture could exceed essentially its value in an ordinary muon capture).

Following the procedure explained in section 4.2, we can obtain an effective non-relativistic Hamiltonian for the radiative muon capture. However, the expression of $\bar{H}_{eff}^{r\mu}$ is very complicated and I refer to references 224 and 271 in order to see the final result.

By the way, $g_P(q^2)$ can be written in the form

$$g_P(q^2) = \frac{m_\pi^2 + m_\mu^2}{m_\kappa^2 + q^2}\, g_P ,$$

where $g_P \equiv g_P(m_\mu^2)$ for normal muon capture in framework of PCAC hypothesis (see sec. 3.7). An alternative form is also possible [272, 273]:

$$g_P = 8\rho \frac{m_\mu^2 + m_\pi^2}{q^2 + m_\pi^2} g_A ,$$

where $\rho$ reflects a possible deviation from the PCAC prediction.

It is possible to consider not only one pion exchange but also the poles that have other intermediate states, such as nucleon anti-nucleon exchange and so on. Such a diagram can be added by using any constant $\delta$, because the mass of the intermediate state is considerably larger than the pion mass. The ratio, $R(x)$ of the photon spectrum of the radiative muon capture for $^{40}Ca$ to ordinary muon capture was investigated in reference 224: $x = k/k_m$, where $k_m$ is the maximum photon energy. This introduces the parameters, $\rho$ and $\delta$, to $g_P^L$, $g_P^H$,

$$g_P^L = 8\rho g_A \frac{m_\pi^2 + m_\mu^2}{m_\pi^2 + 2m_\mu k_m - m_\mu^2 + 2k_m^2 x(1-x)} + \delta$$ , and

$$g_P^H = 8\rho g_A \frac{m_\pi^2 + m_\mu^2}{m_\pi^2 - m_\mu^2 + 2m_\mu k_m (1-x)} + \delta$$ .

Case III in Fig. 31 gives the magnitude and sign of $g_P$, as predicted by Goldberger and Treiman [273].

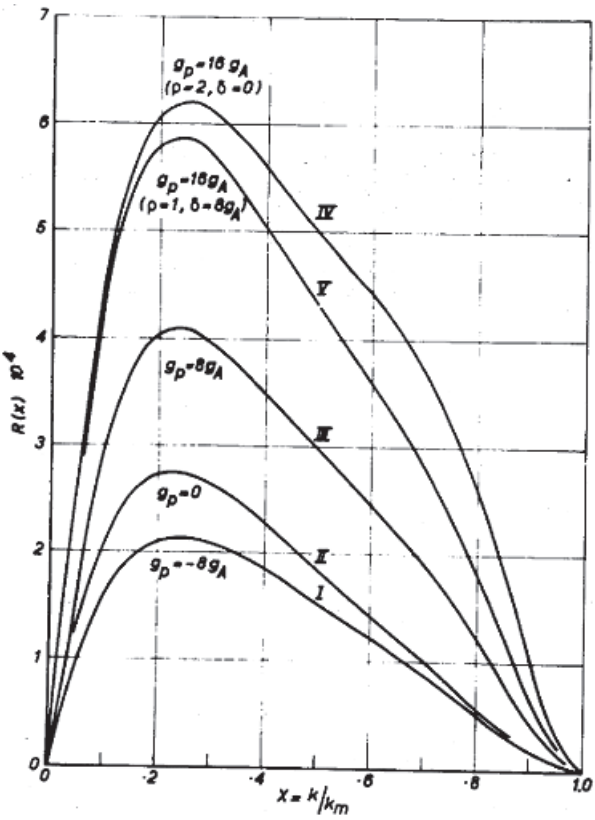


Fig. 31: The energy spectrum for the photon in a radiative muon capture in $^{40}Ca$ (taken from Rood and Tolhoek [224]). In experiments, the typical maximum photon momentum is $k_m = 91 MeV$ and $E_\gamma \geq 57\,MeV$ (i.e., $x = k/k_m \geq 0.63$).

The $g_P(q^2)$ could also be written in the form,

$$g_P(q^2) = \frac{m_\pi^2 + m_\mu^2}{m_\pi^2 + q^2} g_P + \frac{q^2 - m_\mu^2}{m_\pi^2 + q^2} g_A \delta \quad ;$$

this, was used to calculate the photon spectrum for the radiative muon capture in the allowed $j_0 \xrightarrow{\mu} j_0 + 1$ transition presented in Fig. 32, which was taken from references 271 and 274.

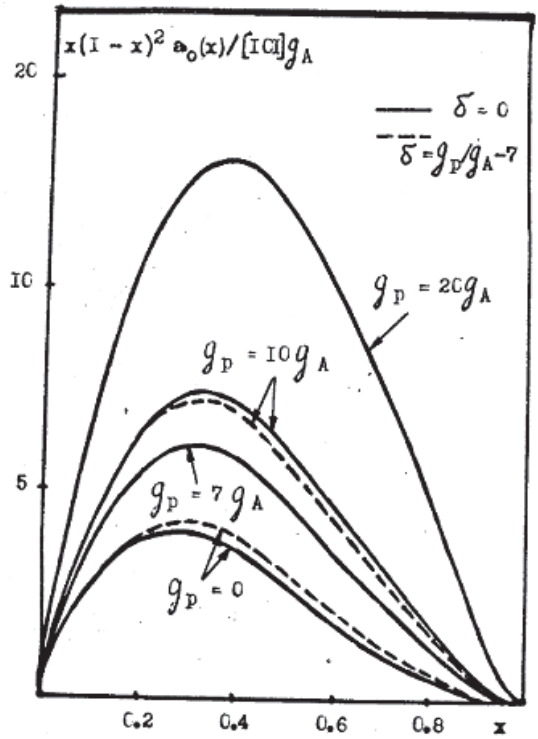


Fig. 32: The energy spectrum for the photon in a radiative muon capture for allowed $j_0 \xrightarrow{\mu} j_0 + 1$ transition. This was taken from references 271 and 274, where the nuclear matrix element [101] is determined by Morita and Fujii in reference 222.

The gamma-gamma correlation, $P_2(\hat{k}_n \cdot \hat{k}_r)$, in the reaction,

$$\mu^- + (A,Z)_{j_0} \rightarrow (A,Z-1)^*_{j_1} + \nu_\mu + \gamma_\gamma$$
$$\downarrow$$
$$(A,Z-1)^*_{j_2} + \gamma_n, \quad ,$$

was calculated in references 244, 271 and 274. The calculated correlation coefficient, $\tilde{a}_2(x)$, was presented in Fig. 33. This demonstrated a strong dependence on $g_P$.

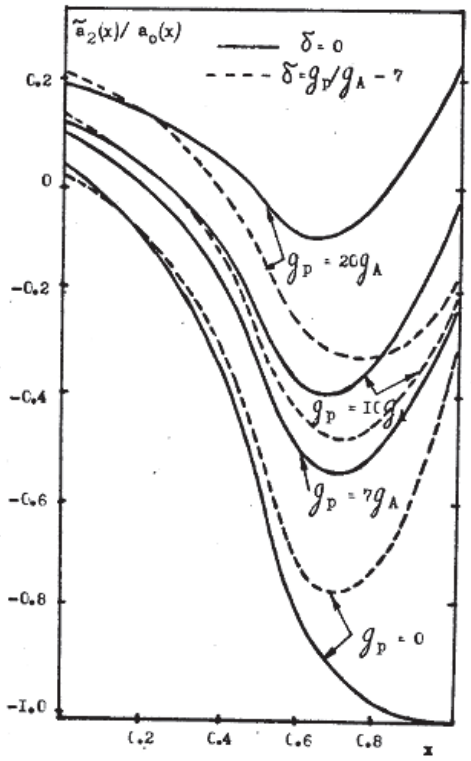


Fig. 33: The gamma-gamma correlation in a radiative muon capture for allowed $j_0 \xrightarrow{\mu} j_0 + 1$ transition taken from references 244, 271, and 274.

The experimental investigation of the whole yield of RMC relative to OMC in $^{40}Ca$ resulted in $R = (1.14 \pm 0.09)\cdot 10^{-4}$ and $R = 0.154\cdot 10^{-4}$ for the photon energy $0.57\ MeV \leq E_\gamma \leq 75 MeV$ in reference 275. They also measured the photon asymmetry relative to the muon-spin direction,

$W \sim 1 + \alpha_\gamma \cos\vartheta_{\mu\gamma}$.

This was inconsistent with the PCAC with an obtained negative value of $g_P$. However, the high energy neutron background could be very important in the experiment.

The branching ratio relative to the ordinary muon capture *R* and the photon asymmetry relative to the muon-spin direction were measured for radiative muon capture in $^{40}Ca$ [276]. For ~1200 photon events, the partial branching ratio was $R = (21.1 \pm 1.4)\times 10^{-6}$ for $E_\gamma > 57 MeV$ and the asymmetry $\alpha_\gamma = 0.90 \pm 0.50$ for $E_\gamma > 63.5 MeV$. Fitting the photon spectrum to the theory gave the value, $g_P = (6.5 \pm 1.6)\, g_A$.

The investigations by RMC of a photon energy spectrum above $57 MeV$ for two nuclear targets $^{16}O$ and $^{40}Ca$ were performed in reference 277. They measured the muon-spin photon angular correlation, $\alpha_\gamma$, which obtained $g_P = (4.5 \pm 1.5)\, g_A$ for $^{40}Ca$ and $g_P$; this exceeded $12\, g_A$ for $^{16}O$.

The photon asymmetry of $\alpha_\gamma$ and the partial branching $R$ in $^{40}Ca$ were measured in reference 278. Based on 2500 events, they obtained the value of $\alpha_\gamma = 1.32^{+0.57}_{-0.47}$ from a fit to the photon time spectrum and $g_P < 5.2 g_A$.

Finally, a photon asymmetry measurement in RMC by $^{40}Ca$, has been carried out for $57MeV < E_\gamma < 95MeV$ at TRIUMF [279]. The data sample consisted of 5200 high-energy RMC photon candidates. They measured the value for the energy-averaged photon asymmetry $\alpha_\gamma = 1.00 \pm 0.23$. The extracted value $g_P / g_A << 14.5$ was obtained using the framework of the modified impulse approximation model.

In spite of the sensitivity of the radiative muon capture to the value $g_P$, its reliable extraction from this rare process is still open, depending also on nuclear models.

## 4.5 Exchange-current effects

The meson-exchange current (MEC) effects in electroweak interactions, including muon capture, in nuclei [280282] could be important when considering the possible renormalization of the weak coupling form factors [283]. The MEC effects were considered for muon capture by simplest nuclei: deuterium [280a, 208a] and $^3He$ [281]. Earlier we considered the impulse approximation (IA), where the effective Hamiltonian was found by summing up the on-shell one-body currents from each of the nucleons with their additive contribution (see sec. 4.2). However, the pion current $J_\pi$ in the equation $(-\Box^2 + m_\pi^2)\varphi_\pi = J_\pi$, as

well as $\varphi_\pi$ should be changed in the presence of MEC. The prediction of the axial constant, $g_A(0)$, in the PCAC framework also could be other, moreover $g_P(q^2)$ determined by the one-pion pole exchange. The MEC is determined by a Feynman graph of a one-pion exchange between a nucleon interacting with a lepton pair and other nucleons of the nucleus, which corresponds to Born's contribution to the MEC. Other nuclear weak MEC operators are defined by the set of Feinman graphs in Fig. 34, taken from reference 183b.

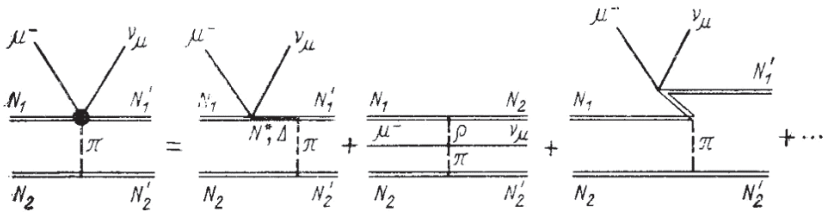


Fig. 34: The MEC diagrams, taken from reference 183b.

The first graph corresponds to $\Delta(1236)$ - isobar excitation with $\pi$-exchange; the second one is responsible for virtual $\rho \to \pi \mu \nu_\mu$ decay and the third graph is the excitation of the nucleon-antinucleon pair. MEC is illustrated by these diagrams, however, many others also exist. At the same time, a single $\pi$ - meson exchange provides a main contribution to MEC with a possible exchange also by $\rho$, $\omega$, $\phi$ and others vector mesons. The contribution of MEC to the muon capture in deuteron is 6.5%, which is in agreement with the pioneering work in reference 280a.

The renormalization of axial and pseudoscalar weak formfactors was predicted [283] up to $g_A^{nucleus} \approx 0.75\, g_A$ and $g_P^{nucleus} \approx \frac{1}{3} g_P$ [183b]. However, the procedure for the extraction of the $g_P^{nucleus}$ from experimental data depends on the nuclear models. The single-nucleon pion production amplitudes and two-body exchange current operators were constructed in reference 280b. The connection between exchange currents and the structure of a nuclear potential was analysed and the theorectical results were compared with the experimental data.

The calculation of MEC contribution for the muon capture by $^3He$ indicated that the dominant addition to the one-nucleon prediction (impulse approximation, IA) for the three-nucleon Gamow-Teller matrix element arose from the $\Delta$ - isobar excitation in the axial current [284] as well as to the magnetic moment in the vector current [280c]. The possible contribution from the MEC corrections to the muon capture by $^3He$ is also discussed in references 228 and 230. These cumbersome and complicated analytical calculations can be found in references 280b and d.

The possible competition between the neutrino mass and the MEC effects is discussed in reference 282.

The matrix element of lepton current was presented in section 3.7 with the massive left-handed Dirac neutrino in section 2.5. Some formulae for the massive left-handed Dirac neutrino have already been indicated in section 2.5. As the MEC corresponds to the relativistic effects, then both components of the muon wave function should be kept. Following the point nucleus solution, (i.e. Coulomb potential), we have

$F(r) \approx -\alpha ZG(r)/2$ , while $\alpha$ is a fine structure constant. Of course, the small radial component of the muon wave function is quenched, which is a relatively large one, especially for light nuclei. The $0^{\pi_i} \xrightarrow{\mu^-} 1^{\pi_f}$ $(\pi_{i,f} = \pm 1)$ muon capture transition was considered in reference 282. Following this paper, the space part of the weak axial MEC originated from the $\Delta$-isobar excitation. In agreement with results of reference 208a and 282, the axial $\Delta$-excitation current with $\pi$-exchange is

$$G_A^{(3)} = -g_A \frac{2}{9} \frac{m_\pi}{M_\Delta - M} \frac{1}{4\pi} f_{\pi N\Delta}^2 = -g_A \, 23.83 \times 10^{-3} \quad ,$$

(i.e. the MEC corrections, $\sim 24 \times 10^{-3}$, against the leading Gamow-Teller contribution in the first forbidden $\mu$-capture transition). The following numerical data were used: $m_\pi = 140\,MeV, M_\Delta = 1232\,MeV$ for the lowest mass state of the $\Delta$-isobar, $M \approx 939 MeV$ and $f_{\pi N\Delta}^2 / 4\pi = 0.2275$ for the $\pi N \Delta$ coupling [281]. The largest relativistic effect arose from $F(r)$ which for $^3He$ corresponds to about $10^{-2}$. As for the massive neutrino, the estimation of spherical Bessel functions for $q < E$ results in a global factor, $(1 + m_\nu^2/(2q^2))$, where $q \approx 100 MeV$ is the neutrino momentum [282]. Supposing the upper limit to be $m_{\nu_\mu} \le 160\,keV$, then the change of the amplitude will correspond to $m_\nu^2/(2q^2) = 1.28 \times 10^{-6}$. This suggests that the relativistic effect is four orders of magnitude stronger than the neutrino mass contribution [282]. However, the supposition of a

possible heavy sterile neutrino of $m_\nu \sim 100 MeV$ results in the opposite situation when the neutrino mass effect is ~100 times stronger than relativistic ones. The investigation of the muon capture process could be very important for the verification of the neutrino mass problem as well as the MEC effects.

The importance of the MEC contribution to the weak axial current in muon capture by oxygen in the transition $0^+ \to 0^-$ was obtained in reference 285a in agreement with the experimental result in 285b.

## 4.6 T-violation in muon capture

If we consider the movement of the stone (in a vacuum), which was thrown up, in comparison with the film about the fall of the stone, which is demonstrated back, we can see the identity of such movements. It is explained by the time-reversal invariance of Newton's equations in homogeneous gravity field.

The problem of time reversal in quantum mechanics has been discussed since the thirties [286]. On the basis of the CPT theorem, one expects a T-violating interaction to violate the CP-invariance. In 1964, Christenson, Cronin, Fitch, and Turlay discovered the CP-violating effect through the decay of the neutral $K_L$ meson to $2\pi$ mesons [287]; this can be found in reference 288. The discovery of the CP violation in the decay of neutral kaons resulted in the 1980 Nobel Prize in Physics for J. Cronin and V. Fitch. In fact, two *K*-mesons exist: $K_1^0 \to \pi^+ + \pi^-$ with CP = +1 (while CP = +1 for the $\pi^+\pi^-$ state), i.e. the even state, and $K_2^0 \to \pi^+ + \pi^- + \pi^0$ with

CP = -1, i.e. the odd state. The lifetime of $K_1^0$ is $\tau_1 \approx 10^{-10} s$, while $\tau_2 \approx 5 \cdot 10^{-8} s$ is for $K_2^0$. Therefore, two states exist: short $K_S = K_1$ and long $K_L = K_2$. However, in agreement with results from reference 287, $K_L$ has a $2\pi$ state (i.e. $K_L^0 = (1+|\varepsilon|^2)^{-1/2}(K_2^0 + \varepsilon K_1^0)$, where $|\varepsilon| = (2.229 \pm 0.012) \cdot 10^{-3}$ [289]) and the CP-symmetry is violated.

The CP violation was discussed in a number of reviews [35, 201, 290].

A large number of CP violation processes in *B* meson decays have been discovered [291] and a hint of the CP violation in the decay of neutral *D*-mesons was also obtained [292]; this includes $D^0 \to K^- K^+$ and $D^0 \to \pi^- \pi^+$ decays [293].

The Universe is made chiefly of matter, rather than consisting of equal parts of matter and antimatter as might be expected. It can be demonstrated that, in order to create an imbalance in matter and antimatter from an initial condition of balance, the Sakharov conditions must be satisfied [294]. One of these is the existence of the CP violation during the extreme conditions in the first seconds following the Big Bang. The Big Bang should have produced equal amounts of matter and antimatter if the CP–symmetry was preserved and, therefore, there should have been a total cancellation of protons with antiprotons, electrons with positrons, neutrons with antineutrons, and so on. This would have resulted in a sea of radiation in the Universe instead of matter. Since this is not the case, physical laws must have acted differently after the Big Bang with regard to matter and antimatter; thereby, violating the CP-symmetry.

Simultaneously with the verification of the CP violation the CPT-theorem is examined [295].

The possible CP violation is associated with the complex weak coupling constants owing to CP-odd interaction of participating particles. The CP violation appears naturally in unified gauge theories with spontaneous symmetry breaking. This mechanism is possible through the complex vacuum expectation value of Higgs fields. The simplest model of CP breaking through the Higgs-field coupling results in a complex phase in the Cabibbo-Kobayashi-Maskawa mass matrix [296]. However, the effect would be too small ~$10^{-10}$ to be observed, such as in the muon capture. Alongside high-energy physics, the hunt for possible T-violating effects is also realized in low energy physics, including nuclear muon capture.

I should like to discuss the information provided by the research into T-violating effects in muon capture reactions [66, 297–300]. In the case of muon capture by a free proton, only neutron transversal polarization in the direction of $\hat{\vec{q}} \times \hat{\vec{\sigma}}_\mu$ can create a T-violating effect (here $\hat{\vec{\sigma}}_\mu$ and $\hat{\vec{q}}$ are the unit vectors of muon polarization and neutrino momentum, respectively). However, experimental investigation of this correlation in muon capture by hydrogen is very difficult. As for the partial nuclear muon capture, muon capture with the excitation of the daughter nucleus (sec.4.3) is more suitable for the investigation of particle correlations, including T-odd observables (such as the correlation $\hat{\vec{\sigma}}_\mu \cdot (\hat{\vec{k}} \times \hat{\vec{q}}) = -(\hat{\vec{\sigma}}_\mu \times \hat{\vec{q}}) \cdot \hat{\vec{k}}$). The interpretation of the data is easier when using the allowed muon capture with the excitation of the daughter nucleus in the region of light nuclei; however, this is limited by the

absence of appropriate candidates. However, in this region of nuclei the first forbidden transitions [237, 239] have been investigated in the muon capture by $^{12}C$ or $^{16}O$ [184]. In the case of a $0^+ \to 1^-$ transition, this correlation with the gamma-ray is analysed in reference 300. The calculation of this correlation was performed in reference 301. The correlation coefficients for the first forbidden nuclear muon capture have been calculated in reference 237. On the contrary with allowed $0^\pm \to 1^\pm$ transitions the correlation coefficients in the first forbidden $0^+ \to 1^-$ transitions are determined at least by four nuclear matrix elements; this means that three phases $\varphi_i$ are possible due to the likelihood of T-violating nuclear forces [302]. As for muon capture by $^{16}O$, the contribution of all nuclear matrix elements is important in principle using the framework of Migdal's quasiparticle nuclear model [303, 304]. In the case of allowed Gamow-Teller transitions in the framework of the main nuclear matrix element [101]-approximation in reference 222, the correlation coefficients do not depend on the nuclear structure. In this case, T-odd correlations are determined by the possible T-violation of the semi-weak interaction. In the first forbidden transitions using the framework of the main nuclear matrix elements [111]-approximation the ratio $[011]/[111]$ determines the correlation coefficients. So, T-odd correlations depend on the sum of the both phases $\phi_w$ and $\phi_s$, where $\phi_w$ is the semi-weak interaction relative phase and $\phi_s$ is the relative phase between the nuclear matrix elements; this may emerge from T-violating nuclear forces. In order to obtain the correlation coefficients for muon capture by $^{16}O$ the nuclear model from reference 303 was used for the

calculations in reference 301. The nuclear model in reference 303 could explain the nuclear magnetic moment, beta-decay rates, and partial transition rates in muon capture by oxygen. It is clear that only two phases (i.e. the semi-weak interactions relative phase $\phi_w$ between the $g_V$ and $g_A$ coupling constants and the relative phase $\phi_s$ of the [111] and [011] nuclear matrix elements), can be important in muon capture by $^{16}O$. As the $\phi_w$ and $\phi_s$ phases are ~$10^{-3}$ from the available experimental limits of the other processes, the correlation coefficient for T-odd correlation $\hat{\vec{\sigma}}_\mu \cdot (\hat{\vec{k}} \times \hat{\vec{q}})$ was obtained in reference 301 ($\xi \approx 2 \times 10^{-4}$) without disagreement with the experimental value of $\xi \leq \sim 10\%$ [300]. The other correlation coefficients were calculated in reference 301 in order to distinguish the T-violating semi-leptonic weak interaction from the T-violating nuclear forces. Of course, the accuracy was not good; however, using the Doppler broadening method, the experimental investigation into the $277keV$ gamma-ray [249] from the de-excitation of the $1^-$ level of $^{16}N$ was very difficult to analyse due to the small effect.

A possible CP or T violation (within the framework of CPT parity conservation) could be due to the presence of electric dipole moment of the particle. Landau writes

> It is easy to show from the foregoing that despite the absence of ordinary parity the particles cannot possess dipole moments. Indeed, the only vector which can be constructed from $\Psi$ -operators for a particle at rest is its spin vector which is even with respect to inversion and odd with respect to charge. It is consequently odd with respect to combined inversion and, in

> accord with the foregoing regarding the electromagnetic field, it defines only a magnetic but not an electric moment [305].

Landau also introduced combined inversion (i.e. CP violation). The search for the electric dipole moment of the neutron was reflected in a number of reviews [306]. The method was found to influence the electric dipole moment on the spin rotation of a neutron in an external magnetic field due to its magnetic moment. The recent experimental result of the electric dipole moment of a neutron corresponds to $d_n < 5.5 \cdot 10^{-26} e \cdot cm \ \ (90\%\ CL)$ [307].

# 5. MUON AND HEAVY NUCLEI

## 5.1 The physics of muonic atoms

As the muon mass is 207 times greater than the electron mass, all the bound states of muon and nucleus are scaled in energy and linear dimensions by this factor or its inverse. The smallest muon orbits (e.g. K-shell) are closer to the nucleus and the approximation of a point charge is grossly wrong for a muonic atom. The finite nuclear size is not a correction and the energy of the muon in the monopole field is dependent on the radial charge distribution. The muonic levels are determined only by electromagnetic interaction (ignoring very small weak interaction) contrary to $\pi^-$ - and $K^-$ - mesic atoms, where a strong interaction plays an essential role. The great mass of the muon results in the increasing difference between the energy levels of muonic atom in comparison with ordinary atom. Different effects resulting in splitting energy levels depend on the mass by other manner, so that the correlation between different effects in a muonic atom is not the same as in an ordinary one. The h.f.s. splitting in an ordinary atom corresponds to $\sim 10^{-3}$ relative to a spin-orbital splitting due to $m_e / M_p \approx 1/2000$ while the such ratio is $m_\mu / M_p \approx 1/9$ and the h.f.s. splitting for a muonic atom is comparable with a spin-orbital one (moreover h.f.s. splitting exceeds spin-orbital for muonic hydrogen). The radiative corrections in muonic atoms exceed h.f.s. splitting contrary to ordinary atoms; therefore, the verification of quantum electrodynamics in a high order of perturbation theory is very important

when using muonic atoms. Finally, many electrons of ordinary atom complicate the calculations, while for $n << 14$ the smallest muon energy orbits are under the K-shell of an ordinary atom; therefore, the electron screening effects are not essential.

The solution of Schrödinger (or Dirac) equation for electron in the field of the point-like nucleus is necessary for the hydrogen-like atom (ion). However, the approximation of the point-like nucleus is not acceptable for the hydrogen-like muonic atom because of the small distance of the muon from the nucleus in the lower muonic levels. The nuclear radius should be taken into account. The solution of the following equation is necessary [218]

$$H\varphi(x_N, x_\mu) = (H_N + H_\mu + H_{\mu N})\Phi(x_N, x_\mu) = E\,\Phi(x_N, x_\mu),$$

where the total Hamiltonian $H$ is separated into three parts: $H_N$ operates only on variables, $x_N$, in the nucleus, while $H_\mu$ only operates on the muon variables, $x_\mu$, and $H_{\mu N}$ which involves both sets of variables to represent the muon-nuclear interaction. The accurate solution of the equation is impossible. However, the appropriate approximations could resolve the problem. The Hamiltonian, $H_{\mu N}$, can been replaced by the static electromagnetic field that is produced by the charges and currents of the nucleus as a whole. In the extreme case of the muonic atom's greater dimension in comparison to the nuclear radius, $H_{\mu N}$ can be replaced by $Ze^2 / |\vec{r}_\mu|$. The static approximation of $H_{\mu N}$ ignores the influence of the

muon on the movement of nucleons in the nucleus. The small corrections from nuclear polarization (not nuclear spin polarization) are ignored. The total wave function can be factorized in two parts: $\Phi(x_N, x_\mu) \approx \phi_N \cdot \varphi_\mu$ (i.e. one, $\phi_N$, representing the internal motions of the nucleus, and the other, $\varphi_\mu$, the muonic atom). This factorization is an expression of the physical independence of the two motions.

The relativistic (Dirac) equation can be written for the Coulomb field as [218]

$$\left[ H_N + \left( c\vec{\alpha} \cdot \vec{p}_\mu - \frac{Ze^2}{|\vec{r}_\mu|} + \beta m_\mu c^2 \right) \right] \phi_N \, \varphi_\mu = E \phi_N \, \varphi_\mu ,$$

where $\vec{\alpha}$ and $\beta$ are Dirac operators; $\vec{p}_\mu, \vec{r}_\mu$ are the momentum and coordinate of the muon, respectively. The part in $( )$ depends only on muon variables. However, the point-Coulomb-field approximation should be replaced with the more accurate potential $eV(\vec{r}_\mu)$, where

$$V(\vec{r}_\mu) = \int \frac{\rho(\vec{r})}{|\vec{r}_\mu - \vec{r}|} d\vec{r} \; ;$$

$$\rho(\vec{r}) = \sum_i e_i \int \phi_N^* \delta(\vec{r}_i - \vec{r}) \phi_N \, d\vec{r}_1, ..., d\vec{r}_i$$

while the muon interacts with the protons of the nucleus.

The common approximation for a two-parameter nuclear-charge distribution corresponds to the Fermi distribution:

$$\rho(r) = \frac{\rho(0)}{1 + \exp\dfrac{r - R}{a}},$$

which is illustrated in Fig. 35. The measurement of the $1s_{1/2}$ level provides a single relation between $c = R$, the half-density radius, and $t = 4a \ln 3$, the surface thickness, as shown in Fig. 36 for the case of Z = 83.

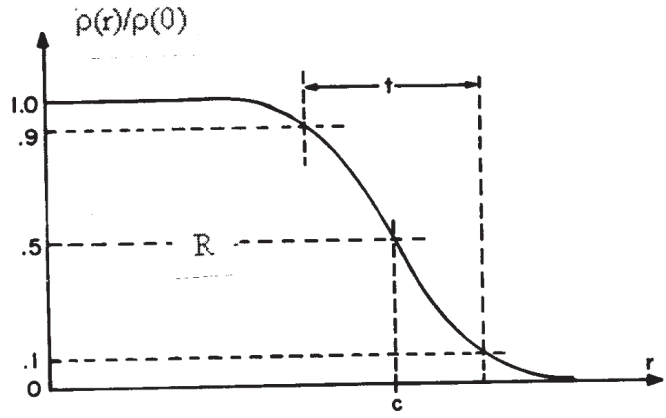


Fig. 35 Fermi distribution, where $c = R$ is the half-density radius and $t = 4a \ln 3$ is the 90% → 10% skin thickness.

A different relation between $c$ and $t$ is also provided by measuring the *2p* levels, and the intersection of the two curves determines $c$ and $t$ for the particular functional dependence of $\rho(r)$ as shown for $^{209}_{83}Bi$ in Fig. 36,

which was taken from references 218 and 308. At the same time, the value of $\left\langle r^2 \right\rangle$ is independent, relative to the nuclear form [218], where

$$\left\langle r^2 \right\rangle = \frac{1}{5}\left[3c^2 + 7(\pi a)^2\right].$$

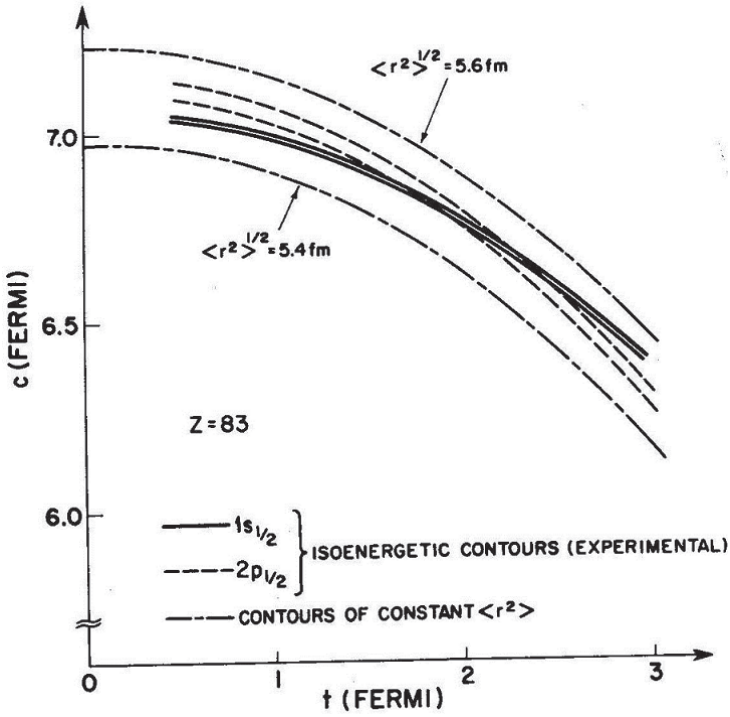


Fig. 36: The possible values of parameters *c* and *t* of the Fermi distribution. The isoenergetic contours are for $E(1s_{1/2}) = 5225.5 \pm 3.9$ *keV* and $E(2p_{1/2}) = 1812.7 \pm 2.7$ *keV* (Z=83). The contours of the constant $\left\langle r^2 \right\rangle^{1/2}$ show that this quantity is determined more accurately than either *c* or *t*.

It is known that $R \approx r_0 A^{1/3}$ for $r_0 \approx$ 1.2 ÷1.3*fm*. Fig. 37 illustrates this using electron scattering on nuclei experiments.

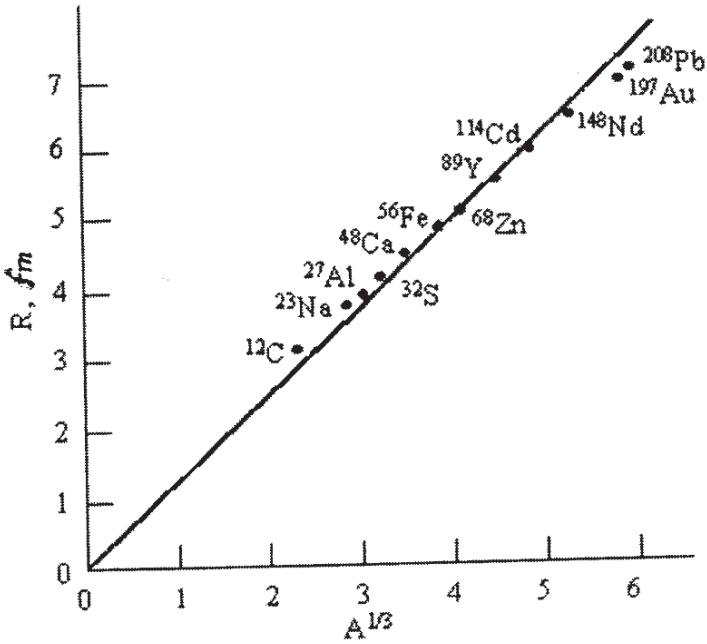


Fig. 37 The nuclear radius obtained from electron scattering on nuclei experiments.

Although most of the measurements of the muonic-energy levels are absolute and have been interpreted in terms of the charge distribution of a particular nucleus, special attention has been paid to the relative measurements, particularly to the small differences between isotopes of the same element: i.e., isotope shifts. It is explained by small energy differences which can be measured with a high accuracy. Apart from this, isotope shifts allow to obtain a small difference in the charge distribution due to the addition of neutrons. Very small differences in the nuclear charge distribution can be obtained by research into the isotope shifts,

especially at the 1s level, which is the most sensitive to this charge distribution. The relevant measurements are comparisons of the energies of the K X-ray. The elements with many stabile isotopes are of interest for this. For example, Z=60, $^{142-150}_{60}Nd$, presented in Fig. 38 (taken from Devons and Duerdoth, reference 218). A summary of the measured isotope shifts for the $2p - 1s$ transitions were shown in Table X with range from $-0.016 \pm 0.02\ keV$ to $21.55 \pm 0.25\ keV$ [218].

The relative shifts of energy levels for muonic atoms with a different $Z$ cannot be effective as the main energy difference arises from difference in $Z$.

A relatively high energy excitation of the nucleus during the muon cascade is possible. The difference between muon atomic levels for middle and heavy muonic atoms can be comparable, or even exceed, the energy of the excitation of nuclear levels. As a rule, resonant excitation is possible, especially in the case of forbidden E1 $\gamma$ ray emission. Particularly interesting is the isomeric shift with the great contribution of the nuclear structure to shift of the nuclear levels in the presence of the muon. The term, isomerism, was taken from organic chemistry, where there are molecules constructed from the same number of identical atoms, but differing in the arrangement of atoms, so they have different properties. In nuclear physics, nuclei that have the same composition (i.e. the same number of protons and neutrons) but differ in properties due to their different energy states, are called isomer nuclei. Such nuclei can exist for a long time in the excited state that exceeds $10^8 \div 10^{21}$ times the normal lifetime of the excited states of nuclei $\sim 10^{-13}\ s$. The justification for this

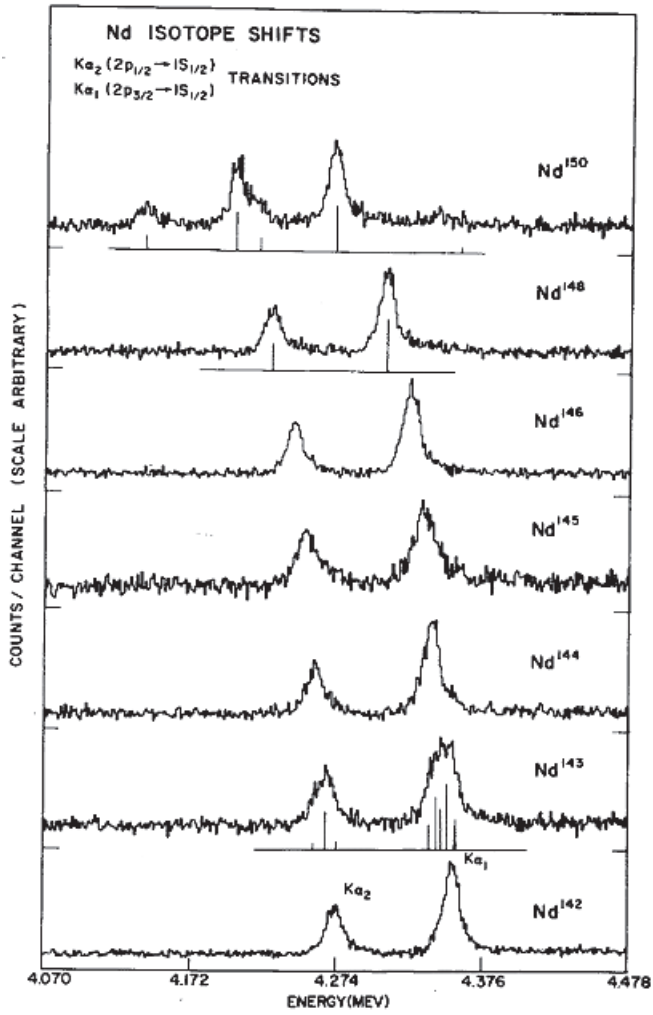


Fig. 38 Isotope shifts in the 2*p*-1*s* muonic transitions of neodymium, taken from reference 218.

was first given by Weizsaecker [309a], for example, $Br^{80}$ with a lifetime of the excited state of 4.4 hours before $\gamma$ decay. In the case of the excitation of the normal nucleus in a muonic atom, the emission of a gamma ray takes place in the presence of the muon on K-orbit. In fact $2p$ – $1s$ mesic atomic transition has a lifetime of $\sim 10^{-17}\, s$ (with the whole cascade lifetime $\sim 10^{-13}\, s$) in comparison with the nuclear cascade for a heavy nuclei $\sim 10^{-9} \div 10^{-11}\, s$. Therefore, the muon reaches $1s$ state in the excited nucleus. The lifetime of the muon, before the weak muon capture by the heavy nucleus, is $\sim 10^{-7}\, s$: i.e., it exceeds nuclear deexcitation**.** So, the nucleus in both excited and ground states (after radiative deexcitation) is in the presence of muon on K-shell. Therefore, the $\gamma$ ray has shifted due to the electromagnetic interaction of muon with nucleus. For example, the charge distribution in the ground and excited states of the nucleus is different, so that the energy of these states of nucleus in the presence of the muon will be shifted in different ways. This shift reflects the important information about nuclear structure. This isomer shift could be experimentally obtained from difference of energy of nuclear gamma quantum in the muonic atom relative to that obtained in an ordinary nucleus excited in beta-decay. The observed shifts were presented in Table XIV from reference, 218 and Fig. 39 for $^{152}Sm$ was also taken from the same reference.

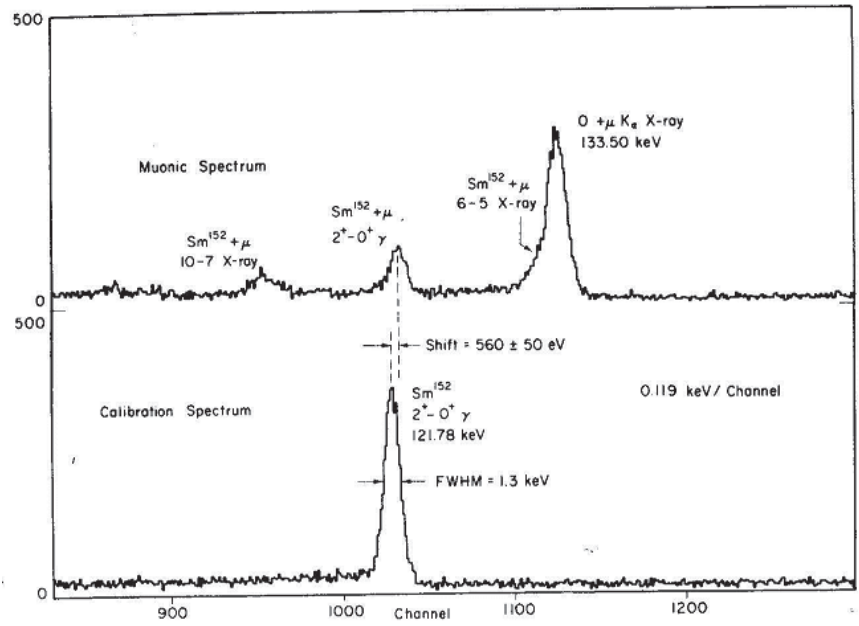


Fig. 39 The experimental shift $(560 \pm 50)\ eV$ in the 122 *keV* $2^+ \rightarrow 0^+$ nuclear $\gamma$ ray of $^{152}Sm$ due to the presence of a $1s_{1/2}$ muon, taken from reference 218.

Nuclear excitation and the isomer shift in muonic atoms are discussed in reference 309 b–d.

This effect is very similar to the well-known isomer shift observed in Mössbauer spectra, where crystal lattice is responsible for the energy shift of nuclear gamma ray.

The shift of muonic levels are due to the radiative corrections (QED). This important point is discussed in a number of reviews and papers, such as in reference 310. The degenerated $2s_{1/2}$ and $2p_{1/2}$ levels of ordinary

hydrogen were shifted into 1058 μHz due to the radiative corrections (Lamb shift) [311]. The calculations of the high order radiative corrections agreed with the experimental data; this proved the truth of QED. At the same time, the verification of QED [311a] by investigating mesic atoms is very important due to the proton radius puzzle, for example (see section 2.4).

For the ordinary electronic atom, the main contribution to Lamb shift is determined by its own energy (Fig. 40a) and the anomalous magnetic momentum of electron (Fig. 40b), while the vacuum polarization [311a] (Fig. 40c) does not exceed some % of a possible shift: i.e. ~ 27 μHz. The opposite situation can be found in a muonic atom, where the vacuum polarization (Fig.40c) corresponds to the main contribution and graphs Fig. 40a,b could be ignored. In fact, the electron receives additional energy due to its interaction with the zero oscillations from vacuum, which are reflected through the renormalization of its mass.

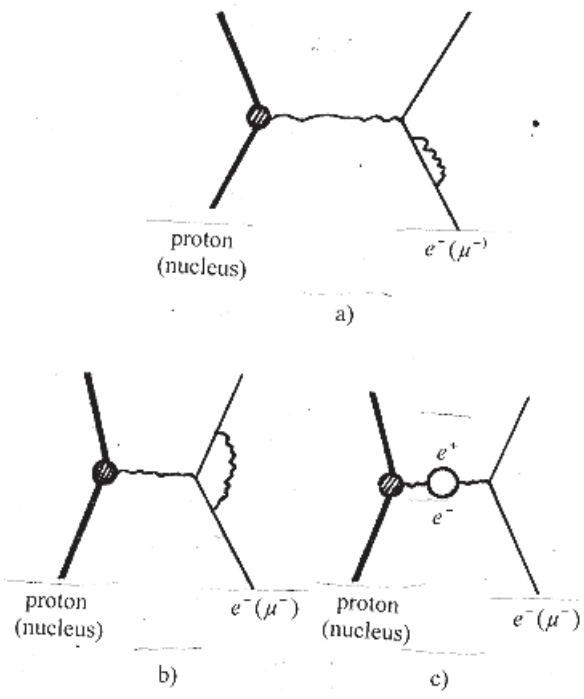


Fig. 40 Graphs showing the radiative QED corrections in various levels of electronic (muonic) atoms.

The interaction, which corresponds to Fig. 40a and b, also changes the potential energy; this results in a shift of atomic levels due to the Coulomb interaction $V_1 \approx \alpha \lambda\!\!\!^{-2}_e \cdot Z e^2 \delta(\vec{r})$, where $\lambda\!\!\!^{-}_e = \hbar / m_e c = 386\ fm$ is the Compton wave length of electron. The $\delta-$ function means that the interaction is limited by $r \le \lambda\!\!\!^{-}_e$: i.e., this potential is more important for the *s*-level. The vacuum polarization (Fig. 40c) corresponds to an interaction with the electron-positron vacuum field; this means that the proton is screened by virtual electrons. Therefore, the proton charge could

be larger for $r < \lambda\!\!\!^{-}_{e}$: i.e., it is increased with an evident shift in the bound states. The estimation of its effective potential corresponds to $V_2 \approx -\frac{4}{15}\alpha \lambda\!\!\!^{-2}_{e} Z e^2 \delta(\vec{r})$. The following was obtained after averaging $\langle V_1 + V_2 \rangle$ the formula for energy shift level $\delta E \approx \alpha \lambda\!\!\!^{-2}_{e} \cdot Ze^2 \int |\psi_e|^2 \delta(\vec{r})\, d\vec{r} \approx \alpha \lambda\!\!\!^{-2}_{e} \cdot Ze^2 \frac{1}{\pi a_e^3} \approx (\alpha Z)^3 e^2 / a_e$, where $a_e = \lambda\!\!\!^{-}_{e} / \alpha Z$ is the Bohr radius of electron. As the level energy is $E_0^e \approx Ze^2 / a_e$, we have $\delta E / E_0^e \approx \alpha^3 Z^2$ for an ordinary electronic atom. Let us consider the energy shift of the muonic atom. In this case, we should replace $\lambda\!\!\!^{-}_{e}$ on $\lambda\!\!\!^{-}_{\mu} = \hbar / m_\mu c = 1.87\, fm.$ in the potential $V_1$, which will be small and the contribution from Figs. 40a and b to $\delta E$ can then be ignored. As for the potential $V_2$, the Compton wave length of electron should be kept in agreement with Fig. 40c, where the electron-positron pair determines the vacuum polarization. Therefore,

$$\frac{\delta E_2^\mu}{E_0^\mu} = \frac{\langle V_2 \rangle}{E_0^\mu} = \left(\frac{m_\mu}{m_e}\right)^2 \approx 10^4$$

(in the calculation of $\delta E_2^\mu$ we should replace $\psi_e \to \psi_\mu \sim 1/a_\mu^{3/2}$ with $\lambda\!\!\!^{-2}_{e} \sim 1/a_e^2$ and $E_0^\mu \sim 1/a_\mu$, where $a_e \sim 1/m_e$ and $a_\mu \sim 1/m_\mu$). This means that the vacuum polarization is the main effect. At the same time, these estimations are preliminary as

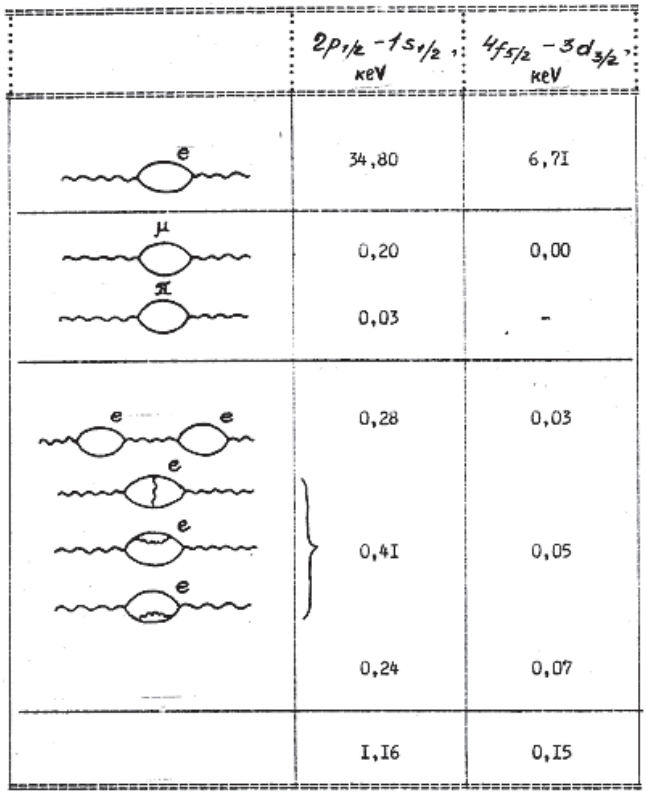


Fig. 41 High order corrections of the QED to vacuum polarization.

$r < \lambda\!\!\!^{-}_{a}$ is not as evident as $a_\mu = \lambda\!\!\!^{-}_{\mu} / \alpha Z = \lambda\!\!\!^{-}_{e.} \frac{m_e}{m_\mu} \cdot \frac{1}{\alpha Z} \approx \lambda\!\!\!^{-}_{e}$. Moreover, the calculations of the radiative correction should consider the nuclear size especially for low levels [312]. At the same time, $a_\mu << \lambda\!\!\!^{-}_{e}$ is for muonic atoms with large *Z*. In fact, vacuum polarization is the main radiative correction for all muonic atoms, including high orbits [313]. The vacuum polarization exceeds with factor ~ 200 the effect of nuclear size

for the transition $5g \rightarrow 4f$ so radiative corrections from the QED of up to $\alpha^4$ can be verified. The high order QED corrections are presented in Fig. 41, where the total contribution is 1.16 keV for the $2p_{1/2} \rightarrow 1s_{1/2}$ transition and 0.15 keV for the $4f_{5/2} \rightarrow 3d_{3/2}$ transition.

## 5.2 The muon and nuclei fission

The process of the prompt fission of heavy nuclei, as induced by a muon was first discussed by Wheeler [314a] and considered in more details by Zaretsky [314b]. The energy of mesic atomic transitions in heavy mesic atoms could exceed the fission threshold. The $2p \rightarrow 1s$ muonic transition of energy 6.6 MeV and $3d \rightarrow 1s$ muonic transition of energy 9.6 MeV result in the excitation of the nuclear giant dipole and giant quadrupole resonances, respectively, following the fission in actinides.

The promt fission arising from the radiationless nuclear excitation occurs in $\sim 10^{-13} s$, while the delayed one arising from weak muon capture by nucleus corresponds to $\sim 10^{-7} s$. As a result of the prompt fission, the muon remains on one of the fragments of the nuclear fission and it can be captured by this fragment or emitted to solid spectrum due to internal gamma-ray conversion. The muon-induced fission has been reviewed [315]. The theoretical consideration of the muon-induced fission was performed in a number of papers [315, 316]. As the nuclear excitation energy is equal, or exceeds the fusion barrier height, it is possible to consider the process classically without barrier tunnelling. Due to the fact that the muon lifetime (both muon decay and weak muon capture by nucleus) has long been compared to that of prompt nuclear fission, the

motion of the muon in the Coulomb field of nucleus could provide information about the dynamics of fission. The process of the prompt muon-induced fission of the actinide nuclei was considered by Oberacker, Umar, and Karpeshin [315]. They investigated the time-dependent Schrödinger equation using Born-Oppenheimer expansion. This method considers fission dynamics classically using quasi-molecular orbitals. They also resolved the relativistic time-dependent Dirac equation with their prediction of a strong mass asymmetry dependence of the probability of muon attachment to the light fission fragment in agreement with the experimental data. According to Teller and Weiss [317], the $3d \rightarrow 1s$ radiationless transition could be dominant in muon-induced fission.[1]

The prompt muon-induced fission was first observed by Diaz et al. [318].

Experiments regarding the prompt fission of the muonic $^{238}U$, reveal that ~ 75 % of all events are due to the $3d \rightarrow 1s$ radiationless transition and only ~ 25 % to the $2p \rightarrow 1s$ transition [319a]. The probability of the non-radiative decay in the $3d$ level of the muonic $^{237}Np$ was also considered [320]. This begs the question of how the yield of prompt fission is shared between the $3d \rightarrow 1s$ and $2p \rightarrow 1s$ radiationless transitions in this mesic atom, where the total prompt fission rate per stopped $\mu^-$ is about 10 times

[1] The giant dipole resonance for $^{238}U$ is located at 12.8 MeV and the giant quadrupole resonance corresponds to 9.9 MeV. The radiationless $3d \rightarrow 1s$ transition is 9.6 MeV and is very close to the giant quadrupole resonance, while the $2p \rightarrow 1s$ transition of 6.6 MeV is far from the giant dipole resonance, which was located at 12.8 MeV.

higher than the corresponding date for $^{238}U$. In order to clarify these points, they performed a correspondent measurement on $^{237}Np$, using the same experimental method as was used in reference 319. The probability of a radiationless $3d \rightarrow 1s$ transition in the muonic $^{237}Np$ was obtained: (9 ± 4) % [320]. This value was compared with the corresponding one in $^{238}U$: (14 ± 5) % [319b]. However, the errors in both experiments are rather large so this difference might not be statistically significant [320a]. The ratio of prompt to delayed muon induced fusion for the muonic

$2p \rightarrow 1s$ transition was obtained in reference 320b. They compare

28.3 ± 0.3) % and (8.8 ± 0.3) % for $^{237}Np$ and $^{238}U$, respectively, and the possible explanation for this is the difference in height of the fission barriers (5.50 MeV in comparison with 6.35 MeV). One may conclude that the radiationless $2p \rightarrow 1s$ transition plays a much more important role for prompt fission in $^{237}Np$ than in $^{238}U$ [320b].

The evidence for atomic muon capture in fragments from the prompt fission of muonic $^{237}Np$, $^{239}Pu$ and $^{242}Pu$ was obtained in reference 321, with an estimated upper limit for the muon attachment probability $\leq 0.1$. The probabilities of muon attachment to fission fragments in the prompt fission of $^{237}Np$ have been determined as a function of fragment mass and total kinetic energy release in reference 322. The ratio of prompt to delayed fission yields for the isotopes, $^{233-236}U$, $^{238}U$, $^{237}Np$, $^{242}Pu$ and $^{244}Pu$, as well as the fission

probabilities relative to each other have been obtained experimentally. Using the value of the total fission probability for $^{237}Np$, the absolute probability for prompt and delayed fission has been determined in reference 323.

# 6. MUON AND CONDENSED MATTER

## 6.1 The μSR-method

Muon spin rotation, relaxation, and resonance - μSR was considered in a number of reviews [3,324]. The muon is produced in the decay of the pion and it has a mean lifetime of $2.6\times10^{-8}\,s$ according to:

$$\pi^{+} \rightarrow \mu^{+} + \nu_{\mu}$$

$$\pi^{-} \rightarrow \mu^{-} + \overline{\nu}_{\mu}$$

To conserve momentum, the muon and the neutrino must be emitted in opposite directions for a pion produced at rest. The information about μSR-method appeared for the first time in the first issue of the *μSR Newsletter* in 1974, by T. Yamazaki, K. Nagamine, K. Crowe and J.H. Brewer: http://musr.ca/intro/musr/htm/musrlogo.htm.

Since the pion has zero spin, the spins of the muon and neutrino must also point in opposite directions. As the neutrino has negative helicity i.e. its spin is aligned antiparallel with its momentum (the helicity is determined by $h = \dfrac{\vec{S}\cdot\vec{p}}{\left|\vec{S}\right|\cdot\left|\vec{p}\right|}$, where $\vec{S}$ is the spin operator and $\vec{p}$ is momentum of the particle) the muon spin is similarly aligned. As $h$ = -1 for $\nu_{\mu}$ and

$h$ = +1 for $\overline{\nu}_{\mu}$, the muon is 100 % polarized in the centre of the mass system (for pion produced at rest in the laboratory frame): i.e., $\mu^{+}$ has a spin antiparallel to its momentum, while $\mu^{-}$ has spin parallel to its momentum. Therefore, by selecting pions which stop in the target (and which are at rest when they decay) one has a means of producing 100 % spin-polarized muon beams used for condensed matter physics research. In the rest frame of the pion, the muons have an energy of 4.1 MeV. The unique possibility exists to obtain monochromatic $\mu^{+}$ beams with

~ 100 % spin polarization, which are antiparallel to the muon momentum. This is achieved by the formation of so-called “surface muons” [325]; these are produced from the decay of $\pi^{+}$, which have lost their energy inside the target bombarded by protons, and have decayed at rest on the target surface. Although muons are produced in a variety of high-energy processes and elementary particle decays, μSR requires low energy muons that will stop in the samples studied. Low-energy muons are only available in the required intensities from pion decay.

The same situation is impossible for $\mu^{-}$ because of prompt capture of the $\pi^{-}$ inside the target; therefore, $\mu^{-}$ can only be produced from $\pi^{-}$ decaying in flight: i.e. with a high energy within a long superconducting solenoid. At the same time, $\mu^{-}$ is captured for the formation of a muonic atom with a cascade de-excitation. During de-excitation the $\mu^{-}$ is depolarized with radiative signal noise. At last $\mu^{-}$ is captured by a

nucleus with high rates for heavy nuclei. Therefore, $\mu^- SR$ is only used in selected cases. Some unique applications where negative muons, $\mu^-$, were used to investigate specific problems in solid state physics were performed by Maier [326] and Nagamine [327].

The spin polarized ~ 4 MeV energy $\mu^+$ beam penetrates only fractions of millimetres into the solid sample. In the magnetically ordered solid, or superconductor, the positive muon $\mu^+$ serves as a very sensitive microscopic magnetic probe of the local magnetic field in the sample seen by the muon. The advantages of μSR are due to the large magnetic moment of the muon $\mu_\mu \approx 3.2\,\mu_p$ in comparison with other microscopic probes: e.g., neutron scattering, synchrotron radiation, or nuclear magnetic resonance (NMR), as discussed in reference 3.

As a result of parity violation, the positrons from decay of $\mu^+$ are distributed asymmetrically with respect to muon polarization. After integration over all possible energies, the angular distribution of emitted positrons from the decay of $\mu^+ \rightarrow e^+ + \overline{\nu}_\mu + \nu_e$ with the polarization of $P_\mu$ can be described as:

$$\frac{dN(\vartheta)}{d\Omega} \propto 1 + \frac{1}{3} P_\mu \cos\vartheta \,.$$

The huge muon polarization for the initial time $t = 0$ (i.e. $P_\mu = 1$), was considered in section 2.2. The angular distribution of emitted positrons is shown in Fig. 42 taken from reference 324c.

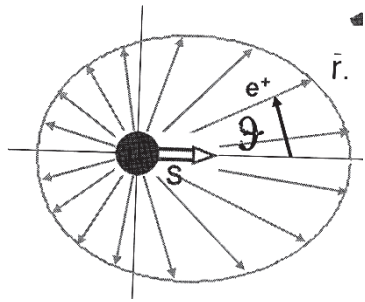


Fig. 42 The angular distribution of emitted positrons with respect to the initial muon-spin direction.

As indicated in Fig. 43, taken from reference 3, there are three types of μSR method: muon spin rotation, muon spin relaxation, and muon spin resonance. I will now discuss these μSR methods.

Muons are implanted into the sample with an energy which is at least 4 MeV. They lose energy very quickly (in 0.1 ÷ 1 ns) to a few keV through ionization of atoms and being scattered with electrons. Then the muon begins to undergo a series of electron captures: i.e. muonium formation which reduces the energy to a few hundred eV on ps. The last few eVs are lost through the inelastic collisions between muonium and the target atoms. The stopping range of muons in a sample varies from 0.1 to 1 mm. These effects are very fast so that the muon (or muonium) is thermalized rapidly. Moreover, all of the effects do not interact with the muon spin so that the muon is thermalized in matter without any appreciable

depolarization. Different principles, including muon spin rotation, relaxation and resonance spectroscopy, are used.

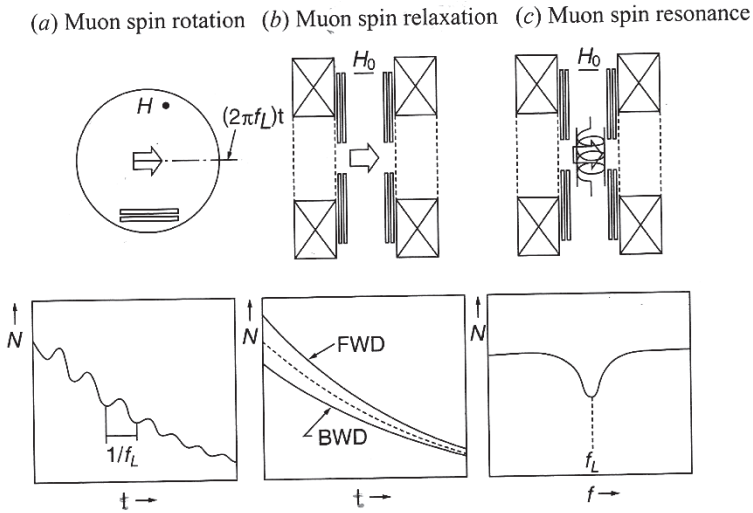


Fig. 43 Schematic illustration of a μSR experiment (FWD $\equiv N_F$ and BWN $\equiv N_B$)

In the magnetic field, $H$, the muon spin precesses with an angular frequency given by $\varpi_\mu = \gamma_\mu H$, where

$$\gamma_\mu = g_\mu \frac{e\hbar}{2m_\mu} = 2\pi \times 13.55342 \ \ kHz \cdot G^{-1}$$

[3] is the gyromagnetic ratio for a muon. This is known as, Larmor precession $\varpi_\mu = 2\pi f_L$.

The Larmor precession is determined by the equation, $\frac{d\vec{\mu}_\mu}{dt} = \left[\vec{\mu}_\mu \times \vec{H}(t)\right]$, where $\vec{H} = \vec{H}_{Loc}$ is the inner magnetic field of the sample. The analogous precession undergoes $\vec{P}_\mu(t) : \frac{d\vec{P}_\mu}{dt} = \gamma_\mu \left[\vec{P}_\mu \times \vec{H}(t)\right]$. $\vec{P}_\mu(t)$ is characterized by precession and /or depolarization/relaxation and contains information about the static and dynamic properties of the sample.

The time evolution of the muon polarization can be obtained via the asymmetry function $A(t) \equiv A_0 P_\mu(t) = \frac{N_B(t) - N_F(t)}{N_B(t) + N_F(t)}$, where $A_0$ is the experimentally observable maximum positron asymmetry which depends on set-up and is generally slightly lower than the initial asymmetry of muon decay $A_0 = 1/3.$ Practically, values $A_0 \approx 0.25$ are routinely obtained. For the determination of $N_F(t)$ and $N_B(t)$ (i.e. the observation of spin rotation), two positron counters could be mounted on opposite sides of the sample in both forward and backward directions. The number of positrons detected by each counter as a function of time (i.e., $N_F(t)$ and $N_B(t)$ in forward and backward directions, respectively), reflects the time dependence of the muon spin polarization along the axis of observation as defined by two detectors:

$$N_F(t) = N(0)\exp\left(-\frac{t}{\tau_\mu}\right)\left[1 - A_0 P_\mu(t)\right],$$

$$N_B(t) = N(0)\exp\left(-\frac{t}{\tau_\mu}\right)\left[1 + A_0 P_\mu(t)\right].$$

The quantities, $A(t) = A_0\, P_\mu(t)$, contain all the information about the interaction of muon magnetic moment with the local magnetic environment from the sample. They can be extracted from the μSR histogram in Fig. 43a from the $e^+$ time spectrum of exponential muon decay. The time evolution of the muon spin polarization depends on the spatial distribution and dynamical fluctuations of the muon's magnetic environment.

The transverse field muon spin rotation involves the application of an external magnetic field which is perpendicular to the initial direction of the muon spin polarization. The muon spin precesses around the transverse field with an angular frequency of $\varpi_\mu$. A frequency spectrum, that has been obtained by means of this experimental arrangement, provides a direct measure of the internal magnetic field intensity distribution. Such a method can be used to measure the magnetic field distribution of the vortex lattice or in the superconductor also for the metallic sample. Another example is the longitudinal field muon spin relaxation, which is involved in the application of an external magnetic field that is parallel to the initial direction of the muon spin polarization.

Then *A(t)* can be described by $A(t) \equiv A_0 P_\mu(t) = A_0\, P_\mu(0)\, G(t)\cos(\varpi_\mu t + \varphi)$, where the Larmor frequency us $\varpi_\mu = \gamma_\mu (H_{ext} + H_{\text{int}})$, and $H_{ext} \equiv H_0$ in Fig. 43;

$\varphi \equiv \vartheta$ in Fig. 42. The $A(t)$ gives information about the average internal field and *G(t)* $\leq 1$ is called the depolarization, or relaxation, function that expresses the damping of the polarization. Alternatively, such measurements may be performed in the absence of an external field. In addition to these methods, the muon spin resonance spectroscupy [328], which is analogous to the nuclear magnetic resonance NMR or electron-spin resonance ESR experiments, can be used. A static magnetic field $H_0$ is applied parallel to the initial muon spin polarization together with the field $H_1$, which is perpendicular to the field $H_0$. This resonance occurs when the resonance frequency matches the precession frequency $f_L$. This condition is detected as a loss of muon polarization (see Fig. 43c).

Numerous examples of use of μSR methods were presented in reviews and papers [324–328].

## 6.2 Muonium physics

Muonium is an exotic atom $\mu^+e^-$ (chemical symbol Mu) with lifetime of a muon ~2.2 μs. It was theoretically discussed by Friedman and Telegdy in 1957 [329] and discovered in 1960 by Hughes et al. [330]. Muonium is more similar to the hydrogen atom than the positronium $e^+e^-$. The muonium contrasts with positronium by having a central nucleus. The electron reduced mass is only ~ 0.5 % lower than in the protium ( $pe^-$ atom), so that its size and binding energy are very similar to those of ordinary atomic hydrogen. The muonium has a Bohr radius of 1.004 $a_B$

and an ionization potential of 0.996 $I_H$. Muonium was considered in a number of reviews [3,329–331].

Energy levels n=1 and n=2 of muonium, including h.f.s. splitting of levels are presented in Fig. 44 taken from reference 331b.

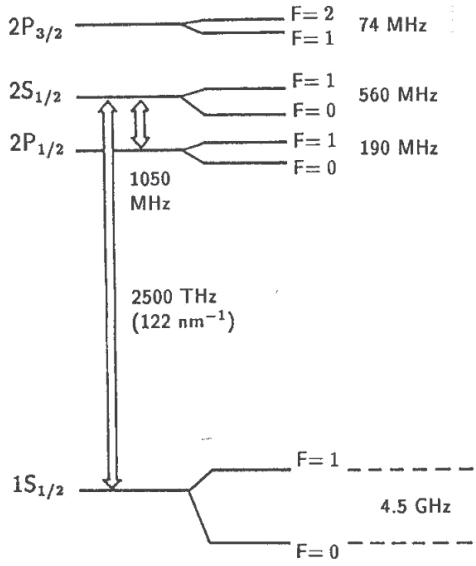


Fig. 44 Energy levels of muonium, including h.f.s. splitting, which is schematically equivalent to atomic hydrogen.

The theoretical calculation for h.f.s. splitting from the ground $1S_{1/2}$ state given in references 331a and b. $\Delta\nu \approx 4.463\ GHz$ is in good agreement with the experimental results. Recent experimental data was used in reference 331c. In the result, more accurate data was indicated for $1S_{1/2} \Leftrightarrow 2S_{1/2}$: i.e.,

2455 THz and for $2P_{1/2}$ h.f.s. splitting 187 MHz, as well as for $2S_{1/2}$ h.f.s. splitting 558 MHz. However, these replacements were not so large.

The possible muonium $\mu^+e^-$ antimuonium $\mu^-e^+$ conversion was analysed in detail by Feinberg and Weinberg [332a]. This process violates lepton numbers (i.e. $\Delta L_\mu = 2$ and $\Delta L_e = -2$). The Standard Model assumes additive lepton family number conservation and any possible violation would be an indication of new physics. In many speculative theories that extend the Standard Model, a possible violation exists: e.g. CP violation or lepton number non-conservation. These theories should explain rare decay modes, neutrino oscillations, and so on. In the framework of gauge models the non-conservation of the lepton number follows on from the spontaneous broken symmetry in the Higgs sector. The interaction with the violated lepton number conservation law is realized through the exchange of Higgs bosons. It is known that processes with $|\Delta L_i| = 1$ are strongly suppressed with a branching ratio of ~ $10^{-12}$ (e.g. $\mu \rightarrow 3e$). The spontaneous conversion of muonium $M$ into antimuonium $\overline{M}$ would violate the additive lepton number conservation (by two units); however, it is allowed by a multiplicative law [332b, 333]. The observation of $M \rightarrow \overline{M}$ conversation could prove the multiplicative lepton number conservation law [332b]. The term, anti-mesonium, was first introduced by Pontecorvo in 1957 with an indication of the possibility of $M \rightarrow \overline{M}$ transition in reference 334. This process could play a decisive role in many speculative models. Pontecorvo supposed the

possible interaction with $|\Delta L| = 2$ would lead to the double beta-decay, as well as to the $M \to \overline{M}$ conversation [335]. The muonium conversion via a neutral Higgs boson with lepton number 2 is shown in Fig. 45, taken from reference 336.

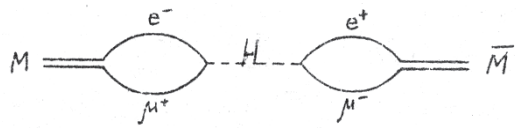


Fig. 45 Transition $M \to \overline{M}$ due to the exchange of Higgs boson.

However, the model with heavy Majorana neutrinos, including doubly charged Higgs bosons, changed the lepton numbers in $\Delta L = 2$ [337]. This could be responsible for $M \to \overline{M}$ conversion. (see Fig. 46 taken from references 336 and 338–340]).

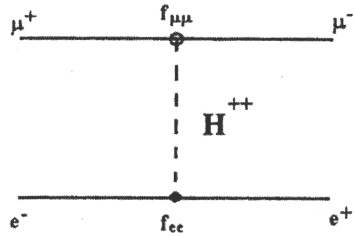


Fig. 46 Transition $M \to \overline{M}$ in a model with the Majorana neutrino.

The $M \to \overline{M}$ conversion in a model with the Majorana neutrinos is shown also in Figs. 47a and b, taken from references 339 and 340. Fig. 47a

reflects the exchange in the correspondent Higgs boson and Fig. 47b in the Majorana neutrinos and W-bosons.

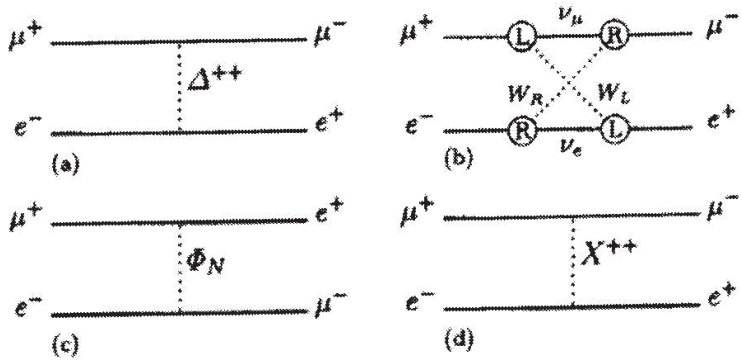


Fig. 47 Muonium-antimuonium conversion in theories beyond the Standard Model, where $\Delta^{++} \equiv H^{++}$.

The $\Phi_N$ in Fig. 47c is a neutral scalar [341] or a supersymmetric $\overline{\nu}_\tau$ [342]. $X^{++}$ is a bileptonic flavour diagonal gauge boson [343].

If Hamiltonian has the standard V-A structure with the coupling constant $G = G_{M\overline{M}}$, the probability will be

$$W_{M\overline{M}} = 2.6 \cdot 10^{-5} \left( \frac{G_{M\overline{M}}}{G_F} \right)^2 = 2.6 \cdot 10^{-5} f^2$$

with a determination of $f$ from its experimental limits [332a, 334]. We have the following model for the Majorana neutrino [337]:

$$\frac{G_{M\overline{M}}}{G_F} = \frac{f_{ee} f_{\mu\mu}{}^*}{g_W^2} \left( \frac{M_W}{M_{++}} \right)^2,$$

where $f_{ee}$, $f^{*}_{\mu\mu}$ are constants indicated in Fig. 46, $g_W^2 = g^2/\sqrt{2}$ is the weak interaction constant ($g$ is determined in section 3.7), $M_W$ is the mass of the W-boson, and $M_{++}$ is the mass of the doubly charged Higgs boson.

A number of experiments have taken place to find $M \to \overline{M}$ conversion. Amato et al. [344] investigated cascade gamma-rays in muonic *Ar* atoms after conversion, using the formation of $\mu^- e^+$ and following the transfer and capture of $\mu^-$ by *Ar* nuclei. The $\gamma$ rays with an energy of 643 keV were registrated. The resulting upper limit of the probability that a muonium atom spontaneously will convert to antimuonium is $2.1\times10^{-6}\,(90\,\%\,CL)$, which corresponds to a limit of $G_{M\overline{M}} \le 0.29\; G_F$; this was obtained by Huber et al. [345]. Later an upper limit for the conversion probability in 0.1 T magnetic field was extracted as $8\cdot10^{-11}\,(90\%\;CL)$ in reference 346. The experimental upper limits were also presented by Abela et al. $W_{M\overline{M}} \le 8\times10^{-9}\;(\,90\%\,CL)$ [347], Gordeev et al. $W_{M\overline{M}} \le 4.7\times10^{-7}\;(\,90\%\;CL)$ with $G_{M\overline{M}} \le 0.14\; G_F$ [338] and Willmann et al. $8.3\times10^{-11}\,(90\%\;CL)$ with $G_{M\overline{M}} \le 3.0\times10^{-3}\,G_F$ [340]. The results of these different experimental techniques were summarized by Patrignani in reference 348. A further perspective could be connected to the Japanese PRISM (Phase Rotated Intense Slow Muon)

project, which was aimed at constructing a high-intense slow muon source with an arrow energy spread [349, 350]. Muonium is used as probe for solid state research [324a, 331b, 351]. The investigations of matter using a muon was presented in a number of reviews [3, 17, 217, 352–354]. The muon provides an exceptional opportunity to investigate basic chemical interactions and $\mu^+$ and $\mu^-$ are used for the investigation of this matter. The muon is used as a probe to research the microscopic magnetic properties of condensed matter, under the assumption that those properties are unchanged by the introduction of the muon. At the same time, studies of microscopic physics and chemistry were created by the introduction of the muon. The creation of a new microscopic condensed matter in the target is realized by the introduction of $\mu^+, Mu$ and $\mu^-$ in order to research the chemical reactions: e.g. by the hydrogen-like *Mu* in semiconductors, polymers, and so on.

# 7. THE MUON IN BIOLOGY AND MEDICINE

The use of muonic physics in biology and medicine was first proposed by Daniel in reference 18. The review of the problem was presented in references 3, 18–20, and 217. Due to the large muon mass in comparison with the electron's, the muonic X rays from formation of $\mu^-$ muonic atoms have energies that are very suitable for gamma-ray spectroscopy and every element is easily recognized. By selecting the primary $\mu^-$ energies any part of the sample, including the inside, can be investigated. The X-ray emission spectrum is a non-destructive method of determining the element content of a given sample. Another possibility is connected with the registration of the muon's decay electron and the lifetime of the bound $\mu^-$ is the determined factor of this method. In both cases the muon transfer from muonic hydrogen (in molecules containing hydrogen atoms) to $Z > 1$ should be taken into account. However, the X-ray method became more popular. The X-ray from the muonic atom formed between the injected $\mu^-$ and the nuclei of the stopping sample is a characteristic photon which is registered by the detector outside the sample. There is a unique correspondence between the atomic number of the stopping element and the energy of the muonic $K_\alpha$ X-ray, as illustrated in Fig. 4.4 in reference 3. The relative intensities of $K_\alpha$ X-rays for animals, such as rats, following aeronautics were presented in Table 22 in reference 217. The correspondence between the elements C, N, O, Na, Mg, P, S, Cl, K,

and Ca were changed after the flight due to hypokinesia. From the intensity of the muonic X-ray after its correction due to the atomic capture process, the transfer from hydrogen to *Z*, and the energy-dependent efficiency, one can obtain the elemental concentrations. Table 7 and Fig. 48 (taken from reference 3) demonstrate the distribution of some elements in the human body (the corresponding energies of $K_\alpha$ .and $K_\beta$ lines are summarised in Table 7).

**Table 7. The distribution of elements in the human body taken from Table 4.5 in reference 3**

| Element | Abundance in the human body (%) | Lifetime (μs) | X-ray energy (keV) of 2p→1s | X-ray energy (keV) of 3p→1s |
|---|---|---|---|---|
| C | 23.0 | 2.026(2) | 75.5 | 13.9 |
| N | 2.6 | 1.907(3) | 102.0 | 18.9 |
| O | 61.0 | 1.795(2) | 133.0 | 24.0 |
| P | 1.1 | 0.611(1) | 458.0 | 88.4 |
| Ca | 1.4 | 0.333(3) | 786.0 | 158.0 |

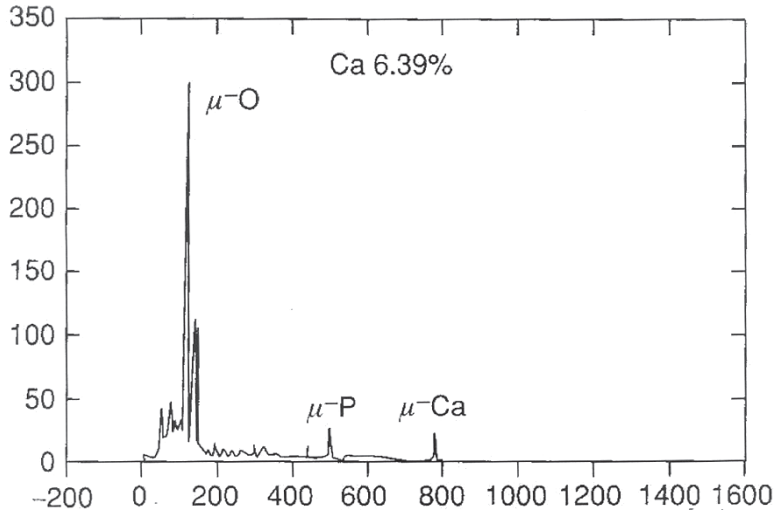


Fig. 48 A muonic X-ray spectrum of the human body.

The consequences for astronauts to stay in imponderability due to hypokinesia are discussed in reference 217. Bone loss has been observed during flights in space since 1960. Astronauts lose an average of 1÷2 % bone mass[2] per month spent in space [355]. There are indications of losses of bone material density >10 % detected in the hip and spine in some astronauts following a 6-month space mission. In the case of spaceflight to Mars, where gravity is about one-third that of Earth, the gravitational forces acting on astronauts would be much lower, causing bones to decrease in mass and density [356]. This problem is connected with a possible osteoporosis risk [357]. The muonic X-ray analysis is used in medical diagnosis especially in the case of osteoporosis (see Fig. 48). The

[2] Although this is in comparison to 1÷1.5 % bone loss per year in the elderly and 2÷3 % in postmenopausal women.

initial research was performed using heel bones because of their homogeneous structure and accessibility [217, 358]. The decrease in mass and density of heel bones was obtained in these experiments. At present, an extensive NASA program exists for medical research into astronauts; this includes muonic X-ray analysis [359].

# 8. NUCLEAR FUSION OF LIGHT NUCLEI IN MUONIC MOLECULES

The study of fusion reactions between light nuclei is relevant to the nuclear reactions which occurred during the primordial nucleosynthesis after the Big Bang; this also occurs in stars [360]. The present understanding of nucleosynthesis in the Galaxy points to a deficiency of light nuclei (except for $^4$He) compared with predictions based on the theory of thermonuclear reactions and existing models. To explain this phenomenon, modified star models are usually proposed, which assume that during the extrapolation of nuclear cross sections from accelerator energies to the astrophysical region no resonances or other anomalies occur. It cannot be excluded, however, that the nuclear cross-sections have a resonant character, which could lead to the intensive burning of the light elements in stars. Therefore, the investigation of nuclear fusion in the astrophysical range of energies is very important.

The investigation of nuclear synthesis in charge-asymmetric muonic molecules, $\mu hZ$, provides an opportunity to investigate strong interactions, including nuclear fusion reactions at low energies. In addition to astrophysics, another important problem is proving the fundamental symmetries, such as charge, time, and the isotopic invariance of strong interactions. These symmetries were experimentally established in the MeV energy region and were only extrapolated with regard to low and very low energies. It is of great importance to test the fundamental symmetries of strong interactions in ultra-low energies. However, small

energies, such as eV ÷ keV, are not accessible in accelerator experiments and there is practically no information about strong interactions in these energy regions.

It is known that deuterium disintegrates in stars at energies $\geq 50\,eV$, lithium at $\geq 200\,eV$, and so on. At the same time the creation of light elements in the keV-range of energies (e.g. the reactions $p+{}^7Li \to 2{}^4He$ and $t+{}^4He \to Li^7+\gamma$) is also very important. As for the fusion of hydrogen-helium isotopes, the following reactions are possible (considering the exothermal fusion reactions in reference 361):

$$d^3He \to \alpha + p + 18.3\,MeV \quad (E_\alpha = 3.5\,MeV;\ E_p = 14.64\,MeV)$$

$$\to {}^5Li + \gamma + 16.4\,MeV$$

The energy yield in the first reaction is divided between two heavy particles: $\alpha$ and $p$ according to the indicated manner.

The radiative channel is strongly suppressed and so is the fusion in $\mu d^4He$ molecule [361, 362]

$$d^4He \to {}^6Li + \gamma + 1.48\,MeV$$

Five fusion channels are possible for the $t-{}^3He$ system

$$t^3He \to \alpha + p + n + 12.1\,MeV$$

$$\to \alpha + d + 14.32\,MeV$$

$$\rightarrow {}^{5}He + p + 11.2\,MeV$$

$$\rightarrow {}^{5}Li + n + 10.13\,MeV$$

$$\rightarrow {}^{6}Li + \gamma + 15.8\,MeV$$

and only one for $t-{}^{4}He$

$$t\ {}^{4}He \rightarrow {}^{7}Li + \gamma + 2.47\,MeV\ .$$

Nuclear fusion reactions for the $h - Li$ system (see references 361 and 362) are presented in reference 363:

$$p\,{}^{6}Li \rightarrow \alpha + {}^{3}He + 4\,MeV$$

$$\rightarrow {}^{7}Be + \gamma + 5.6\,MeV$$

$$d\,{}^{6}Li \rightarrow 2\alpha + 22.4\,MeV$$

$$\rightarrow {}^{7}Li + p + 5\,MeV$$

$$\rightarrow {}^{8}Be + \gamma + 22.3\,MeV$$

$$p\,{}^{7}Li \rightarrow 2\alpha + 17.34\,MeV$$

$$\rightarrow {}^{8}Be + \gamma + 17.3\,MeV$$

$$d\,{}^{7}Li \rightarrow \alpha + {}^{5}He + 14.2\,MeV \quad (E_{\alpha} = 7.9MeV;\ E_{He} = 6.3\,MeV)$$

All the fusion reactions mentioned above occur in the corresponding *μhHe* and *μhLi* muonic molecules. The deexcitation and decay of such molecules (with rates $\geq 10^{11}\, s^{-1}$) were discussed in section 3.3. As follows from the calculations (see section 3.3), the nonradiative decay of *μpHe* and *μpLi* via predissociation prevails over the radiative and Auger decay channels. Predissociation corresponds to the transition between the molecular terms, $2p\sigma \to 1s\sigma$ for *μhHe* and $3d\sigma \to 2p\sigma$ for *μhLi* (see Fig.1 and 2 in reference 364). Due to the fact that internuclear separation is relatively large in such molecules (about $\sim 10^3\ fm$), nuclear reactions occur with relatively small rates $\sim 10^6\, s^{-1}$. The possible enhancement of a fusion rate may be due to the presence of a threshold resonance, which close to the threshold energy of some two-body channels (e.g. in the reaction $d\ {}^6Li \to {}^8Be + \gamma + 22.3\, MeV$ that has $\lambda_f = 1.83 \times 10^9\, s^{-1}$ as calculated in reference 365). The nuclei *d* and ${}^6Li$ form the threshold resonant state of ${}^8Be^*(2^+,0)$ [365, 366]; this situation is analogous to nuclear fusion in the *dtμ* molecule. Consequently, the value of the overlap integral to the probability of a transition between the molecular and the nuclear resonance wave function is relatively large. Therefore, long-range nuclear transition can be expected in the molecule.

The nuclear fusion rate in muonic molecules is usually calculated on the basis of Jackson's idea [12a], which allows the factorization of nuclear and molecular coordinates. In this case, the nuclear fusion rate of $\lambda_f$ for small collision energy is given by

$$\lambda_f = C\left|\psi(0)\right|^2,$$

where $C = S/(\pi M Z_1 Z_2)$ is described by the astrophysical *S*-factor, the reduced mass of the system *M*, the nuclear charges $Z_1$ and $Z_2$, and the three body system wave function $\psi(0)$. This was averaged over the muon's degree of freedom and taken at distance comparable with the size of the nuclei: i.e., at an internuclear distance of $r \to 0$, since the nuclear force is short ranged ($\hbar = c = 1$). Different methods of calculation of $\psi(0)$ were used to create various approximate solutions in the Schrödinger equation for the three particles with a Coulomb interaction. Adiabatic expansion schemes were used as a rule without, however, any consideration of the important problem of the convergence of the expansions over the adiabatic basis at small distances. However, the direct solution of the Faddeev equations exists in the configuration space [367], where the problem of convergence is absent.

Conventionally the extrapolation of the cross sections for nuclear reactions to the low energy region (s-wave scattering) is performed with *S*-factor.

Investigation into nuclear fusion in the asymmetric muonic molecules, $\mu hZ$, is a very difficult experimental task, which has only been realized in PSI, to determine the rate of the nuclear fusion of $\mu d^3He$ molecule. The nuclear fusion process following $\mu d^3He$ molecular formation can occur via the intermediate resonant compound state $^5Li^*$, leading to an expected high fusion rate resulting from the large *S*-factor for the

$d^3He \to \alpha + p$ reaction [362]. In reference 368, the author used a small variation basis and the experimental value of the $S \approx 6.32$ *MeV* x *b* and found the nuclear fusion rate for the $\mu d^3He$ in the $J = 0$ state to be $3.8 \times 10^6 s^{-1}$. In reference 364, the nuclear fusion rate in the $\mu d^3He$ from the $J = 0$ was calculated using various methods. Since the nuclear fusion rate in the $1s\sigma$ states of the $\mu d^3He$ molecule is much higher than the fusion rate from the $2p\sigma$ state because of a far smaller potential barrier (see Fig. 13), the under-barrier $2p\sigma \to 1s\sigma$ transition was calculated by finding the transition point in the complex *r*-plane with fusion rate $\lambda_f = 0.88 \times 10^6 s^{-1}$. This procedure is ambiguous and so, therefore, the reaction rate for nuclear fusion in the $\mu d^3He$ was also calculated using the *S*-factor and the experimental data for low-energy scattering in the $^3He(dp)^4He$ process. The result equalled $\lambda_f = 0.32 \times 10^6 s^{-1}$. However, the approximation procedure of the experimental data for the ultra-low energy region leads to some ambiguity in the results. The results of the calculation by the two methods may differ by a factor of three [364]. The fusion rate $\lambda_f = 0.19 \times 10^6 s^{-1}$ was evaluated in reference 369. By the way, all theoretical predictions of this fusion rate correspond to $\sim 10^6 s^{-1}$.The experimental study of the nuclear fusion reaction in the charge-asymmetrical $\mu d^3He$ was presented in reference 370. The 14.64 *MeV* protons were detected by three pairs of

Si(*dE*-*E*) telescopes placed around the cryogenic target filled with $D_2 + {}^3He$ gas at 34 K. They were made of a 4 mm thick Si(*E*) detector and a thin, 360 μm thick, Si(*dE*) detector, respectively. The 6.85 keV gamma-rays emitted during the de-excitation of the $\mu d\,{}^3He$ (see Fig.13) from reaction

$$\mu d + He \rightarrow \left[(\mu dHe)^* e^-\right]^+ + e^-$$

$$\downarrow \lambda_\gamma$$

$$\left[(\mu dHe)^+ e^-\right] + \gamma$$

were detected by a germanium detector. Muon decay electrons were detected by four pairs of scintillators placed around the vacuum housing of the target. To suppress muon decay electrons in the Si(*dE*-*E*) telescope, provision was made in the electronic logic of the experiment to connect each of the electron detectors in anti-coincidence with the corresponding Si(*dE*-*E*) telescope. The experiment included two runs with the $D_2 + {}^3He$ mixtures at different densities and with a helium atomic concentration of 5%. The measurements were performed at two target densities, $\varphi = 0.0585$ and $\varphi = 0.168$ (relative to LHD). The values of the $J = 0$ nuclear fusion rate in $\mu d\,{}^3He$ was derived :

$$\lambda_f = \left(9.7\,{}^{+5.7}_{-2.6}\right) \times 10^5 s^{-1} \quad (\varphi = 0.0585)$$

and

$$\lambda_f = \left(12.4\,^{+6.5}_{-5.4}\right)\times 10^5\, s^{-1} \quad (\varphi = 0.168)$$

.

The effective rates of nuclear fusion found in two runs coincide within the measurement errors. A comparison of the measured $\lambda_f$ rates with the theoretical calculations agrees with reference 364, but slightly disagrees with the results in references 368 and 369.

The study of reactions between light nuclei (p, d, t, He, Li, Be) in asymmetrical muonic molecules were presented in reference 366 without any experimental results for $Z \geq 3$.

# 9. CONCLUSION

The muon plays a very important role in modern physics [371]. I have discussed the contribution of the research into muons in elementary particle physics, atomic investigations, nuclear physics, solid state research, and applied physics. The muon and the muon neutrino, with the correspondent quarks, determine the second generation of the Standard Model. The quality of the μ-decay constant to the vector coupling of ß-decay proved the conserved vector current (CVC) of a weak interaction. In this case, as for the electric charge of elementary particles, the weak charge represented by the vector form factor is not renormalized by the presence of a strong interaction. This implies that all form factors of the hadronic weak current are bound to be equal to the corresponding form factors of the electromagnetic current. So, if the CVC holds, the scalar coupling constant $g_S$ is zero. Furthermore, it obtains the value of the weak-magnetism coupling constant $g_M(q^2) \approx 3.7$ at the vanishing momentum transfer of $q \rightarrow 0$. The confirmation of the partial conserved of axial current (i.e. PCAC hypothesis, including the pseudoscalar $g_P$ constant of a weak interaction) was obtained in the muon capture by light nuclei, especially by hydrogen. From a physical point of view, one may qualitatively understand the idea of a PCAC by observing that the pion mass, which is responsible for the non-conservation of such a current, is actually small with respect to the nucleon mass. The conservation of leptonic numbers could also be obtained by an investigation into muonic

processes. The upper limits for second-class currents were obtained from a nuclear muon capture, especially in hydrogen. Second-class currents have the opposite behaviour under the *G*-parity transformation. The *G*-operation produces a rotation of $180^0$ around the 2-axis in the isospin space with the charge conjugation. According to this definition, one can see that the scalar and tensor currents are second-class. The induced scalar interaction, $g_S$, is zero as a consequence of the CVC hypothesis and the conservation of *G*-parity. It is known that second-class currents are absent in the framework of the Standard Model. The weak muon capture process, as well as the neutrino-deuteron medium-energy interaction, which takes place at higher momentum transfer than *β*-decay, may well represent a better possibility to investigate this problem. Further planned experiments with improved sensitivity were discussed in reference [4]; this includes very rare reactions beyond the Standard Model $\mu \to e\gamma, \mu \to e$ conversion, $\mu \to 3e$, muon anomalous magnetic moment, (g – 2) experiments, h.f.s. of the muonium, proton radius puzzle, and muon capture by deuterium for determination with a 1.5 % precision of the two nucleon weak axial constant, especially $g_P$. At the same time, the understanding of μCF together with the future perspective on fusion energy have been discussed in references 3 and 12g. The further investigation of μCF in the high density and condensed matter phase of the D-T mixture at the RIKEN-RAL Muon Facility with J-PARC is very important. The goal of this research is the realization of at least 300 fusions per muon, due to the decrease of the effective sticking probability. At the same time, an increase in the order of magnitude of the intensity of the muon beam is necessary. Also, the use of μCF as a source of intense

14 MeV neutrons [372] should be further investigated. The small size muonic atoms are an effective possibility to investigate nuclear characteristics, including the electric and magnetic charge distributions of nuclei as well as QED corrections in the high order of perturbation theory. The μSR method using the polarized muon, including muonium, is very effective at investigating the different materials, especially solid-state samples. The method of muonic X-ray diagnosis became the standard practice, which is similar to nuclear magnetic resonance (NMR) and so on. The problem of research into the muon in aerospace medicine is connected to X-ray analysis in medical diagnosis (particularly with regard to osteoporosis) and high-energy galactic cosmic radiation, which emanates from outside the solar system and is sporadically exposed to the burst of energetic particles from the sun, including muons [373]. Fig.1 in reference 373 demonstrates the calculated effective dose rate as a function of altitude for various component particles of galactic cosmic radiation in the atmosphere. Therefore, the possibilities of using $\mu^{\pm}$ muons to solve different problems is extensive.

# REFERENCES


1. a) G. Feinberg and L. Lederman, Ann. Rev. of Nucl. Sci. **13**, 1963;
   b) A.O. Vaisenberg, Mu-Meson, Nauka, Moscow, 1964 (in Russian)
2. Muon Physics, **vol. 1-3**, Eds.V.W. Hughes, C.S. Wu, Academic Press, New York, 1975; The Future of Muon Physics, Eds.: K. Jungmann, V.W. Hughes, G. zu Putlitz, Springer Verlag, Berlin-Heidelberg, 1992
3. K. Nagamine, Introductory Muon Science, Cambridge University Press, 2003
4. T.P. Gorringe, D.W. Hertzog, Progress in Particle and Nuclear Physics **84**, 73, 2015
5. C.D. Anderson and S.H. Neddermeyer, Phys. Rev. **50**, 263, 1936; **51**, 884, 1937; **54**, 88, 1938; J.C. Street, E.C. Stewenson, Phys. Rev. **52**, 1003, 1937
6. C.M.J. Lattes, H. Muirhead, G.P.S. Occhialini and C.F. Powell, Nature **159**, 694, 1947
7. H. Georgy, H.S.L. Glashow, Phys. Rev. Letters **32**, 438, 1974 G. Ross, Grand Unified Theories, Westview Press, ISBN 978-0-8053-6968-7, 1984
8. D.F. Measday, Phys. Reports **354**, 243, 2001, and references therein
9. A. Bertin and A. Vitale, "Strangeness-Conserving Semi-Leptonic Weak Processes", p. 130, in book "Fifty Years of Weak-Interaction Physics", Eds.: A. Bertin, R.A. Ricci and A. Vitale, Italian Physical Society, Bologna, 1984, and references therein
10. D.H. Wilkinson, Proc. Phys. Soc**. 80**, 997, 1962

11 a) F.C. Frank, Nature **160**, 525, 1947;
   b) A.D. Sakharov, P.N. Lebedev Physical Institute, Acad. Sci. USSR, Moscow 1948 (English translation in Muon Cat. Fusion **4**, 235, 1991);
   c) Ya.B. Zel'dovich, Dokl. Acad. Nauk USSR **95**, 493, 1954;
   d) L.W. Alvarez et al., Phys. Rev. **105**, 1127, 1957

12. a) J.D. Jackson, Phys. Rev., **106**, 330, 1957;
   b) S.S. Gerstein and L.I. Ponomarev, Phys. Lett. **72B**, 80, 1977; G. Fiorentini, Nucl. Phys. **A374**, 607c, 1982; L. Bracci and G. Fiorentini, Phys. Rep. **86**, 171, 1982; Yu.V. Petrov, Nature **285**, 466, 1980, Atomkernenergie / Kerntechnik **46**, 25, 1985; Muon Cat. Fusion **3**, 525, 1988; L.I. Ponomarev, Atomkernenergie / Kerntechnik **43**, 175, 1983S.E. Jones, Nature **321**, 127, 1986; S.S. Gershtein, Yu.V. Petrov and L.I. Ponomarev, Sov. Phys. Usp. **33**, 591, 1990;

c) L.I. Ponomarev, Contemp. Phys. **31**, 219, 1990,
d) S.S. Gerstein, "μ-atomic and μ-molecular processes in hydrogen isotope mixtures and muon catalyzed fusion", p.113 in book "Exotic Atoms in Condensed Matter", Eds. G. Benedek, H. Schneuwly, Springer Verlag, Berlin, 1992;
e) J.S. Cohen, „Atomic and molecular processes in muon-catalyzed fusion", Chapter 2 in "Review of Fundamental Processes and Applications of Atoms and Ions", Ed. C.D. Lin, World Scientific, Singapore, 1993;
f) L.I. Ponomarev, Hyperfine Int. **103**, 137, 1996;
g) K. Nagamine and M. Kamimura, Advances in Nuclear Physics **24**, 151, 1998;
K. Ishida, K. Nagamine, T. Matsuzaki, N. Kawamura, Nuclear Physics **B** – Proceedings Supplements **149**, 348, 2005;
h) J.D. Jackson, Phys. Perspect **12**, 74, 2010;
N. Kawamura et al., Journal of Phys.: Conference Series **225**, 012025, 2010; T. Matsuzaki, K. Ishida, and M. Iwasaki, J. Radioanalytical Nucl. Chem. **305**, 889, 2015;
i) K. Nagamine and L. Ponomarev, Nuclear Physics **A721**, 863c, 2003
13. Ya.B. Zel'dovich and S.S. Gershtein, Soviet Phys. Usp., **3**, 593, 1961
14. P. Froenlich, Advances in Physics **41**, 405, 1992
15. E. Borie and G.A. Rinker, Rev. Mod. Phys. 54, 67, 1982; E. Borie, "Lamb schift in light muonic atoms – revised", http://arXiv:1103.1772v7, and references therein
16. V.E. Oberacker, A.S. Umar and F.F. Karpeshin, "Promt Muon-Induced Fission: a Sensitive Probe fort Nuclear Energy Dissipation and Fission Dynamics" in Muon: New Research, Ed. J. Caparthy, p.179, Nova Science Pub., Inc., 2005, ISBN 1-59454-175-2
17. Parts II, V and VI of book "Exotic Atoms in Condensed Matter", Eds.: G. Benedek, H. Schneuwly, Springer Verlag, Berlin, 1992; Muon Science: Muons in Physics, Chemistry and Materials, Eds.: S.L. Lee, S.H. Kilcoyne, R. Cyminski, CRC Press, 1999; K. Stierstadt, Physik der Materie, VCH Verlagsgesellschaft, Weinheim, Basel, Cambridge, New York, 1989, ISBN 3-527-26921-5
18. H. Daniel, Nuclear Medizin **8**, 311, 1969
19. A.L. Huddeleston, Quantitative methods in bone densitometry, Kluwer Academic Pub., Norwell, ISBN-13: 978-1-4612-8971-5, 1988
20. R.K. Hobbie and B.J. Roth, Intermediate Physics for Medicine and Biology, Springer Int. Pub., Switzerland, 2015

21. L.C.L. Yuan and C. Wu, Methods for the determination of fundamental physical quantities, Academic press, New York/London, 1963
22. W. Liu et al. Phys. Rev. Lett. **82**, 711, 1999
23. P.J. Mohr, B.N. Taylor, D.B. Newell, Rev. Mod. Phys. **84**, 1527, 2012
24. R. Winston, Phys. Rev. **129**, 2766, 1963
25. R.F. Christy, S. Kusaka, Phys. Rev. **59**, 405, 414, 1941
26. S. Belenkiy, Avalanche processes in cosmic rays, OGIZ, Moscow, 1948 (in Russian); S. Hirokawa, H. Komori, S. Ogawa, Nuovo Cim. **4**, 736, 1956
27. G. Bardin et al., Phys. Lett. **B 137**, 135, 1984
28. J.P. Miller et al. Ann. Rev. Nucl. And Part. Sci. **62**, 237, 2012
29. F. Rasetti, Phys. Rev. **59**, 706, 1941; **60**, 198, 1941
30. B. Rossi, N. Nereson, Phys. Rev. **62**, 417, 1942
31. K.L. Giovanetti et al., Phys. Rev. **D29**, 343, 1984; M. Balandin, V. Grebenyuk, V. Zinov, A. Ponomarev, Sov. Phys. JETP **40**, 811, 1975
32. A. Barczyk et al., Phys. Lett. **B663**,172, 2008
33. V. Tishchenko et al., Phys. Rev. **D87**, 052003, 2013
34. R.W. Williams and D.L. Williams, Phys. Rev. **D6**, 737, 1972
35. T.D. Lee and C.S. Wu, Weak Interactions, Annual Review of Nuclear Science, **vol. 15**, p.381-476, 1965; vol. **16**, p.471-590, 1966, Annual Reviews, Inc., Palo, Alto, California, U.S.A.
36. J. Adam, et al., Phys. Rev. Lett. **110**, 201801, 2013
37. U. Belgardt, et al., Nuclear Phys. **B299**, 1, 1988
38. W.H. Bertl, et al., Eur. Phys. J. **C47**, 337, 20039
39 C.N. Yang, R.L. Mills, Phys. Rev. **96**, 191, 1954; S.L. Glashow, Nuclear Physics **22**, 579, 1961; S. Weinberg, Phys. Rev. Lett. **19**, 1264, 1967; A. Salam. Elementary Particle Physics: Relativistic Grouls and Analyticity. Ed. N. Svartholm, Eighth Nobel Symposium, Stockholm: Almquvist and Wiksell, p.367, 1968
40. F. Englert, R. Brout, Phys. Rev. Lett. **13**, 321, 1964
41. P.W. Higgs, Phys. Rev. Lett. **13**, 508, 1964
42. G.S. Guralnik, International Journal of Modern Physics, **24**, 2601, 2009
43. J. Bernauer, et al., Phys. Rev. Lett. **105**, 242001, 2010
44. R. Pohl, et al., Nature **466**, 213, 2010
45. a) A. Antognini, et al., Science **339**, 417, 2013;
b) A. Antognini for the CREMA collaboration, WSPC Proceedings, 2016, https://arXiv:1512.01765v2
46. W. Pauli, Noyaux Atomiques (VII Conseil de Physique Solvay 1933), Paris, p.324, 1934

47. F. Reines and C.L. Cowan, Nature **178**, 446, 1956
48. B. Pontecorvo, Sov. Phys. JETP **6**, 429, 1957; Sov. Phys. JETP **26**, 984, 1968
49. R. Devis, D.S. Harmer and K.C. Hoffmanm, Phys. Rev. Lett. **20**, 1205, 1968
50. V.N. Gribov and B.M. Pontecorvo, Phys. Lett. **B28**, 463, 1969
51. E. Majorana, Nuovo Cimento, **14**, 171, 1937
52. Neutrinos (Graduate Texts in Contemporary Physics), Ed. H.V. Klapdor, Springer-Verlag, Berlin, Heidelberg, ISPN-13: 978-3642477502, 1988; Massive neutrinos, Flavor Mixing of Leptons and Neutrino Oscillations (Advanced Series on Directions in High Energy Physics, vol. 25), Ed. Harald Fritzsch (Ludwig-Maximilians-University of Munich, Germany), World Scientific, New Jersey, London, Singapore, Berlin, Shanghai, ISBN 978-9814704762, 2015; F. Boehm and P. Vogel, Physics of massive neutrinos, Cambridge University Press, Cambrige, New York, New Rochelle, Melbourne, Sydney, 1992; S.M. Bilenky and S.T. Petcov, Rev. Mod. Physics, **50**, 671, 1987; Proceeding of XVI INS International Symposium "Neutrino Mass and Related Topics", Eds. S. Kato and T. Ohshima, Tokio, 16-18 March, 1988, World Scientific, Singapore, New Jersey, London, Hong Kong, 1988; T.K. Kuo and J. Pantaleone, Rev. Mod. Physics, **61**, 937, 1989; A. Dar and S. Nussimov, Part. World **2,** 117, 1991; L. Oberauer and F. von Feilitzsch, Rep. Prog. Phys. **55**, 1093, 1992; F. Reines, Rev. Mod. Physics, **68**, 317, 1996
53. E. Fermi, Nuovo Cimento **11**, 1, 1934
54. V.N. Aseev et al., Phys. Rev. **D84**, 112003, 2011
55. Ch. Kraus et al., Eur. Phys. J. **C40**, 447, 2005
56. P.A.R. Ade et al., Astron. Astrophys. **A16**, 571, 2014
57. K. Abe et al., Phys. Rev. Lett. **107**, 041801, 2011
58. P. Adamson et al. (MINOS Collaboration), Phys. Rev. Lett. **112**, 191801, 2014; **110**,171801, 2013; **110**, 251801, 2013; **108**, 191801, 2012; Phys. Rev. **D86**, 12082915, 2012; **D82**, 05110, 2010; L.H. Whiterhead, Nucl. Phys. **B908**, 130, 2016; K. Abe et al., Phys. Rev. Lett. **112**, 181801, 2014; **110**, 251801, 2013; G.L. Folgi et al., Phys. Rev. **D86**, 013012, 2012
59. T. Goldman and G.J. Stephenson, Jr., Phys. Rev. **19**, 2215, 1979
60. A. Aguilar et al. (LSND Collaboration), Phys. Rev. **D64**, 112007, 2001
61. A. Aguilar-Arevalo et al. (MiniBooNE Collaboration), Phys. Rev. Lett. **110**, 161801, 2013
62. N. Okada and O. Yasuda, Int. J. Mod. Phys. **A12**, 3669, 1997; S.M. Bilenky, C. Guinti and W. Grimus, Eur. Phys. J. **C1**, 247, 1998; C.

Guinti and E.M. Zavanin, Mod. Phys. Lett. **A31**, 1650003, 2016; J. Kopp, P.A.N. Machado, M. Maltoni and T. Schwetz, J. High Energy Phys. **05**, 050, 2013
63. P. Adamson et al., Phys. Rev. Lett. **117**, 151801, 2016
64. Andre de Gouvea and A. Kobach, Phys. Rev. **D93**, 033005, 2016
65. N. Cabibbo, Phys. Lett. **B72**, 333, 1978; S.M. Bilenky, J. Hosek, S.T. Petcov, Phys. Lett. **B94**, 495, 1980; M. Doi et al., Phys. Lett. **B102**, 323, 1981; L. Wolfenstein, Nucl. Phys. **B186**, 147, 1981
66. S. Ciechanowicz and N. Popov, Z. Phys. **C57**, 623, 1993; N. Popov and S. Ciechanowicz, "Neutrino mass and T-violation in nuclear muon capture" in Proceeding of the International Workshop on Low Energy Muon Science – LEMS'93, Ed. M. Leon, LA-12698-C, UC-410, Los Alamos, 1994
67. H.F. Schopper, Weak interactions and nuclear beta decay, North-Holland Pub. Co., Amsterdam, 1966
68. E. Fermi and E. Teller, Phys. Rev. **72**, 399, 1947
69. A.S. Wightman, Phys. Rev. **77**, 521, 1950
70. M. Leon and H. Bethe, Phys. Rev. **127**, 636, 1962
71. V.E. Markushin, Sov. Phys. JETP, **53**, 16, 1981; Phys. Rev. **A50**, 1137, 1994
72. a) J.S. Cohen, Rep. Prog. Phys. **67**, 1769, 2004; and references therein
b) Phys. Rev. **A27**, 167, 1983
73. J.E. Russel and G.L. Shaw, Phys. Rev. Lett. **4**, 369, 1960
74. A.P. Bukhvostov and N.P. Popov, Sov. Phys. JETP **55**, 13, 1982
75. L.I. Menshikov, Muon Cat. Fusion **2**, 173, 1988
76. A.V. Kravtsov, A.I. Mikhailov, I.A. Mikhailov, L.I. Ponomarev, Hyperfine Int. **138**, 103, 2001
77 A.V. Kravtsov, A.V. Mikhailov, I.A. Mikhailov, Phys. Rev. **A67**, 042713, 2003
78. L. Bracci and G. Fiorentini, Nuovo Cimento **A43**, 9, 1978
79. W. Czaplinski, A. Gula, A. Kravtsov, A. Mikhailov, N. Popov, S. Ovcinnikov, Muon Cat. Fusion **5/6**, 59, 1990/91; "Coulomb deexcitation of muonic hydrogen", p.159 in book "Exotic atoms in condesed matter", Eds. G. Benedek, H. Schneuwly, Springer Verlag, Berlin, 1992
a) W. Czaplinski, A. Gula, A. Kravtsov, A. Mikhailov and N. Popov, Phys. Rev. **A50**, 525, 1994
80. A.V. Kravtsov and A.I. Mikhailov, Phys. Rev. **A58**, 4426, 1998; JETP **80**, 822, 1995; Phys. At. Nucl. **69**, 371, 2006
81. A. Kravtsov, Hyperfine Int. **119**, 45, 1999

82. L.I. Ponomarev and E.A. Solovyov, JETP Letters **64**, 135, 1996; **68**, 7, 1998; Hyperfine Int. **119**, 55, 1999; Phys. At. Nucl. **65**, 1575, 2002
83. A.V. Kravtsov, A.I. Mikhailov, L.I. Ponomarev and E.A. Solovyaov, Hyperfine Int. **138**, 99, 2001
84. A.V. Kravtsov and A.I. Mikhailov, Phys. At. Nucl. **69**, 371, 2006
85. J. Heading, An introduction to phase-integral methods, London, New York, 1962; N. Fröman and P.O. Frömanm JWKB approximation, North-Holland Publishing Company; Amsterdam, 1965
86. S.S. Gershtein and L.I. Ponomarev, "Mesomolecular processes induced by $\mu^-$ and $\pi^-$ mesons" in book "Muon physics" vol. **3**, p. 141, Eds. V. Huges and C.S. Wu, Academic Press, New York, 1975
87. A. Bertin, "Elastic scattering of muonic hydrogen atoms against protons: status and experiments" in book "Exotic Atoms'79. Fundamental Interactions and Structure of Matter", Eds. Kenneth Crowe, Jean Duclos, Giovanni Fiorentini, and Gabriel Torelli, vol. 4 of the series Ettore Majorana International Science Series p.161, Series Ed. Antonino Zichichi, Physical Sciences, Plenum Press, New York, London, 1979
88. J.S. Cohen, Phys. Rev. **A34**, 2719, 1986
89. S.E. Jones, Nature **321**, 127, 1986
90. N.P. Popov, Muon Cat. Fusion **2**, 207, 1988;
    A.V. Kravtsov, A.I. Mikhailov and N.P. Popov, Phys. Lett. **A223**, 129, 1996
91. A.V. Kravtsov, A.I. Mikhailov, N.P. Popov, Phys. Lett. **A116**, 180, 1986
92. A.V. Kravtsov, A.I. Mikhailov, N.P. Popov, J.Phys. **B19**, 1323, 1986
93. A. Adamczak, V.S. Melezik, L.I. Menshikov, Z. Phys. **D4**, 153, 1986
94. A. Bertin, A. Vitale, and A. Placci, Riv. Nuovo Cim. **5**, 423, 1975; A. Bertin et al., Nuovo Cim. **72A**, 225, 1982; A. Bertin and A. Vitale, Riv. Nuovo Cim. **7,** 1, 1984
95. V. Bystritsky, W. Czaplinski, J. Wozniak, E. Gula, A. Kravtsov, A. Mikhailov, N. Popov, Phys. Rev. **A53**, 4169, 1996
96. V.S. Melezhik, L.I. Ponomarev, M.P. Faifmanm Sov. Phys. JETP **85,** 254, 1983
97. V.S. Melezhik, J. Wozniak, Phys. Lett. **A116**, 370, 1986
98. P. Kammel et al., Phys. Rev. **A28**, 2611, 1983
99. V.P. Dzelepov et al., Sov. Phys. JETP **22**, 275, 1966;
    A. Alberigi et al., Nuovo Cim. **47B**, 72, 1967;
    A. Bertin et al., Phys. Lett. **85B**, 458, 1979

100. N.P. Popov, “Charge exchange processes”, p.151 in book “Exotic Atoms in Condensed Matter”, Eds. G. Benedek, H. Schneuwly, Springer Verlag, Berlin, 1992
101. A. Adamczak, M.P. Faifman, L.I. Ponomarev, V.I. Korobov, V.S. Melezhik, R.T. Siegel and J. Wozniak, Atomic data and nuclear data tables **62**, 255, 1996
102. L.I. Menshikov and L.I. Ponomarev, Sov. Phys. – JETP Lett. **39**, 663, 1984
103. L.I. Menshikov and L.I. Ponomarev, Z.Phys. **D2**, 1, 1986
104. A.V. Kravtsov, A.I. Mikhailov and N.P. Popov, Phys. Lett. **132**, 124, 1988
105. A.V. Kravtsov, A.I. Mikhailov, S.Yu. Ovchinnikov, and N.P. Popov, Muon Cat. Fusion **2**, 183, 1988
106. A.V. Kravtsov, A.Yu. Mayorov, A.I. Mikhailov, S.Yu. Ovchinnikov, N.P. Popov, V.M. Suvorov and A.I. Shchetkovsky, Muon Cat. Fusion **2**, 199, 1988
107. A. Gula, A. Kravtsov, A. Mikhailov, Z. Oziewicz and N. Popov, Muon Cat. Fusion **4**, 217, 1989
108. A. Gula, Z. Oziewicz and N. Popov, Postepy Fizyki **6**, 319, 1990
109. L.I. Menshikov and L.N. Somov, Sov. Phys. Usp. **33**, 616, 1990
110. W. Czaplinski, A. Gula, A. Kravtsov, A. Mikhailov and N. Popov, Muon Cat. Fusion **5/6**, 55, 1990/91
111. N. Popov, Hyperfine Int. **82**, 83, 1993
112. W. Czaplinski, A. Gula, A. Kravzsov, A. Mikhailov and N. Popov, Phys. Rev. **50**, 518, 1994
113 W. Czaplinski, M. Filipowicz, A. Gula, E. Gula and N. Popov, „Muon catalyzed fusion: kinetics of muonic atoms in mixtures of hydrogen isotopes”, in Proc. of 2nd Nat. Symposium “Plasma’95” (Polish Academy of Sciences) Warsaw, June 26-28, Poland, p.217, 1995
114. W. Czaplinski, A. Gula, A.V. Kravtsov, A.I. Mikhailov and N. Popov, Hyperfine Int. **101/102**, 151, 1996
115. W. Czaplinski, A. Kravtsov, A. Mikhailov and N. Popov, Acta Physica Polonica **A93**, 617, 1998
116. M. Filipowicz, W. Czaplinski, E. Gula, A. Kravtsov, A. Mikhailov and N. Popov, Nuovo Cim. **D20**, 155, 1998
117. N. Rozen and C. Zener, Phys. Rev. **40**, 502, 1932;
Yu.N. Demkov, Sov. Phys, JETP **18**, 138, 1964
118. S.Yu. Ovchinnikov and E.A. Solov’ev, Sov. Phys. JETP **63**, 538, 1986; T.P. Grozdanov and E.A. Solov’ev, Phys. Rev. **A42**, 2703, 1990; E.A. Solov’ev, Sov. Phys. Usp. **32**, 228, 1989

119. L.I. Ponomarev, $6^{th}$ Int. Conf. on Atomic Physics Proc. Aug. 17-22, 1978, Zinatne Riga, p.182, Plenum Press, New York, London, 1979
120. V.S. Melezik, Muon Cat. Fusion **2**, 117, 1988
121. A.A. Vorobyov, Muon Cat. Fusion **2**, 17, 1988
122. K. Kobayashi et al., Muon Cat. Fusion **2**, 191, 1988
123. V. M. Bystritsky et al., Sov. Phys. JETP **53**, 877, 1980
124. S.E. Jones et al., Phys. Rev. Lett. **56**, 588, 1986
125. P.K. Haff, E. Rodrigo, T.A. Tombrello, Ann. Phys. **104**, 363, 1977
126. A. Placci et al. Nuovo Cim. **52A**, 1274, 1967
127. L. Schellenberg, A. Adamczak et al., Hyperfine Int. **101/102**, 215, 1996; D. Bakalov, A. Adamczak, M. Stoilov and A. Vacchi, Phys. Lett. **A379**, 151, 2015
128. S.S. Gershtein, Sov. Phys. JETP **16**, 501, 1963
129. L. Landau, Phys. Z. Sow. **1**, 88, 1932; **2**, 46, 1932; C. Zener, Proc. Roy. Soc. **A137**, 696, 1932;
a) L.D. Landau and E.M. Lifshitz, Quantum Mechanics: Non-relativistic Theory, Pergamon, London, 1977; N.F. Mott and H.S.W. Massey, The theory of atomic collisions, Oxford University Press, London-New York, 1965
130. E. Lacopini et al., Nuovo Cim. **67A**, 201, 1982
131. G. Fiorentini and G. Torelli, Nuovo Cim. **36**, 317, 1976
132. A.S. Coolidge, H.M. James and R.D. Present, J. Chem. Phys. **4**, 193, 1936
133. A.V. Matveenko and L.I. Ponomarev, Sov. Phys. JETP **36**, 24, 1973
134. Ya.A. Aristov, A.V. Kravtsov, N.P. Popov, G.E. Solyakin, N.F. Truskova, M.P. Faifman, Sov. J. Nucl. Phys. **33**, 564, 1981; Phys. Lett**. 83A**, 379, 1981; J. Gronowski, W. Czaplinski and N. Popov, Acta Physica Polonica **106**, 795, 2004
135. F.H. Mies, Molecular Physics **26**, 1233, 1973;
F.H. Mies and A.L. Smith, J. Chem. Phys. **45**, 994, 1966
136. V.M. Bystritsky et al., Sov. Phys. JETP **57**, 728, 1983
137. R. Jacot-Guillarmod et al., Phys. Rev. **A38**, 6151, 1988
138. A.A. Vorobyov, Muon Cat. Fusion **2**, 17, 1988
139. A.J. Caffrey et al., Muon Cat. Fusion **1**, 53, 1987
140. S. Hara and T. Ishihara, Phys. Rev. **A39**, 5633, 1989
141. A.V. Kravtsov, A.I. Mikhailov and V.I. Savichev, Z. Phys. **D29**, 49, 1994
142. W. Czaplinski, A. Kravtsov, A. Mikhailov and N. Popov, Phys. Lett. **A233**, 405, 1997
143. V.B. Belyaev, O.I. Kartavtsev, V.I. Kochkin, E.A. Kolganova, Z. Phys. **D41**, 239, 1997

144. T. Matsuzaki et al., Muon Cat. Fusion **2**, 217, 1988;
K. Nagamine et al., in Muon Catalyzed Fusion, p.23, Sanibel Island, Fl., 1988, AIP Conf. Proc. No.181, Eds. S.E. Jones, J. Rafelski, H.J. Monkhorst, AIP, New York, 1989;
a) B. Gartner et al., Hyperfine Int. **101/102**, 249, 1996;
b) S. Tresh et al., Hyperfine Int. **101/102**, 221, 1996
145. a) A.V. Kravtsov, N.P. Popov, G.E. Solyakin, Sov. J. Nucl. Phys. **35**, 876, 1982;
b) V.K. Ivanov, A.V. Kravtsov, A.I. Mikhailov, N.P. Popov and V.I. Fomichevm Sov. Phys. JETP **64**, 210, 1986;
c) W. Czaplinski, M. Filipowicz, E. Gula, A. Kravtsov, A. Mikhailov and N. Popov, Z. Phys. **D41**, 165, 1997;
d) V.K Ivanov, A.V. Kravtsov, A.I. Mikhailov, and N.P. Popov, Z. Phys. **D7**, 349, 1988
146. E.A. Vesman, Sov. Phys. JETP **5**, 91, 1967
147. S.I. Vinitskii, L.I. Ponomarev, I.V. Puzynin, T.P. Puzinina, L.N. Somov and M.P. Faifman, Sov. Phys. JETP **47**, 444, 1978
148. V.B. Belyaev, S.S. Gershtein, B.N. Zakhar'ev and S.P. Lomnev, Sov. Phys. JETP **10**, 1171, 1960
149. S. Cohen, D.L. Judd and R.J. Riddel, Phys. Rev. **119**, 384, 1960
150. W.H. Breunlich et al., Phys. Rev.Lett. **58**, 329, 1987;
C. Petitjean et al., Muon Cat. Fusion **2**, 37, 1988
151. V.P. Dzhelepov, P.F. Ermolov, V.I. Moskalev and V.V. Filchenkov, Sov. Phys. JETP **23**, 820, 1966
152. J. Zmeskal, P. Kammel, A. Scrinzi, W.H. Breunlich, et al., Proc. Few Body XII Conference, Vancouver, **A32**, 1989
153. S.E. Jones, A.N. Anderson, A.J. Gaffrey, Phys. Rev. Lett. **56**, 588, 1986
154. V.D. Balin, A.A. Vorobyov et al., JETP Lett. **40**, 1112, 1984; Phys. Lett. **B41**, 173, 1984
155. V.M. Bystritsky, V.P. Dzelepov, V.I. Petrukhin et al., Sov. Phys. JETP **49**, 232, 1979
156. L.I. Menshikov, L.I. Ponomarev, T.A. Strizh, M.P. Faifman, Sov. Phys. JETP **65**, 656, 1987
157. W. Czaplinski, Phys. Rev. **A88**, 032706-1, 2013;
W. Czaplinski and M. Rybski, Phys. Lett. **A380**, 869, 2016
158. A.I. Mikhailov, W. Czaplinski and A. Gula, Hyperfine Int. **77**, 119, 1993; W. Czaplinski, "Transitions between hyperfine-structure states of the 2s metastable muionic hydrogen in collision processes", PhD Dissertation, AGH, University of Science and Technology, Faculty of Physics and Applied Computer Science, Cracow, 1992

159. S.S. Gerstein, Sov. Phys. JETP **7**, 318, 1958; **13**, 488, 1961
160. A.V. Matveenko and L.I. Ponomarev, Sov. Phys. JETP, **32,** 871, 1971
161. V.S. Melezik and J. Wozniak, Phys. Lett. **A116**, 370, 1986
162. L. Bracci et al., Muon Cat. Fusion **4**, 247, 1989
163. G. Kodosky and M. Leon, Nuovo Cim. **1B**, 41, 1971; R.O. Mueller et al., Phys. Rev. **A11**, 1175, 1975 J.S. Cohen and J.N. Bardsley, Phys. Rev. **A23**, 46, 1981
164. G. Carbonu and G. Fiorentini, Nuovo Cim. **39B**, 281, 1977
165. A.V. Matveenko, communication of JINR E2-81-135, Dubna, 1981
166. A.I. Mikhailov and V.S. Fomichev, Sov. J. Nucl. Phys. **52**, 74, 1990
167. H.A. Bethe and E.E. Salpeter, Quantum Mechanics of One- and Two-Electrons Atoms, Diver Pub. Inc., 2008
168. E. Borie and M. Leon, Phys. Rev. **A21**, 1460, 1980
169. J. Sheffield, Rev. Mod. Phys. **56**, 1015, 1994
170. S.V. Putvinskii, Phys. Usp. **41**, 1127, 1998; V.E. Fortov and A.A. Makarov, Phys. Usp. **52**, 1249, 2009; E.A. Azizov, Phys. Usp. **55**, 190, 2012
171. S.E. Jones et al. Phys. Rev. Lett. **51**, 1757, 1983
172. S.S. Gershtein et al., Sov. Phys. JETP **53**, 872, 1981;
L. Bracci and G. Fiorentini, Nucl. Phys. **A364**, 383, 1981
173. J.S. Cohen, Phys. Rev. Lett. **58**, 1407, 1987; Muon Cat. Fusion **1**, 179, 1987; **3**, 421, 1988
174. C.D. Stodden, H.J. Monkhorst, K. Szalewicz, and T.G. Winter, Phys. Rev. **41**, 1281, 1990
175. S.S. Gershtein, Yu.V. Petrov, L.I. Ponomarev, N.P. Popov, L.P. Presnyakov, L.N. Somov, Sov. Phys. JETP **53**, 872, 1981
176. R. Rice, G. Basbasm F.D. Mc Daniel, Atomic Data and Nuclear Data Tables **20,** 503, 1977;
R.K. Janev, L.P. Presnyakov, V.P. Shevelko, Phys. Lett. **76A**, 121, 1980;
R.K. Janev, L.P. Presnyakov, J.Phys. **B13**, 4233, 1980; Phys. Rep. **70**, 1, 1981
177. K.T. Dolder, M.F.A. Hasrrison, P.C. Thonemann, Proc. Roy. Soc. **A264**, 367, 1961; B. Peart, D.S. Walton, K.T. Dolder, J.Phys. **B2**, 1347, 1969; J.B. Mitchell, K.F. Dunn, G.C. Angel, R. Browning, H.B. Gilbody, J.Phys. **B10**, 1897, 1977; B. Peart, R. Grey, K.T. Dolder, J.Phys. **B10**, 2675, 1977; G.C. Angel, K.F. Dunn, E.C. Sewell, H.B. Gilbody, J.Phys. **B11**, 149, 1978; G.C. Angel, E.C Sewell, K.F. Dunn, H.B. Gilbody, J.Phys. **B11**, 1297, 1978
178. L.I. Menshikov and L.I. Ponomarev, JETP Lett. **42**, 13, 1985

179. A.V. Kravtsov, A.I. Mikhailov, S.Yu. Ovchinnikov and N.P. Popov, Muon Cat. Fusion **2**, 183, 1988; A.V. Kravtsov, A.I. Mikhailov and N.P. Popov, Phys. Lett. **132**, 124, 1988; W. Czaplinski, A. Gula, A. Kravtsov, A. Mikhailov and N. Popov, Muon Cat. Fusion **5/6**, 55, 1990/91; F. Filipowicz, W. Czaplinski, E. Gula, A. Kravtsov, A. Mikhailov and N. Popov, Nuovo Cim. **20D**, 166, 1998
180. P. Ackerbauer et al., Hyperfine Int. **101/102**, 67, 1996
181. K. Ishida, K. Nagamine, T. Matsuzaki, N. Kawamura, Nuclear Phys. **B149**, 348, 2005
182. T. Kase et al., Muon Cat. Fusion **5/6**, 521, 1990/91
183. a) H. Primakoff, in book "Muon Physics" **vol. 2**, p. 3, Eds. V. Huges and C.S. Wu, Academic Press, New York, 1975;
b) V.V. Balashov, G.Ya. Korenman and R.A. Eramzhyan, Absorption of mesons by atomic nuclei, Atomizdat, Moscow, 1978 (in Russian);
c) E. Cremmer, Nucl. Phys. **B2**, 409, 1967
184. L. Grenacs, Ann. Rev. Nucl. Part. Sci. **35**, 455, 1985
185. L.B. Okun, "Weak Interactions of Elementary Particles", Int. Ser. Monogr. in Natural Philosophy, vol.**5**, Pergamon, Oxford,1965
186. R.P. Feynmann and M. Gell-Mann, Phys. Rev. **109**, 193, 1958
187. E.C.G. Sudarshan and R.E. Marshak, Phys. Rev. **109**, 1860, 1958: R.E. Marshak, Riazuddin, C.P. Ryan, "Theory of Weak Interactions in Particle Physics", Ed. R.E. Marshak, N.Y., Wiley, 1969
188. N. Cabibbo, Phys. Rev. Lett. **10**, 531, 1963
189. a) E.A. Paschos and U. Türke, Phys. Lett. **B116**, 360, 1982;
b) J.-M. Gaillard and G. Sauvage, Ann. Rev. Nucl. Part. Sci. **34**, 351, 1984;
c) M. Ademollo, "Cabibbo Theory and Current Algebra", p. 193 in book "Fifty Years of Weak-Interaction Physics", Eds.: A. Bertin, R.A. Ricci and A. Vitale, Italian Physical Society, Bologna, 1984
190. W.-Y.P. Hwang and H. Primakoff, Phys. Rev. **C16**, 397, 1977
191. S. Weinberg, Science **210**, 1212, 1980
192. J. Ellis, Physica Scripta **25**, 107, 1982
193. N.C. Mukhopadhyay, Phys. Rep. **30c**, 1, 1977; Nucl. Phys. **A335**, 111, 1980; in Proc. of the Int. Conference on Weak and Electromagnetic Interactions in Nuclei (Montreal, May 1989), p.51, Ed. P. Depommier, Editions Frontieres, 1989
194. a) K. Olive et al., Chin. Phys. **C38**, 090001, 2014;
b) J. Beringer et al., Phys. Rev. **D86**, 010001, 2012
195. H. Abramowicz, F. Dydak, J.G.H.DE Groot et al., Z. Phys. **C12**, 225, 1982
196. S. Weinberg, Phys. Rev. **112**, 1375, 1958

197. J. Hardy and L. Towner, Phys. Rev. **C79**, 055502, 2009
198. K. Minamisono et al., Phys. Rev. **C84**, 055501, 2011
199. M. Gell-Mann and M. Levy, Nuovo Cim. **16**, 705, 1960
200. S.S. Gershtein and Ya.B. Zel'dovich, Sov. Phys. JETP **2**, 576, 1956
201. L.B. Okun, "Leptons and Quarks", North-Holland, Amsterdam, N.Y., Oxford, 1982, and references therein
202. M.M. Nagels et al., Nucl. Phys. **B109**, 1, 1976
203. V. Bernhard, L. Elouadrhiri and U.G. Meissner, J. Phys. **G28**, R1, 2002
204. V.A. Andreev et al., Phys. Rev. Lett. **110**, 012504, 2013
205. A. Fujii and H. Primakoff, Nuovo Cim. **12**, 327, 1959; C. Kim and H. Primakoff, Phys. Rev. **B140**, 566, 1965
206. S. Knaack, PhD thesis, UIUC, 2012208
207. P. Kammel and K. Kubodera, Annu. Rev. Nucl. Part. Sci. **60**, 327, 2010
208. N. Tatara, Y. Kohyama and K. Kubodera, Phys. Rev. **C42**, 1694, 1990; M. Doi, T. Sato, H. Ohtsubo and M. Morita, Progr. Theor. Phys. **86**, 13, 1991;
a) J. Adam, E. Truhlik, S. Ciechanowicz and K. Schmitt, Nucl. Phys. **A507**, 675, 1990
209. a) A. Placci, E. Zavattini, A. Bertin and A. Vitale, Phys. Rev. Lett. **25**, 475, 1970;
b) A. Bertin et al., Phys. Rev.**D8**, 3774, 1973;
c) G. Bardin et al., Nucl. Phys. **A453**, 591, 1986;
d) M. Cargnelli et al., Workshop on fundamental $\mu$ physics, Los Alamos, 1986, LA 10714C; Nuclear Weak Process and Nuclear Structure, Yamada Conference XXIII, Eds. M. Morita, H. Ejiri, H. Ohtsubo and T. Sato, Word Scientific, p. 115, 1989
210. P. Kammel, "Precision Muon Capture at PSI", the 7th Int. Workshop on Chiral Dynamics, August 6-10, 2012, Jefferson Lab. Newport News, Virginia, USA, Proceeding of Science; Nucl.Phys. **A844**, 181c, 2010
211. C. Petitjean, "Muon Capture Experiments in Hydrogen and Deuterium", Elsier Science
212. Xiao Luo, "MuSun: muon capture on the deuteron", EPJ Web of Conferences **95**, 04037, 2015
213. V. Andreev et al. (MuSun collaboration), Muon capture on the deuterium, arXiv: 1754 V1/nucl-ex/ Apr'2010
214. Roy Kreswell Neely, "A first experimental limit on the relative rates of muon capture by deuterium from the quartet and doublet

hyperfine spin states of μd atom", Thesis and Dissertation (PhD) – Physics and Astronomy, University of Kentucky, 2017, https://doi.org/10.13023/ETD.2017.045
215. a) J.A. Bistirlich et al., Phys. Rev. Lett. **36**, 942, 1976;
b) J. Torre, B. Goulard, Phys. Rev. Lett. **43**, 1222, 1979
216. S.S. Gershtein, V.I. Petrukhin, L.I. Ponomarev and Yu.D. Prokoshkin, Sov. Phys.Usp. **12**, 1, 1970
217. V.S. Evseev, T.N. Mamedov and V.S. Rosanov, Negative Muons in Matter, Energoatomizdat, Moscow, 1985 (in Russian)
218. S. Devons and I. Duerdoth, Advances in Nuclear Physics, vol.2, p.295, Plenum Press,1969
219. V.G. Kirillov-Ugrumov, Yu.P. Nikitin and F.M. Sergeev, Atoms and mesons, Atomizdat, Moscow, 1980 (in Russian)
220. D. West, Rept. Progr. Phys. **21**, 271, 1958
221. M. Morita, Beta decay and muon capture, Benjamin, New York, 1973
222. M. Morita and A. Fujii, Phys. Rev. **118**, 606, 1960
223. a) H. Primakoff, Rev. Mod. Phys. **31**, 802, 1959;
A. Fujii and H. Primakoff, Nuovo Cim. **12**, 327, 1959
224. a) H.P.C. Rood, On the theory of muon capture in nuclei, Thesis, promoter H.A. Tolhoek, University of Groningen, 1964;
b) H.P.C. Rood and H.A. Tolhoek, Nucl. Phys. **70**, 658, 1965
225. P. Ackerbauer et al., Phys. Lett. **B417**, 224, 1998
226. V.M. Bystritsky et al., Phys. Rev. **A69**, 012712, 2004
227. C.W. Kim and H. Primakoff, Phys. Rev. **B140**, 566, 1965
228. J.G. Congleton and H.W. Fearing, Nucl. Phys. **A552**, 534, 1993
229. D. Gazit, Phys. Lett. **B666**, 472, 2008;
Nucl. Phys. **A827**, 409C, 2009
230. L.E. Marcucci, J. Phys.: Conference Series **336**, 012026, 2011; L.E. Marcucci et al., Phys. Rev. **C83**, 014002, 2011
231. J. Golak et al., EPJ Web of Conferences **113**, 04029, 2016
232. a) M.M. Block et al., Nuovo Cim. **55**, 501, 1968;
b) N.C. Mukhopadhyay et al., "Inclusive muon capture in loght nuclei", RPI-98N116, FTUV 98/20, IFIC 98/20, https://arXiv:nucl-th/9802060v1
233. a) C. Biedenharn and M.E. Rose, "Theory of angular correlation of nuclear radiations", Rev. Mod. Phys. **25**, 729, 1953; G. Frauenfelder and P. Steffen, "Angular distribution of radiation", in book "Alpha-, beta-and gamma-ray spectroscopy", vol. 3, Ed. K. Siegbahn, North-Holland Publishing Co., Amsterdam, 1965; A.Z. Dolginov, "Angular

correlations in radiative transitions of nucleus", in book "Gamma-ray", p. 523, Academy of Sciences of the USSR, Moscow, 1961 (in Russian)
234. R.M. Sundelin and R.M. Edelstein, in book "High Energy Physics and Nuclear Structure", p. 150, Ed. S. Devons, Plenum Press, New York, 1970
235. N.P. Popov, Sov. Phys. JETP **17**, 1130, 1963
236. G.M. Bukat and N.P. Popov, Sov. Phys. JETP **19**, 1200, 1964
237. Z. Oziewicz and N. Popov, Phys. Lett. **15**, 273, 1965
238. A.P. Bukhvostov and N.P. Popov, Phys. Lett. **24B**, 497, 1967
239. Z. Oziewicz and A. Pikulski, Acta Phys. Polonica **32**, 873, 1967; **34**, 291, 1968
240. A.P. Bukhvostov and N.P. Popov, Sov. J. Nucl. Phys. **6**, 589, 903, 1968
241. A.P. Bukhvostov and N.P. Popov, Nucl. Phys. **A147**, 385, 1970
242. N.P. Popov, "Particle correlations and hyperfine effects in muon capture", in book "High Energy Physics and Nuclear Structure", p. 188, Ed. S. Devons, Plenum Press, New York, 1970; "The correlations of neutrino and nuclear gamma-quantum from muon capture", in Proc. Conf. on Electron Capture and Higher Order Processes in Nuclear Decays, p.321, Debrecen, Hungary, July 15-18, 1968
243. S. Ciechanowicz and Z. Oziewicz, "Angular Correlation for Nuclear Muon Capture", Fortschr. Phys. **32**, 61, 1984
244. Z. Oziewicz and N. Popov, "Gamma-gamma correlation in radiative partial muon capture", in book "High Energy Physics and Nuclear Structure", p. 185, Ed. S. Devons, Plenum Press, New York, 1970
245. T.A. Dmitrieva, Z. Oziewicz and A. Pikulski, Nucl. Phys. **A155**, 205, 1970
246. A.P. Bukhvostov, A.M. Chatrchan, G.E. Dogotar, R.A. Eramzhyan, N.P. Popov and V.A. Vartanian, Acta Physica Polonica, **B3**, 375, 1972; A.P. Bukhvostov, S. Ciechanowicz, G.E. Dogotar, R.A. Eramzhyan, N.P. Popov and V.A. Vartanian, Acta Physica Polonica **B4**, 495, 1973
247. Z. Oziewicz, "Muon capture phenomenology (spin zero targets)", Preprint JINR, E4-8350, Dubna, 1974; Acta Physica Polonica, **B8**, 563, 1977
248. M.E. Rose, Multipole Fields, John Wiley & Sons, Inc. New York, 1955; Elementary Theory of Angular Momentum, John Wiley & Sons, Inc., New York, 1957
249. L. Grenacs, J.P. Deutsch, P. Lipnik and P.C. Mack, Nucl. Instrum. Methods **58**, 164, 1968
250. G.H. Miller, M. Eckhause, F.R. Kane, P. Martin and R.E. Welsh, Phys. Rev. Lett. **29**, 1194, 1972

251. G.H. Miller, "Gamma rays following negative muon capture in medium Z nuclei", Ph.D. Thesis, College of William & Mary, WM-39-72, 1972
252. V. Brudanin et al., Nucl. Phys. **A587**, 577, 1995
253. B.A. Moftah, E. Gete, D.F. Measday, D.S. Armstrong, J. Bauer, T.P. Gorringe, B.L. Jonson, B. Siebels and S. Stanislaus, Phys. Lett. **B395**, 157, 1997
254. S. Ciechanowicz, Nucl. Phys. **A267**, 472, 1976
255. R. Parthasarathy and V.N. Sridhar, Phys. Rev. **C23**, 861, 1981
256. a) K. Junker, V.A. Kuz'min, A.A. Ovchinnikova and T.V. Tetereva., WEIN'95 – IV Int. Symp.on Weak and Electromagnetic Interactions in Nuclei, p. 394, Osaka, June 1995;
b) K. Junker et al., Phys. Rev. **C61**, 044602, 2000;
c) T. Siiskonen et al., Phys. Rev. **C59**, R1839, 1999
257. B.L. Johnson et al., Phys. Rev. **C54,** 2714, 1996, and references therein
258. Ch. Brianson, V. Brudanin, J. Deutsch, et al., Nucl. Phys. **A671**, 647, 2000
259. L. Wolfenstein, Nuovo Cim. **7**, 706, 1958
260. M.E. Rose and R.H. Good, Jr., Ann. Phys. **9**, 211, 1960
261. M. Morita and D. Greenberg, Phys. Rev. **119**, 435, 1960
262. M. Morita, Phys. Rev. **161**, 1028, 1967
263. V.V. Balashov and R.A. Eramzhyan, Atomic Energy Rev. **5**, 3, 1967
264. A.P. Bukhvostov, V.A. Vartanyan, Z. Oziewicz, N.P. Popov and R.A. Eramzhyan, Sov. J. Nucl. Phys. **13**, 468, 1971
265. G. Dugan, C.S. Wu, W. Hughes et al., "Measurement of the residual muon polarization in $^3He$ muonic atom; Part 2. Angular correlations in the capture of polarized muons in gaseous $^3He$", (exp. 529) in Progress at LAMPF, p. 8-9, 135, LA-8768-PR, Los Alamos, 1981
266. K. Huang, C.N. Yang and T.D. Lee, Phys. Rev. **108**, 1340, 1957; G.K. Manacher and L. Wolfenstein, Phys. Rev. **116**, 782, 1959; G.A. Lobov and T.S. Shapiro, Sov. Phys. JETP **16,** 1286, 1963; G.I. Opat, Phys. Rev. **B134**, 428, 1964; D. Beder, Nucl. Phys. **A258**, 447, 1976; W.-Y.P. Hwang and H. Primakoff, Phys. Rev. **C18**, 414, 1978; H.W. Fearing, Phys. Rev. **C21**, 1951, 1980 E. Truhlik and F.C. Khanna, "On radiative muon capture in hydrogen", in AIP Conference Proceedings, **603**, 535, 2001, http://dx.doi.org/10.1063/1.1436680
267. P. Pascual, Preprint TH 1081 – CERN, 1969
268. a) P. Depommier et al., Chinese Journal of Physics, **32**, 1247, 1994
b) G. Jonkmans et al., Phys. Rev. Lett. **77**, 4512, 1996;

c) D.H. Wright et al., Phys. Rev. **C57**, 373, 1998;
d) Shung-ichi Ando, F. Myhrer and K. Kubodera, Phys. Rev. **C65**, 043501, 2002
269. R.M. Cantwell, "Internal bremstrahlung in the capture of $\mu$-mesons by nuclei", Doct. Dissertation, Washington University, 1956
270. M. Bernstein, Phys. Rev. **115**, 694, 1959
271. N. Popov, "Radiative processes in muon capture by light nuclei and muonic molecule formation", Doct. Dissertation, Academy of Sciences of the USSR, Nuclear physics institute, Leningrad, 1983 (in Russian)
272. L. Wolfenstein, Nuovo Cim. **8**, 882, 1958
273. M.L. Goldberger and S.B. Treiman, Phys.Rev. **111**, 354, 1958
274. Z. Oziewicz, "Partial muon capture", Doctoral Thesis, University of Wroclaw, Institute of Theoretical Physics, Wroclaw, 1970;
Preprint ITP UWr, No. 208, 1970
275. L. DiLella, I. Hammerman and L.M. Rosenstein, Phys. Rev. Lett. **27**, 830, 1971
276. R.D. Hart et al., Phys. Rev. Lett. **39**, 399, 1977
277. M. Döbeli et al., "Radiative muon capture and induced pseudoscalar coupling in nuclei", in Weak and Electromagnetic Interaction in Nuclei, Ed. H.V. Klapdor, Springer Verlag, Berlin, Heidelberg, 1986,
https://link.springer.com/chapter/10.1007/978-3-642-71689-8_163
278. C.J. Virtue et al., Nucl. Phys. **A517**, 509, 1990
279. A. Pouladdej, T.P. Gorringe et al., Phys. Rev. **C68**, 034605, 2003
280. M. Chemtob and M. Rho, Nucl. Phys. **A163**, 1, 1971
a) F. Dautry, M. Rho, D.O. Riska, Nucl. Phys. **A264**, 507, 1976;
R.J. Blin-Stoyle, in Progress in Particle and Nuclear Physics, p.5, Ed. D.W. Wilkinson, Pergamon Press, Oxford, 1978;
b) E. Ivanov and E. Truhlik, Nucl. Phys. **A316**, 437, 1979; "Exchange Currents in Nuclei", Sov. J. Part. Nucl. **12**, 198, 1981; D.O. Riska, Prog. Part. Nucl. Phys. **11**, 199, 1984 W. Donnelly and I. Sick, Rev. Mod. Phys. **56**, 461, 1984; M. Kirschbach and E. Truhlik, Sov. J. Part. Nucl. **17**, 93, 1986; B. Frois and C.N. Papanicolas, Ann. Rev. Nucl. Part. Sci. **37**, 133, 1987;
c) I.S. Towner, Phys. Rep. **155**, 263, 1987;
d) M. Lifshitz and P. Singer, "Meson-exchange currents and energetic particle emission from μ-capture", CERN-TH. 4822/87, 1987; J.-F. Mathiot, Phys. Rep. **173**, 63, 1989
281. J.G. Congleton and E. Truhlik, Phys. Rev. **C53**, 956, 1996
282. S. Ciechanowicz, Z. Oziewicz and N. Popov, J. Phys. **G22**, 1601, 1996

283. S.L. Adler and R.F. Dashen, Current Algebras and Applications to Particle Physics, W.A. Benjamin Inc., New York, Amsterdam, 1968;
S. Wycedch, Nucl. Phys. **B14**, 133, 1969; K. Ohta and M. Wakamatsu, Phys. Lett. **B51**, 325, 1974; Nucl. Phys. **A234**, 445, 1974; M.Rho, Nucl. Phys. **A231**, 493, 1974; J. Delorme et al., Ann. Phys. **102**, 273, 1976; M. Ericson, J.Phys. **G3**, 173, 1977

284. J. Adam Jr., Ch. Hajduk, H. Henning, P.U. Sauer and E. Truhlik, Nucl. Phys. **A531**, 623, 1991

285. a) H.-U. Jäger, M. Kirchbach and E. Truhlik, Nucl. Phys. **A404**, 456, 1983;
b) P. Guichon et al., Phys. Rev. **C19**, 987, 1979

286. E. Wigner, Gruppentheorie und ihre Anwendungen auf die Quantenmechanik der Atomspekten, Friedr. Vieweg und Sohn, Baunschweig, 1931; Nachr. Gesell. der Wissen., Math.-Phys. Klasse **5**, 546, 1932

287. J.H. Christenson, J.W. Cronin, L. Fitch and R. Turlay, Phys. Rev. Lett. **13**, 138, 1964

288. V. Fanti et al., NA48 Collaboration, "A new measurement of direct CP violation in two pion decays of the neutral kaon", Phys. Lett. **B465**, 335, 1999; A. Alavi-Harat et al., KTeV collaboration, "Observation of Direct CP violation in $K_{S,L} \to \pi\pi$ Decays", Phys. Rev. Lett. **63**, 22, 1999

289. C. Amsler et al., Particle Data Group, Phys. Lett. **B667**, 1, 2008

290. L. Wolfenstein, "CP violation", North-Holland Publishing, ISBN 0-444-88081-X, 1989; I. Bigi, "CP Violation - An Essential Mystery in Nature's Grand Design", Surveys of High Energy Physics **12**, 269, 1997; J.-M. Gerard, "CP-violation", Contribution to the Joint International Lepton-Photon Symposium and Europhysics Conference on High Energy Physics, Geneva, July 1991; UCL-IPT-91-21; I.B. Khriplovich, Nucl. Phys. **B352**, 385, 1991; I. Bigi and A. Sanda, "CP violation", Cambridge University Press, ISBN 0-521-44349-0, 1999; G.C. Blanco, L. Lavoura, J.P. Silva, CP violation, Claredon Press, ISBN 0-19-850399-7, 1999; M.S. Sozzi, "Discrete symmetries and CP violation", Oxford Universita Press, ISBN 978-0-19-929666-8, 2008; P. Kooijman and N. Tuning, "CP Violation", 2011, http://master.particles.nl/LectureNotes/2011-CP.pdf ; V. Cirigliano et al., Rev. Mod. Phys. **84**, 399, 2012, http://rmp.aps.org/abstract/RMP/v84/il/p399_1

291. B. Aubert et al., Phys. Rev. Lett. **86**, 2515, 2001; K. Abe et al., Phys. Rev. Lett. **87**, 091802, 2001

292. A. Carbone, LHCb Collaboration, Phys. Rev. Lett. **108**, 111602, 2012; R. Aaij et al., LHCb Collaboration, Phys. Rev. Lett. **110**, 221601, 2013; Journal of High Energy Physics (JHEP) **7**, 041, 2014
293. R. Aaij et al., LHCb Collaboration, Phys. Rev. Lett. **116**, 191601, 2016
294. A.D. Sakharov, JETP Letters **5**, 24, 1967; Sov. Phys. Usp. **34**, 392, 1991
295. J. Schwinger, Phys. Rev**. 82**, 914, 1951; G. Luders, Det Kongelige Danske Videnskabernes Selskab, Matematisk-fysike Meddelelser, **28**, Nu.5, 1954; Ann. Phys. **2**, 1, 1957; W. Pauli, "Forbidden Principle, Lorentz Group, Reflection of Space, Time and Charge", in Niels Bohr and the Development of Physics, Eds. W. Pauli, L. Rosenfeld and V. Weisskopf, London, Pergamon Press Ltd., 1955 M. Kobayashi and A.I. Sanda, Phys. Rev. Lett. **69**, 3139, 1992; O.W. Greenberg, Phys. Rev. Lett. **89**, 231602, 2002; M. Chaichian et al., Phys. Lett. **B699**, 177, 2011; V.A. Kostelecky and N. Russell, Rev. Mod. Phys. **83**, 11, 2011
296. N. Cabibbo, Phys. Rev. Lett. **10**, 531, 1963;
N. Kobayashi and T. Maskawa, Progr. Theor. Phys. **49**, 652, 1973
297. Z. Oziewicz, Acta Physica Polonica **31**, 501, 1967
298. S. Ciechanowicz, Z. Phys. **A337**, 97, 1990
299. J. Deutsch and P. Quin, "Symmetry-Tests in Semileptonic Weak Interactions: a Search for new Physics", in Precision Tests of the Standard Electroweak Model, Ed. P. Langacker, World Scientific Advanced Series on Directions in High Energy Physics, 1993; J. Deutsch, "A comment on T-violating triple-correlations in muon-capture", in Workshop on Fundamental Muon Physics: Atoms, Nuclei and Particles, LAMPF, Los Alamos, 1986
300. Anne-Sophie Carnoy, „Il est possible de mesurer une violation T dans la capture μ", Thesis, Universite Catholique de Louvain, Faculte des Sciences, Institut de Physique Nucleaire, Louvain-la-Neuve, 1991
301. Z. Oziewicz and N. Popov, Phys. Lett. **B324**, 10, 1994
302. L.I. Schiff, Phys. Rev. **132**, 2194, 1963; F.C. Michel, Phys. Rev. **133**, B329, 1964; E.M. Henley, Ann. Rev. Nucl. Sci. **19**, 367, 1969; E. Fischbach and D. Tadic, Phys. Rep. **6**, 124, 1973; M.Gari, Phys. Rev. **C6**, 318, 1973; O.P. Sushkov et al., Sov. Phys. JETP **60**, 873, 1984; E.M. Henley and J.B. Khriplovich, Phys. Lett. **B289**, 223, 1992; V.P. Gudkov, Phys. Rep. **212**, 77, 1992; Z.Phys. **A343**, 437, 1992
303. M. Rho, Phys. Rev. **161**, 955, 1967
304. A.M. Green and M. Rho, Nucl. Phys. **A130**, 112, 1969
305. L.D. Landau, Nucl. Phys. **3,** 127, 1957

306. N.F. Ramsey, Ann. Rev. Nucl. Part. Sci. **32**, 211, 1982; E.P. Schabalin, Sov. Phys. Usp **26**, 297, 1983; V.V. Flambaum, I.B. Khriplovich and O.P. Sushkov, Nucl. Phys. **A449**, 750, 1986
307. A.P. Serebrov et al., Phys. Part. Nuclei Lett.**12**, 286, 2015
308. H.L. Acker et al., Nucl. Phys. **87**, 1, 1966
309. a) C.F. Weizsaecker, Naturwiss. **25**, 284, 1937;
b) H.K. Walter, Nucl. Phys. **A234**, 504, 1974;
c) H.K. Walter et al., Nucl. Phys. **A234**, 469, 1974;
d) H.K. Walter et al., Phys. Lett. **38B**, 64, 1972
310. R.C. Barrett, Phys. Lett. **B28**, 93, 1968;
H.K. Walter et al., Phys. Lett. **40B**, 197, 1972;
E. Borie, Helvetica Physica Acta **48**, 671, 1975;
F. Scheck, Electroweak and strong interactions: an introduction to theoretical particle physics, Springer Verlag, Berlin, Heidelberg, 1996;
S.G. Karshenboim and V.G. Ivanov, Phys. Lett. **A235**, 375, 1997;
A. Czarnecki, Uni. Alberta, RADCOR-LoopFest, Los Angeles, 2015
311. W.E. Lamb Jr. and R.C. Retherford, Phys. Rev. **72**, 241, 1947;
H.A. Bethe, Phys. Rev. **72**, 339, 1947;
H.A. Bethe and E.E. Salpeter, Phys. Rev. 82, 309, 1951;
E.E. Salpeter, Phys. Rev. **87**, 328; **89**, 92, 1952;
a) S.S. Schweber, A introduction to relativistic quantum field theory, Row, Peterson and Co, Evanston, Ill., Ellmsford, New York, 1961
312. J. Arafone, Phys. Rev. Lett. **32**, 560, 1974
313. E. Zavattini, "On vacuum polarization in muonic atoms and some related topics", in Ettore Majorana Centre for Scientific Culture, Exotic atoms and related topics; Erice: Cicily, 1977;
T. Dubler, K. Kauser, B. Robert-Tiscot, L.A. Schaller, L. Schellenberg, H. Schneuwly. Nucl. Phys. **A294**, 397, 1978;
E.Yu. Korzinin, V.G. Ivanov and S.G. Karshenboim, Eur. Phys. J. **D41**, 1, 2007
314. a) J.A. Wheeler, Rev. Mod. Phys. **21**, 133, 1949;
b) D.F. Zaretsky, Proc. of the Second United Nation Int. Conf. on the Peasful Uses of Atomic Energy, vol.**15**, p.175, Geneva, 1958
315. V.E. Oberacker, A.S. Umar and F.F. Karpeshin, "Prompt muon-induced fission: a sensitive probe for nuclear energy dissipation and fission dynamics", in Muons: New Research, p. 179, Ed. J. Caparthy, Nova Science Publishers Inc., 2005, ISBN 1-59454-175-2, and refrences therein,
http://arXiv:nucl-th/0403087v1
316. J.A. Maruhn et al., Phys. Rev.Lett. **44**, 1576, 1980;
Z.Y. Ma et al., Nucl. Phys. **A348**, 446, 1980;

P. Olanders et al., Phys. Lett. **B90**, 193, 1980;
Z. Ma et al., Phys. Lett**. B106**, 159, 1981;
A.H. Blin and G. Wolshin, Phys. Lett. **B112**, 113, 1982;
L. Bracci and G. Fiorentini, Nucl. Phys. **A423**, 429, 1984;
F.F. Karpeshin and V.O. Nesterenko, J. Phys. **G17**, 705, 1991;
V.E. Oberacker et al., Phys. Lett. **B293**, 270, 1992;
V.E. Oberacker et al., Phys. Rev. **C48**, 1297, 1993;
V.E. Oberacker, Heavy-Ion Physics, **10**, 221, 1999;
F.F. Karpeshin, J. Phys. **G30**, 1, 2004; **G16**, 1195, 1990; Nucl. Phys. **A617**, 211, 1997; Phys. At. Nucl. **63**, 729, 2000;
Yu. Demkov, D.F. Zaretsky, F.F. Karpeshin et al., JETP Lett. **28**, 263, 1978
317. E. Teller and M.S. Weiss, Trans. N.Y. Acad. Sci**. 40**, 222, 1980
318. J.A. Diaz et al., Nucl. Phys. **40**, 54, 1963
319. a) T. Johansson et al., Phys. Lett. **B97**, 29, 1980;
b) T. Johansson et al., Phys. Lett. **B116**, 402, 1982
320. a) P. David et al., Phys. Lett. **B180**, 324, 1986;
b) P. David et al., Z. Phys. **A330**, 397, 198
321. W.U. Schroder et al., Phys. Rev. Lett. **43**, 672, 1979
322. F. Risse et al., Z. Phys. **A339**, 427, 1991
323. Ch. Rösel et al., Z. Phys**. A345**, 89, 1993
324. A. Schenck, Muon Spin Rotation Spectroscopy: Principles and Applications in Solid State Physics, A. Hilger, Bristol, 1985; S.F.J. Cox, J. Phys. **C20**, 3187, 1987; E.B. Karlsson, Solid State Phenomena as seen by Muons, Protons, and Excited Nuclei, Oxford University Press, Oxford, 1995; A. Schenck and F.N. Gygax, "Magnetic Materials Studied by Muon Spin Rotation Spectroscopy", p.57, in "Handbook of Magnetic Materials", vol. **9**, Ed. K.H.J. Buschow, Elsevier, Amsterdam, 1995; G. Schatz and A. Weidinger, Nuclear Condensed Matter Physics; Nuclear Methods and Applications, John Wiley, Chichester, 1996; P. Dalmas de Reotier and A. Yaouanc, J. Phys.: Condensed Matter **9**, 9113, 1997; A. Amato, Rev. Mod. Phys. **69**, 1119, 1997; V.G. Storchak and N.V. Prokof'ev, Rev. Mod. Phys. **70**, 929, 1998; S.L. Lee, S.H. Kilcoyne and R. Cywinski, Muon Science: Muons in Physics; Chemistry and Materials, IOP Publishing, Bristol and Philadelphia, 1999;
a) S.J. Blundell, Contemporary Physics **40**, 175, 1999;
J.E. Sonier, J.H. Brewer and R.F. Kiefl, Rev. Mod. Phys. **72**, 769, 2000;
b) P. Bakule, E. Morenzoni, Contemporary Physics **45**, 203, 2004;
A. Yaouanc and P. Dalmas de Reotier, Muon Spin Rotation, Relaxation and Resonance, Oxford University Press, Oxford, 2010;

P. Dalmas de Reotier, Introduction to muon spin rotation and relaxation (μSR), CEA and University Joseph Fourie, Grenoble, France, 2010, http://inac.cea.fr/Pisp/pierre.dalmas-de-reotier/introduction_muSR.pdf

c) E. Morenzoni, Introduction to μSR, Muon Spin Rotation / Relaxation, Script of lecture ETH-Z / Uni ZH: Physics with muons, 2012, http://people.web.psi.ch/morenzoni
A. Bungau et al., Simulations of Muon Production Targets, RAL Technical Reports, RAL-TR-2016-003, 2016, http://purl.org/net/epubs/manifestation/24721603

325. A.E. Pifer et al., Nucl. Instr. Methods **135**, 39, 1976;
T. Bowen, Phys. Today **38**, 22, 1985

326. K. Maier, "Light Particles in Solids - $\mu^-$ in Semiconductors", p. 63, in book "Exotic Atoms in Condensed Matter", Eds G. Benedek, H. Schneuwly, Springer Verlag, Berlin, 1992

327. K. Nagamine, "Condensed Matter Studies with Polarized Bound Negative Muons", p.73, in book "ExoticAtoms in Condensed Matter", Eds G. Benedek, H. Schneuwly, Springer Verlag, Berlin, 1992

328. R. Scheuermann et al., Hyperfine Int. **106**, 295, 1997;
J.H. Brewer, "Muon Spin Rotation/Relaxation/Resonance" in Encyclopedia of Applied Physics, vol.**II**, p.23, VCH Publishers Inc., New York, 1994

329. J.I. Friedman and V.L. Telegdi, Phys. Rev. **105**, 1681, 1957

330. V.W. Hughes et al., Phys. Rev. Lett. **5**, 63, 1960;
V.W. Hughes, Phys. Today **20**, 29, 1967; Z. Phys. **C56**, 535, 1992; Ann. Rev. Nucl. Part. Phys. **50**, 1, 2000

331. a) G. Feinberg and L.M. Lederman, Ann. Rev. Nucl. Sci. **13**, 1963;
V.L. Telegdi, in Festschrift in honor V.W. Hughes, p. 65, Ed. M. Zeller, World Sci., Singapore, 1991;

b) S.P.J. Cox, "Muonium and Hydrogen Defect Centres in Solid", p.213, in book "ExoticAtoms in Condensed Matter", Eds G. Benedek, H. Schneuwly, Springer Verlag, Berlin, 1992; R. Prepost, "Muonium – the early experiments", in The memory of Vernon Willard Hughes, p.26, Eds. E.W. Hughes and F. Iachello, World Sci. Pub. Co, Pte, Ltd, 2004; http://arXiv:nucl-ex/0404013v1; B. Liu, Muonium-Antimuonium Oscillations in an Extended Minimal Suppersymmetrie Standard Model, Springer, ISBN-131: 978-1441983299, 2011; P.Percival, Muonium, TRIUMF Summer Institute 2011, Lecture 9; Monsen Emami-Razavi, J. Theor. App. Phys. **9**, 1, 2015;

c) K.P. Jungmann, "Precision Muonium Spectroscopy", Journal Phys. Society of Japan, **85**, Nu.9, 2016; http://arXiv:1603.01195v1

332. a) G. Feinberg and S. Weinberg, Phys. Rev. **123**, 1439, 1961;
b) G. Feinberg and S. Weinberg, Phys. Rev. Lett. **6**, 381, 1961
333. N. Cabibbo, Nuovo Cim**. 19**, 612, 1961
334. B. Pontecorvo, Sov. Phys. JETP **6**, 429, 1957
335. B. Pontecorvo, Phys. Lett. **B26**, 630, 1968
336. E. Drukarev, V.A. Gordeev and A.I. Mikhailov, Preprint LNPI 1317, 1987
337. A. Halprin, Phys. Rev. Lett. **48**, 1313, 1982
338. V.A. Gordeev et al., JINR Rapid Communications No.4 (78) 1996
339. P. Herczeg and R.N. Mohapatra, Phys. Rev. Lett. **69**, 2475, 1992
340. L. Willmann et al., Phys. Rev. Lett. **82**, 49, 1999
341. E. Derman, Phys. Rev. **B19**, 317, 1979
G.G. Wong and W.S. Hou, Phys. Rev. **D50**, R2962, 1994;
W.S. Hou and G.G. Wong, Phys. Rev. **D53**, 1537, 1996
342. R.N. Mohapatra, Z.Phys. **C56**, 117, 1992;
A. Halprin and A. Mariero, Phys. Rev. **D48**, 2987, 1993
343. H. Fujii et al., Phys. Rev. **D49**, 559, 1994;
P.H. Frampton, Phys. Rev. Lett. **69**, 2889, 1992
344. J.J. Amato et al., Phys. Rev. Lett. **21**, 1709, 1968
345. T.M. Huber et al., Phys. Rev. **D41**, 2709, 1990
346. V. Meyer et al., "Increased sensitivity to possible muonium to antimuonium conversion", in API Converence Proceedings **412**, 429, 1997
347. R. Abela et al., Phys. Rev. Lett. **77**, 1950, 1996
348. C. Patrignani et al., (Particle Data Group), Chin. Phys. **C40**, 100001, 2017
349. Y. Kuno, "PRISM" in Preceedings on new initiatives on lepton flavour violation and neutrino oscillation with high intense muon and neutrino sources, p.96, Eds. Y. Kuno, W.B. Molzon and S. Pakvasa, World Sci. Publishing Co. Pte., Ltd., New Jersey, London, Singapore, Hong Kong, ISBN 981-238-084-1, 2002
350. M. Aoki, "PRISM experiment", p.106, *ibid*
351. S.P.J. Cox, "Muonium Substituted Molecules", p.229 in book "ExoticAtoms in Condensed Matter", Eds G. Benedek, H. Schneuwly, Springer Verlag, Berlin, 1992
352. D.C. Walker, Muon and Muonium Chemistry, Cambridge University Press, London, UK, ISBN: 9780521103374, 2009
353. I.I. Gurevich et al., "Physics and Chemistry of $\mu^+$-Meson and Muonium", Phys. Elem. Part. At. Nuclei **8**, Part 1, 1977

354. V.A. Zhukov et al., "μSR Investigation at Phasotron of the Laboratory of Nuclear Physics of JINR", Phys. Elem. Part. At. Nuclei **28**, Part 3, 1997

355. "Space Bones", NASA, 2001, https://science.nasa.gov/headlines/y2001/ast01oct_1.htm
356 "Trip to Mars Will Challenge Bones, Muscles: Former Astronaut calls for More NASA Research on Exercidse in Space", American College of Sports Medicine, April 12, 2006, http://www.spaceref.com/news/viewpr.html?pid=19543
357. J.D. Sibonga, Curr. Osteoporos Rep. **11**, 92, 2013
358. R.J. Friedman and J.M. Fogel, Rev. Med. Aeronautique et Spatiale **12**, 322, 377, 1973
359. K. Terada et al., Sci. Rep. **4**, 5072, 2014; https://worldwidescience.org/topicpages/i/international+muon+ionization.html
360. C. Rolfs, in Nuclear Astrophysics, Research Reports in Physics, Springer Verlag, p.162, 1988
361. F. Ajzenberg-Selove, Nuclear Physics **A490**, 1, 1988
362. G.R. Caughlan, W.A. Fowler, At. Data Nucl. Data Tables **40**, 283, 1988
363. V.B. Belyaev, A. Bertin, Vit.M. Bystritsky, Vaych.M. Bystritsky, A. Gula, O.I. Kartavtsev, A.V. Luchinsky, G.A. Mesyats, L.A. Rivkis, N.A. Rotakhin, A.A. Sinebryukhov, S.I. Sorokin, S.G. Stetsenko, V.A. Stolupin, A. Vitale, J. Wozniak, Nucleonika **40**, 85, 1995
364. W. Czaplinski, A. Kravtsov, A. Mikhailov, and N. Popov, Phys. Lett. **A219**, 86, 1996; Eur. Phys. J. **D3**, 223, 1998
365. S.A. Rakityansky, S.A. Sofianos, V.B. Belyaev, V.I. Korobov, Phys. Rev. **A54**, 1242, 1996
366. V.B. Belyaev, M. Decker, H. Fiedeldey, S.A. Rakityansky, W. Sandhas, S.A. Sofianos, Nucleonika **40**, 3, 1995
367. A.A. Kostrykin, A.A. Kvitsinsky, S.P. Merkuriev, Few-Body Systems **6**, 97, 1989; Sov. J. Part. Nucl. **21**, 553, 1992; Chi-Yu Hu, A.A. Kvitsinsky, S.P. Merkuriev, Phys. Rev. **A45**, 2723, 1992; Chi-Yu Hu, A.A. Kvitsinsky, Phys. Rev. A46, 7301, 1992; A.A. Kvitsinsky, J. Carbonell, C. Gignoux, Phys. Rev. **A46**, 1310, 1992
368. F.M. Pen'kov, Phys. Atom. Nucl. **60**, 897, 1997
369. L.N. Bogdanova, V.I. Korobov, L.I. Ponomarev, Hyperfine Int **118**,

183, 1999
370. V.M. Bystritsky, M. Filipowicz, V.V. Gerasimov, P.E. Knowles, F. Mulhausen, N.P. Popov, V.P. Volnykh, and J. Wozniak, Eur. Phys. J. **D38**, 455, 2006
371. S. Weinberg, A, Sci. American **13**, 4, 1999; http://www.drtulsian.com/interestingReading/physics/unified-physics-by-2050.pdf
372. I.N. Ruskov et al., Physics Procedia **64**, 163, 2015; A. Gandhi et al., Proceeding of the DAE Symp. on Nucl. Phys. 62, 2017; http://www.sympnp.org/proceedings/62/G42.pdf
373. M. Bagshaw and F.A. Cucinotta, Fundamentals of aerospace medicine, cosmic radiation, https://ntrs.nasa.gov/search.jsp?R=20070028831 2018-06-01T18:58:25+00:00Z